EFFICIENT MOORING SYSTEMS FOR SEMISUBMERSIBLE FLOATING OFFSHORE WIND TURBINES

A Thesis

by

CHONG-SUK SHIN

Submitted to the Office of Graduate and Professional Studies of
Texas A&M University
in partial fulfillment of the requirements for the degree of

MASTER OF SCIENCE

Chair of Committee,	Robert Randall
Co-Chair of Committee,	Charles Aubeny
Committee Member,	Steven DiMarco
Head of Department,	Sharath Girimaji

May 2017

Major Subject: Ocean Engineering

ABSTRACT

This thesis examines critical components of the mooring system for Floating Offshore Wind Turbines including chain cables, anchors and soil. The mooring line is investigated using OrcaFlex models to assess the characteristics of both catenary and semi-taut mooring system. Then, the analysis is advanced to look into the effects of water depth variation on the performance of the mooring system. The continental shelf located at the northern California coastal area is selected as a study region. Based on the information of macro-scale study on the region, soil properties are developed to aid in understanding the performance of the mooring system. Combining the results from the mooring analysis and soil data base, considerations for appropriate anchor types are presented. The anchor types include: driven piles, drag embedment anchors, and direct embedment plate anchors. This study seeks to provide a novel mooring and anchor concept which can be used to design efficient mooring systems relevant to Floating Offshore Wind Turbines.

ACKNOWLEDGEMENTS

I have a great appreciation for several people who have contributed to the realization of this report. I would like to thank Professor Robert Randall and Professor Charles Aubeny for their immensely helpful discussions and notes. Special thanks to Professor Steven DiMarco for his attentiveness and positivity. Thanks to my family for their never-failing support, and another thanks to my friends in Texas for their fantastic friendships. I'm grateful to Ashwin Gadgil and Brian Diaz for their knowledge and experience with this research. And of course, final gratitude is addressed to the Stinchcomb family for providing all the wonderful memories in the United States.

CONTRIBUTORS AND FUNDING SOURCES

This work was supervised by a thesis committee consisting of Professor Robert Randall of the Ocean Engineering Department, Professor Charles Aubeny of the Department of Civil Engineering and Professor Steve DiMarco of the Oceanography Department. All work for the thesis was completed independently by the student.

There are no outside funding contributions to acknowledge related to the research and compilation of this document.

NOMENCLATURE

H_f	Horizontal Force at the Top
V_f	Vertical Force at the Top
ω	Mooring Line Weight in Fluid
L	Unstretched Mooring Line Length
EA	Line Extensional Stiffness
C_B	Seabed Drag Coefficient
S_f	Current Speed at Surface
S_b	Current Speed at Seabed
n	Power Law Exponent
Z_f	Water Surface Level in Z-axis
Z_b	Seabed Level in Z-axis
C_d	Drag Coefficient
ρ_{air}	Density of Air
V_{wind}	Wind Velocity
A	Exposed Area of Platform Surfaces
T_e	Effective Tension
v	Poisson ratio
P_i	Internal Pressure
P_o	External Pressure
A_i	Internal Cross Sectional Area

A_o	External Cross Sectional Area
L_s	Suspended Mooring Length
x_a	Distance to the Anchor from the Origin
θ_n	Angle between the Nodes
μ	Friction Coefficient for the Cable Material
n_A	Number of Anchors in the Wind Farm
n_T	Total number of Floating Turbines
n_{AT}	Number of Anchor Points per Turbine
n_{MA}	Number of Mooring Lines per Anchor
$F_{r,0}$	Resultant Force Parallel to Wind-Wave-Current Direction
$F_{r,90}$	Resultant Force Perpendicular to Wind-Wave-Current Direction
F_r	Total Resultant Force

TABLE OF CONTENTS

Page

LIST OF FIGURES

Page

LIST OF TABLES

Page

1. INTRODUCTION

Background

Although oil & gas continue to persist as dominant energy resource, the ill effects of fossil-fuel emissions have been pushing the U.S. to secure a low-carbon future. This expanded awareness of greenhouse gas resulted in rapid growth of the renewable energy demand.

According to a report by EERE (The Office of Energy Efficiency and Renewable Energy), wind energy could provide 20% of American electricity by 2030 (Lindenberg, 2008). Abundant wind resources often originate from onshore locations that require transmission lines to deliver energy coastal states. As a result, such limited access to interstate grid transmission entraps the availability of land-based wind energy in coastal areas in the United States. Moreover, the oceanic states of Mid-Atlantic and Northeastern coasts have higher usage of the nation's electricity than that of inland states (Beaudry-Losique et al., 2011).

In states further from land wind turbines, offshore wind deployment can potentially lower retail electricity rates and dependence on hydrocarbon deposits with minimized transmission capacity. Energy department's national offshore wind strategy indicates that annual average wind speeds of nation's coastal waters are greater than 7.0 m/s (Schwartz et al., 2010). Due to the close relationship between average wind speeds and accessible energy, the database estimates the total gross of the national offshore wind resources to be 4,150 GW (Lindenberg, 2008).

While the potential installed capacity of offshore wind energy is four times the current supply of the country's electric power system, more than 60 percent of this capacity is in water deeper than 60 m (Beaudry-Losique et al., 2011). Although wind installations have expensive capital costs requiring upgrades in conventional platform and foundation for operation in deep-water, harnessing large scale wind resource addresses the barriers of making viable renewable energy in the future. As in Figure 1, a grid array of platforms tethered to seabed with interconnected piles is a cost effective proposition (Diaz et al., 2016).

Several companies in the U.S. have been attempting to apply the concept of a multiunit floating windfarm, but the scope of design is still beyond the current practices. In order to convert the theoretical capacity of offshore windfarms to the nation's superior renewable energy mix, an extensive research ought to focus on the effect of mooring lines on various types of foundation system. As the station-keeping system plays a crucial role in overall performance for floating wind farms, the proposed thesis aims to assess suitable types for both mooring and foundation systems, considering marine soil behavior (Bhattacharya, 2014). This paper assumes an Offshore Code Comparison Collaborative Continuation (OC4) model, a semisubmersible design developed for a U.S.-based offshore wind project, deployed in the coastal area of Central Pacific (Figure 2).

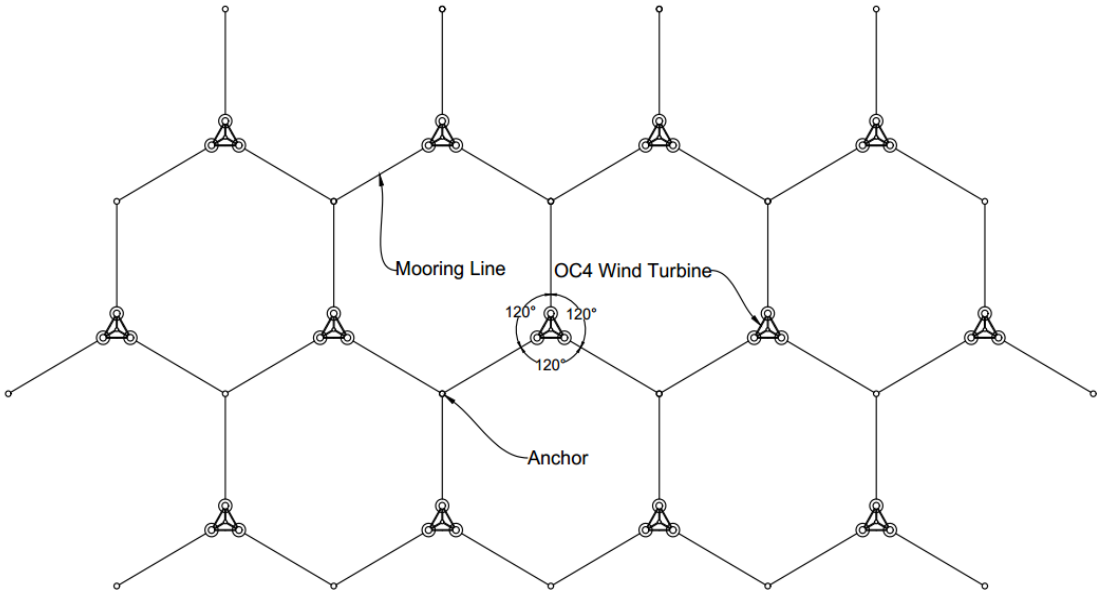

Figure 1: Wind farm configuration

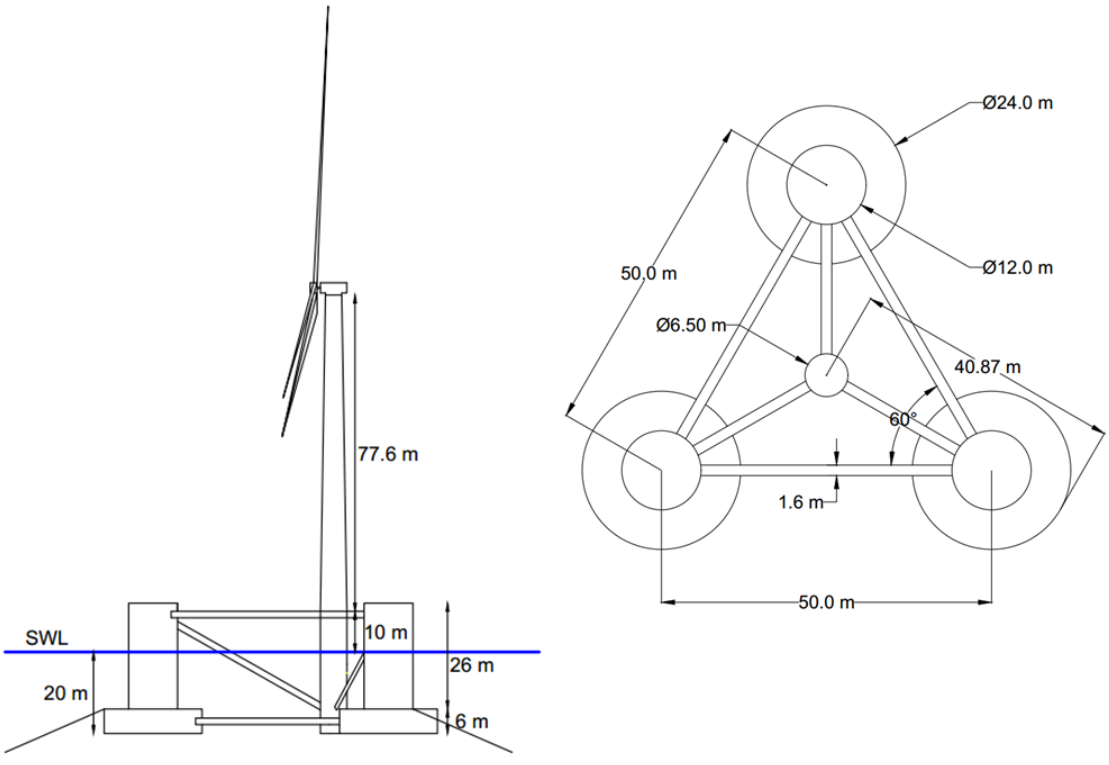

Figure 2: Side (left) and plan (right) view of the OC4 semisubmersible design

Literature Review

Jonkman (2014) devotes an entire chapter of his paper to mooring the OC4 model. The author provides a thorough numerical derivation of mooring loads that are dependent on the horizontal distance between the fairlead and anchor. Finally, the author writes data that was determined by running FAST (Fatigue, Aerodynamics, Structures, and Turbulence) in time-domain simulations. Unfortunately, Jonkman (2014) does not account for a different water level from the default depth (200 m). However, the fundamentals for constructing a catenary mooring model are included in this paper and can be developed to study the effects of water depth variation.

Lin and Sayer (2015) presents a comparative study of mooring behaviors at different water depths. The author discusses the variety of deepwater environments and provides an assessment of mooring a Spar platform for water depths between 300m and 3,000m. For line tension response, Lin shows how to obtain accurate results when coupled with floating body in time domain. Additionally, Lin presents the interdependency between mooring system and platform motion. Such techniques will be employed in this proposal to reveal the effect of water depth variation on mooring lines. Aiming to ensure that the OC4 Semisubmersible wind turbine is coupled in this work; FAST will operate the simulation and present the output.

The Fast-Orcaflex coupling module was developed for coupling the offshore wind turbine simulation tool with an improved mooring cable emulator. Masciola (2011) assesses the fidelity of this tool and reports a promising stability by comparing results with those obtained with the default FAST model. Although the method uses OC3-

HyWind spar, which is a simpler form of offshore wind turbine compared to OC4-Semisubmersible, Masciola notes an expanded functionality of wind turbine simulation. The FASTlink achieves a greater applicability by enabling Orcaflex to model taut mooring lines. The analysis Masciola developed will be used to investigate the effects of converting the existing catenary shaped mooring lines to a taut leg system.

The National Centers for Environmental Information collects the information about the U.S. coastal areas on a geological scale. One of the reports presented in this database conducts granulometric analyses of the sediment samples from the continental shelf off the Washington coast (Robertson, 1974). The document includes the percentage of gravel, sand, silt, clay contents as well as the location of all the samples arranged by latitude, longitude, and water depth. Robertson (1974) plots the data in a tabulated form for each locality and identifies dominant sediment type in the seafloor. While this investigation does not account the details of soil profile data, Alpine Geophysical Associates, Inc in conjunction with the Offshore Sand Inventory Program, obtains soil profile data by recovering drilled cores 10 to 12ft in length. As it exposes the vertical section of the soil in depth, layers of soil types are identified that may be useful in assessing stratification conditions. Devoted to listing factors of site specific information and soil profile data, NOAA may be helpful in terms of establishing important parameters for anchor studies.

Instead of costly direct measurements, Dalyander (2014) developed a methodology for estimating bottom stress through modelling hydrodynamic functions of orbital velocity, wave periods and current near the bed. The estimates of sea floor stress

were added to the U.S. Geological Survey (USGS) data layer to address issues in U.S. coastal environments. A geographic mapping tool, known as ArcGIS, contributes to shaping the data format by locating the values on the bathymetry with the corresponding site location. All stress values contained in the data base will be used as similar factors as the other soil properties in regards to exploring various suitable anchor types for floating wind farm.

The Naval Facilities Engineering Command (NAVFAC) has an engineering manual aimed to help marine geotechnical engineering applications. This Handbook for Marine Geotechnical Engineering (Thompson & Beasely 2012) discusses techniques for determining soil properties as well as designing foundations and anchors. This manual refers to guidance for estimating soil properties based on the related geological province which addresses the concerns of lacking field data. Moreover, as a general guide, the handbook covers the design of piles, direct-embedment anchors, and drag-embedment anchors, which will be the examined types for this study. Overall, the document of Marine Geotechnical Engineering will be devoted to applying the knowledge and measurements attained from the previous sections for assessing design feasibility of various anchor types.

The American Petroleum Institute guidelines for station keeping (API 2SK, 2005) provides a similar guideline as the one from NAVFAC. The standard suggests predicting the anchor holding capacity when credible performance data is missing. The design curves are used to estimate the holding power of drag embedment type in different soils based on the weight of the anchor and soil. API 2SK, (2005) also defines

the factors of safety which are used to calculate the allowable holding capacity. According to Table 1, factors of safety for piles and direct embedment anchors are higher than for drag embedment anchors because the horizontal penetration of drag embedment anchors develop stronger holding capacity.

Table 1: Anchor safety factors (API 2SK, 2005)

Condition	Piles				Direct Embedment		Drag Embedment	
	permanent		Mobile		permanent	mobile	permanent	mobile
	Lateral	Axial	Lateral	Axial				
Intact	1.6	2	1.2	1.5	2	1.5	1.5	1
Damaged	1.2	1.5	1	1.2	1.5	1.2	1	0.8

Aubeny (2016) conducted research that concentrates on examining amenable anchor types to multiline systems. The study not only assesses suitable soil conditions but also considers the mooring restrictions for each anchor alternative. Building off Aubeny (2016), this thesis uses the methodologies for resolving issues caused by introducing a multiline configuration to the anchor. Another objective is to examine the relationship between taut and catenary mooring configurations concerning various anchor types.

Mooring System Design Problem

With regard to the worldwide extensive investigation on Floating Offshore Wind Turbines, OC4 is an international joint project developed under International Energy Agency (Jonkman, 2014). The project organizes 22 research teams from 11 different

countries to verify simulated results of a standardized semisubmersible. According to the outputs computed by different simulation tools, the mooring forces fixing the platform to the 200m deep seabed are consistent in a certain range of values (Robertson et al., 2014). However, the U.S. offshore sites differ in depth and the influence of water depth variation on mooring behavior can be significant enough to affect the overall dynamic response of the structure. Because the weight of mooring lines hanging in the water dictates the pretension of cables, change in water depth requires a complete redesign of the station keeping system with modification in line cross sections, lengths, and anchor positions (Kim et al., 2014).

The concept of OC4-DeepCwind semisubmersible is moored by three catenary lines (Jonkman, 2014). The catenary shape is commonly found as it is economically sound in shallow water depth but the move into deepwater increasingly requires optimal mooring systems to extend the capability of the supporting platform. Unlike the given conditions in European nations, the U.S. outer continental shelf rapidly drops off; hence semi-taut leg mooring is potentially preferable. This thesis compares a catenary system and a semi-taut leg system, and also obtains mooring responses for a water depth outside of the default depth to determine the effective combination of station-keeping components.

The assessment of novel foundation options for moored platforms in the deep ocean requires a thorough investigation on the bottom soil. Based on Randall (2016), when the mooring line reaches the anchor embedded in the seafloor, 15 to 20% of the overall mooring length is grounded to the seafloor and the friction between the line and

surface is dependent on the physical properties of the contact area. Moreover, soil properties such as sediment type, stratigraphy and consolidation state initiate the sizing procedure of adequate anchor type for existing loading conditions. Although the geotechnical aspects of seafloor environment guide optimum foundation type selection, naval engineers find difficulty in acquiring such information due to a lack of precedence for underwater construction. While the oil and gas industry distributes documents containing soil properties beneath the Gulf of Mexico, there is still a low level of publication for Northwest Pacific and Mid-Atlantic geotechnical topics. In this thesis, the research concentrates on generating geotechnical data used for understanding seafloor soil behavior in the central California coastal area.

Along with the summaries of mooring line tensions and seafloor geology, the development of the array wind farm requires an anchor design that has multiline attachments. In contrast to conventional anchor subjected to a single load, applying multi loads to an anchor not only lowers the design loads by counter-pulling line loads but also reduces the number of foundation structures needed (Burns et al., 2009). As there are large financial implications caused by expensive foundation installations, the proposed anchor design concept will potentially enhance the cost efficiency of the overall project (Chung & Maynard, 2007). Because the existing floating wind turbine systems practice individual anchoring connection, the study examines the feasibility of adapting the multiline concept to three types of anchor; Driven Piles, Direct-Embedment Plate Anchors (DEPAs), and Drag-Embedment Anchors (Figure 3, Figure 4 and Figure 5). Despite the fact that each type has its own features in terms of resisting multiple line

loads, this thesis assesses the given options of anchor types with considerations on interdependences between mooring and soil properties.

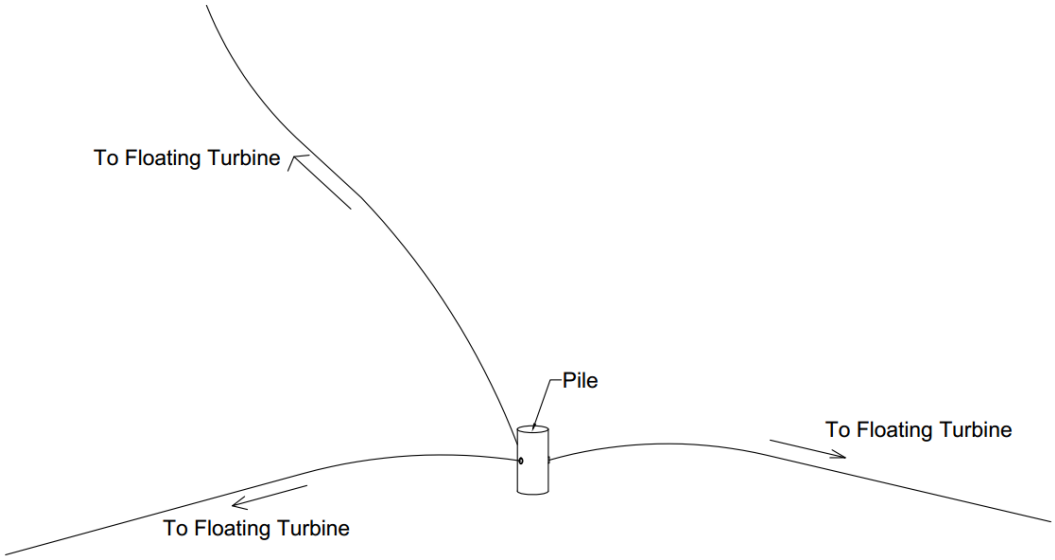

Figure 3: Driven piles

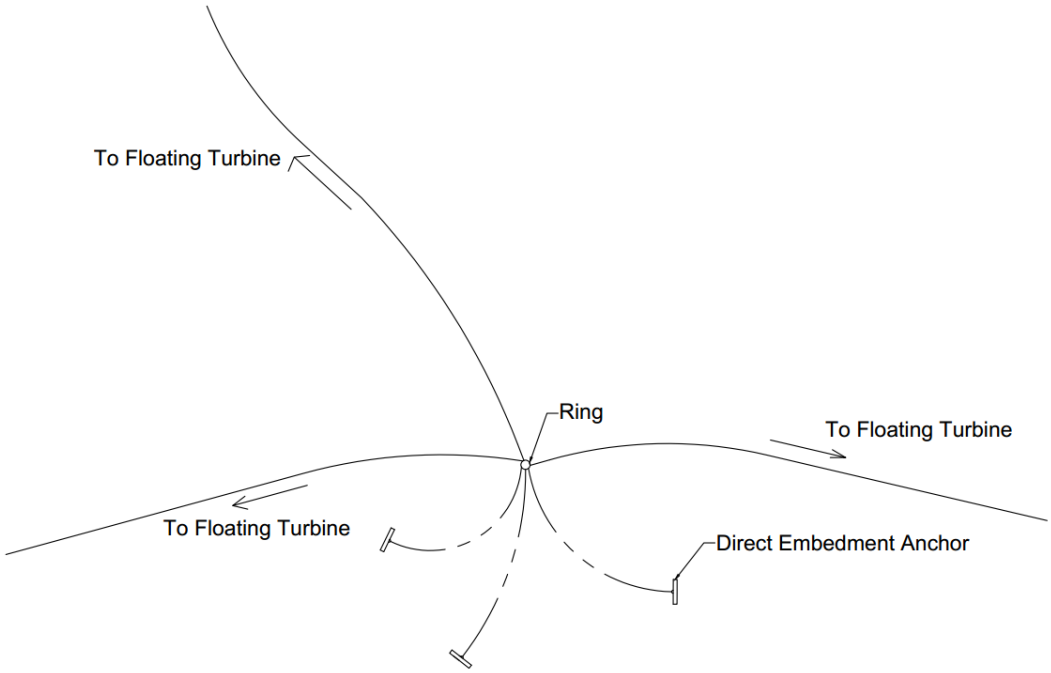

Figure 4: Direct embedment plate anchors

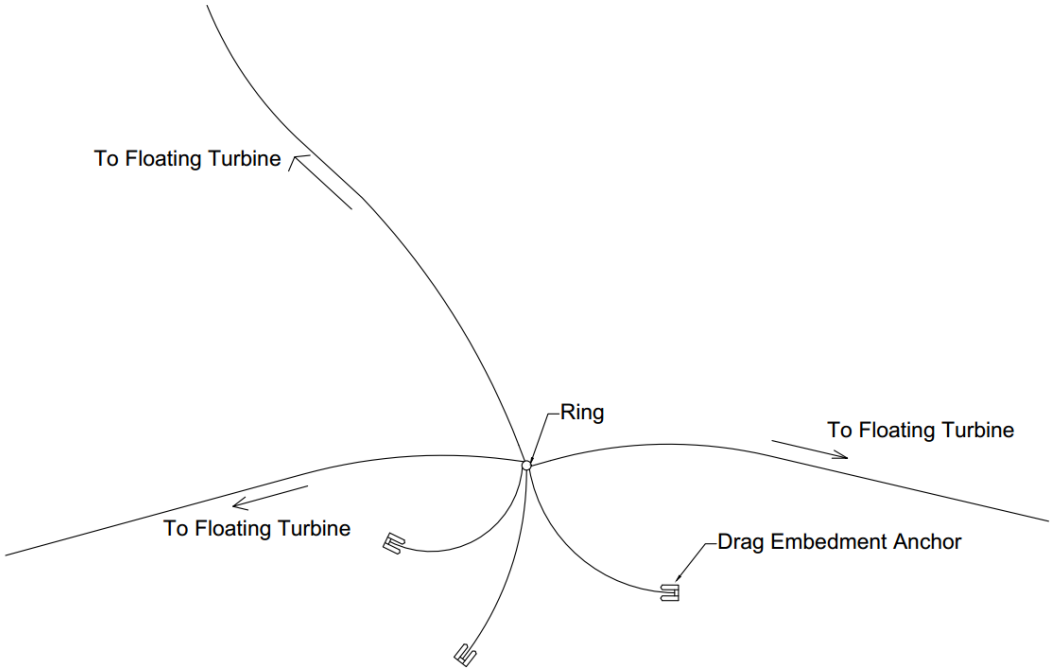

Figure 5: Drag embedment anchors

Modeling Tools for Mooring Systems

The inputs into calculating anchor tensions are the properties of the mooring lines being used for station-keeping. Some examples of these inputs are line diameter, anchor positions, and mooring mass in water. In the first step, a static mooring line analysis will determine initial anchor positions based on the submerged weight of the mooring line. The general approach of mooring analysis breaks a line into N evenly-sized segments and the count of each node, N, starts from the location of the anchor (Hall & Goupee, 2015). During the computation, each weight of the half-segment is assigned to the nodes at both ends as shown in Figure 6.

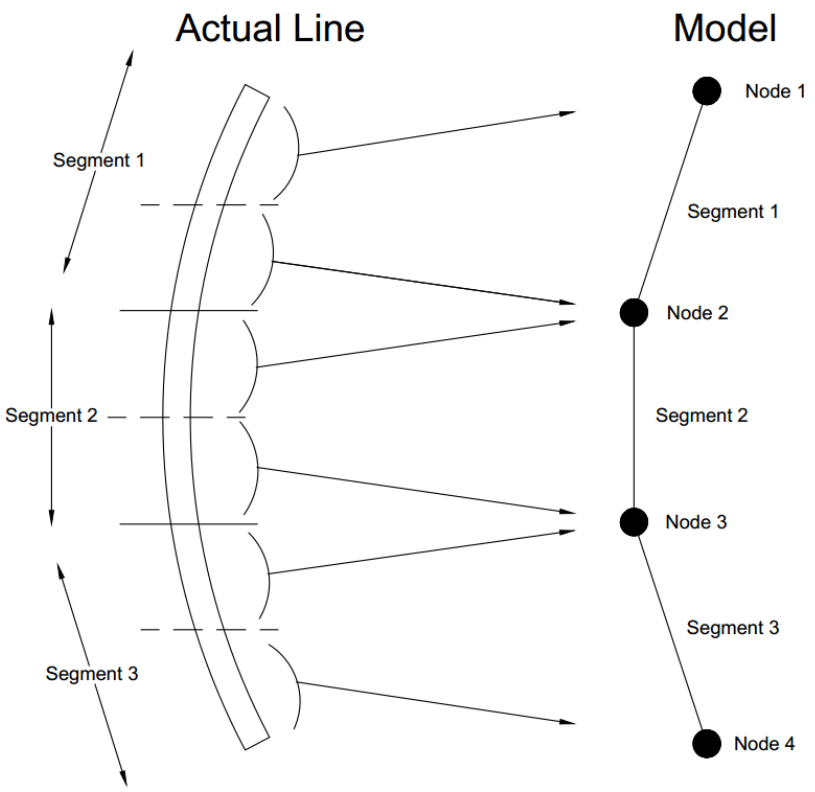

Figure 6: Line model structure

Due to the identical properties but increasing vertical coordinates of each segment, the horizontal tension for each node will remain the same while each vertical tension will reduce as the mooring line reaches the sea floor (OrcaFlex Manual, 2006). At the desired water depth, the results of vertical and horizontal components permit estimation of coordinates for each node including the fairlead (Tomasicchio et al., 2012). The computation is an iterative process of alternating multiple catenary equations to provide locations of connections that will be added as input parameters to the next step (Jonnkman, 2007). The iterative equations are

$$x_f(H_F,V_F)=\frac{H_F}{\omega}\left\{ln\left[\frac{V_F}{H_F}+\sqrt{1+\left(\frac{V_F}{H_F}\right)^2}\right]-ln\left[\frac{V_F-\omega L}{H_F}+\sqrt{1+\left(\frac{V_F-\omega L}{H_F}\right)^2}\right]\right\}+\frac{H_F L}{EA} \quad (1)$$

and

$$z_F(H_F,V_F)=\frac{H_F}{\omega}\left[\sqrt{1+\left(\frac{V_F}{H_F}\right)^2}-\sqrt{1+\left(\frac{V_F-\omega L}{H_F}\right)^2}\right]+\frac{1}{EA}\left(V_F L-\frac{\omega L^2}{2}\right) \quad (2)$$

in which ω is the submerged line weight in fluid per unit length, L the unstretched line length, EA the line extensional stiffness, and H_f and V_f horizontal force and vertical force at the top. When a portion of line is lying on the sea bottom:

$$x_F(H_F,V_F)=L-\frac{V_F}{\omega}+\frac{H_F}{\omega}ln\left[\frac{V_F}{H_F}+\sqrt{1+\left(\frac{V_F}{H_F}\right)^2}\right]+\frac{H_F L}{EA}+\frac{C_B}{2EA}\left[-\left(L-\frac{V_F}{\omega}\right)^2+\left(L-\frac{V_F}{\omega}-\frac{H_F}{C_B\omega}\right)MAX\left(L-\frac{V_F}{\omega}-\frac{H_F}{C_B\omega},0\right)\right] \quad (3)$$

where C_B is the seabed drag coefficient.

Although the variability in depth allows single line catenary solver to set the fundamentals for computing mooring loads, the limitation exists as the method excludes the aero-hydro-servo-elastic dynamics of the floating wind turbine.

In the next step, a simulation tool called FAST, developed by the US National Renewable Energy Laboratory (NREL) is used in this thesis to resolve the matter of tower and rotor blades coupling. FAST is an open-source software which combines the interfaces of aerodynamics, hydrodynamics, and structural dynamics in order to simulate an offshore turbine in time domain. Among the coupled modules, MoorDyn addresses the modelling of the mooring system. The application of MoorDyn model further refines the estimation and thus determines anchor tensions with more accuracy than the values from the previous step (Hall, 2015).

Load Case Descriptions

With various ranges of particular water depth, determination of mooring responses in two steps above will focus on the influence of deep water environment on mooring characteristics as part of the thesis. This thesis considers six different load cases (Table 2) throughout the study. The first two cases focus on sea conditions in the absence of wind and current while the third and fourth case account for the wind incidents. The last two cases assume three types of load excitations including wave, wind and current.

Table 2: Load cases for mooring analysis

	Wave	**Wind**	**Current**
Case 1	Regular waves, H=6 m, T=10 s	No air	No current
Case 2	Irregular waves, H_s=6 m, T_p=10 s, γ=2.87, JONSWAP spectrum	No air	No current
Case 3	Regular waves, H=6 m, T=10 s	Shear wind, 10 m above surface=8 m/s, $1/7^{th}$ power law	No current
Case 4	Irregular waves, H_s=6 m, T_p=10 s, γ=2.87, JONSWAP spectrum	Shear wind, 10 m above surface=8 m/s, $1/7^{th}$ power law	No current
Case 5	Regular waves, H=6 m, T=10 s	Shear wind, 10 m above surface=8 m/s, $1/7^{th}$ power law	$1/7^{th}$ Power law current, 0.5 m/s at surface
Case 6	Irregular waves, H_s=6 m, T_p=10 s, γ=2.87, JONSWAP spectrum	Shear wind, 10 m above surface=8 m/s, $1/7^{th}$ power law	$1/7^{th}$ Power law current, 0.5 m/s at surface

All the conditions are oriented in the same +X direction and the current is 0.5 m/sec at the surface with a 1/7th power law decrease with depth. A power law current profile is given as:

$$S = S_b + (S_f - S_b)\left(\frac{Z - Z_b}{Z_f - Z_b}\right)^{\frac{1}{n}} \quad (4)$$

where S_f is the current speed at the surface, S_b the current speed at seabed, Z_f the water surface level in Z-axis, Z_b the seabed level in Z-axis, and n the power law exponent. After specifying the given variables, Figure 7 shows a vertical view of the profile graph.

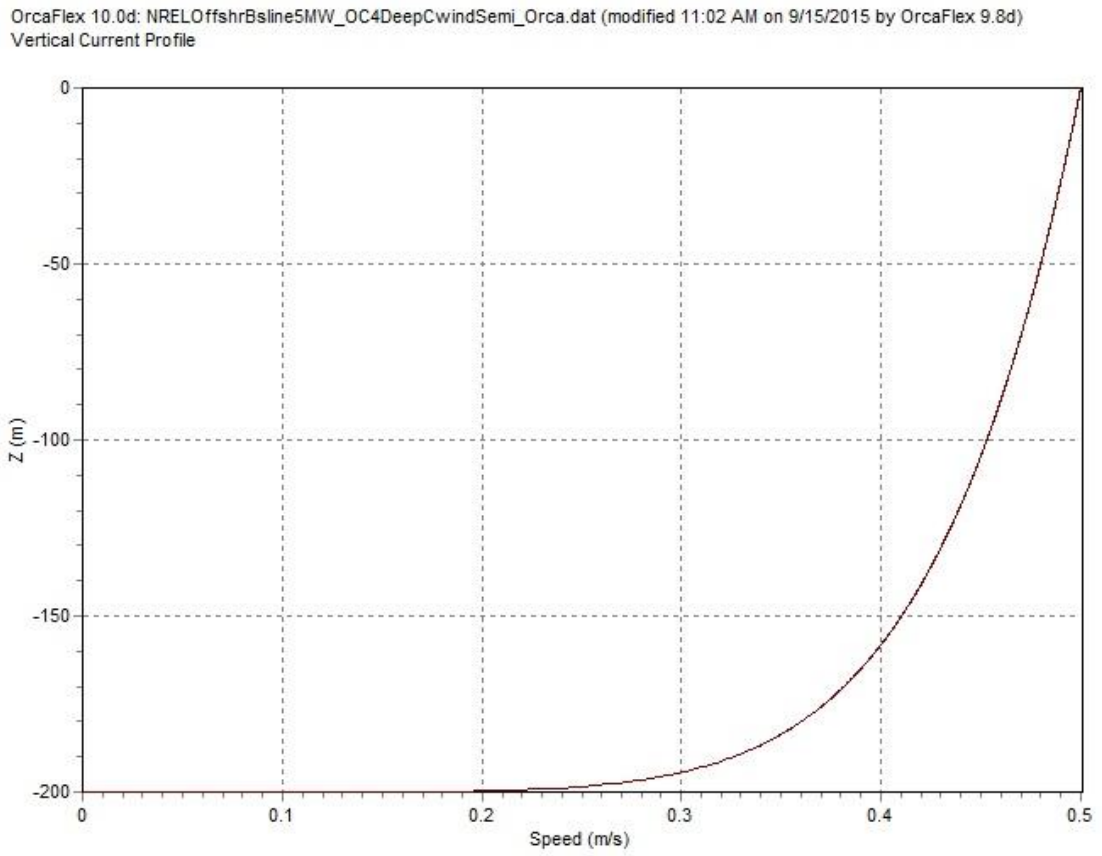

Figure 7: Vertical current profile with 7th power law

The wind condition is also taken as a $1/7^{th}$ power law profile with a velocity of 8 m/sec at 10 meters above the water surface. The effect of wind load is accounted by the wind load formula in the following

$$F_{wind} = \frac{1}{2} C_d \rho_{air} V_{wind}^2 A \quad (5)$$

where C_d is the drag coefficient, ρ_{air} the density of air, V_{wind} the wind speed, and A the exposed projected area of platform surfaces. The vertical profile of wind velocity is shown in Figure 8 below.

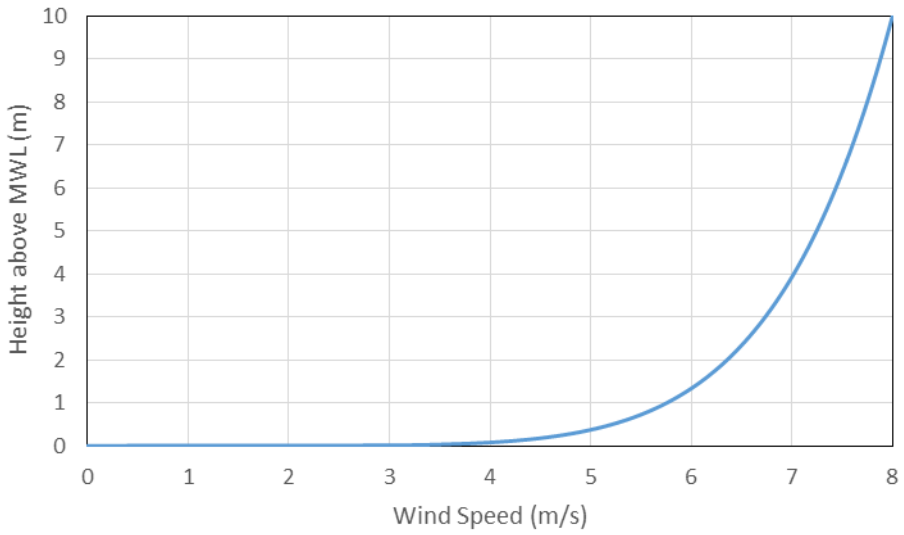

Figure 8: Vertical wind profile with 7th power law

After looking at the effects of water depth variation, another simulation is generated to review the influence of converting the existing catenary model to a semi-taut leg mooring model. The procedure for the modified system analysis is the same as above except a program OrcaFlex, a time domain based commercial software, is used to conduct the part of refining multisegmented mooring responses (Andersen et al., 2016). The OrcaFlex calculates effective tensions at the anchors as below:

$$T_e = EA\left(\frac{L-\lambda L_o}{\lambda L_o}\right) - 2v(P_o A_o - P_i A_i) + EA\left(\frac{\lambda_a}{100}\right)\sqrt{\frac{2ML_o}{EA}}\left(\frac{dL}{dt}\right)/L_o \quad (6)$$

in which T_e is the effective tension, EA the axial stiffness of line, L the length of line, λ the expansion factor, L_o the unstretched mooring length, *v* the Poisson ratio, P_i and P_o the internal and external pressure respectively, A_i and A_o the internal and external cross sectional stress areas respectively, λ_a the axial damping, M the segment mass, and dL/dt the rate of increase of length. The line theory behind the OrcaFlex software identifies dynamic effects of the mooring lines that are ignored in FAST simulation. Though the FAST's quasi-static mooring model is a more simplified analysis, the dynamic mooring model provides a more advanced prediction associated with time-varying conditions such as line damping and platform motions. For deep-water where line damping often creates significant impact on mooring behavior, simulating both the dynamic and quasi-static models across the six load cases will allow valuable investigation on the overall performance of the wind turbine system (Rabe, 2015).

OrcaFlex also enables a variety of cable configuration including semi-taut leg and solves mooring dynamics problems (Masciola, 2011). In this work, FASTlink, a coupling module, will integrate the OrcaFlex model with the data sets of wind turbine to avoid the mismatching of reference frames between these two programs. The aim of the mooring analysis is to compare representative features of the two mooring types in different water depths to aid in the assessment of suitable foundation system (Figure 9, Figure 10).

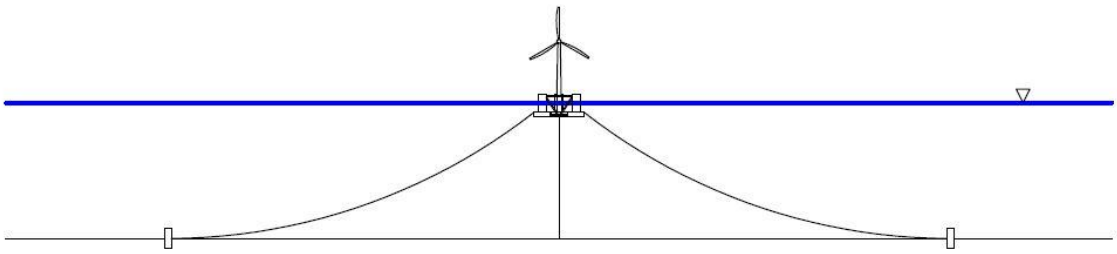

Figure 9: Catenary mooring shape

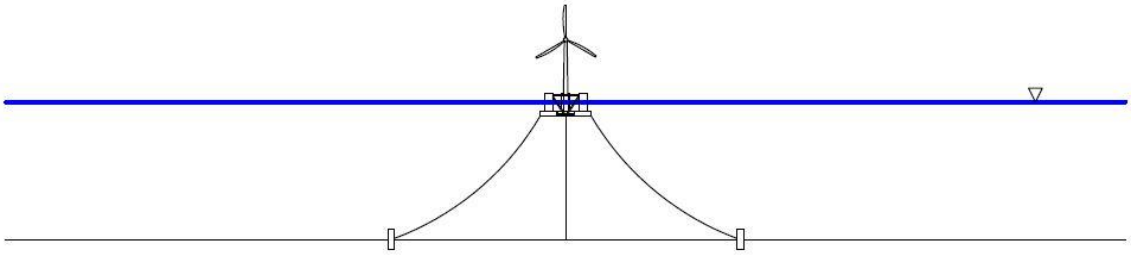

Figure 10: Semi-taut leg shape

Soil Data Development

The summary of geologic site data required for engineering application varies from regional area information to detailed site-specific information (Thompson & Beasley, 2012). The project-specific information is to be obtained from marine geology data repositories available online. In this study, National Oceanic and Atmospheric Administration (NOAA) will be a primary source of finding regional data as well as more detailed information. As a governmental institution, NOAA is one of the prevalent sources that provides geographical database along U.S. coasts. With its complex geologic mapping framework, each coastal system is subdivided into different regions. Understanding the difference in geologic frameworks is an important source of

information because it produces dissimilar design conditions required for the foundation (UNC Chapel Hill, 2009). Such knowledge is included through a macro-scale survey of each shelf component by exploring its operational water depth as well as the according dominant soil type.

Though regional studies can set the basic parameters for foundation design, the behavior of soil is typically determined by other properties. Sediment texture of the bottom seafloor is high value information when characterizing soil behavior because of its impact on holding strength. The U.S. Geological Survey which is another source concerning marine geology has been observing patterns in sea bottom surface with regional variation and converted the output to geographical data. Within the data observed by USGS, textural analyses of the sediment aid in estimating anchor strength capacity by identifying how much the soil's strength is available.

However, in highly stratified seabed, soil profile is another critical performance consideration for foundation because while some types are versatile, some types are restricted to heterogeneous soil deposits (Aubeny, 2016). When dealing with such an issue, the soil profiles from the areas of interest must be identified. This thesis selects specific information points and obtains soil profile information to find out whether the soil layers vary. The presentation of this information will help examining the efficient anchor type in stratified soil conditions.

A review of basic geotechnical data of soils is another matter that needs to be addressed after the investigations for the geophysical property of the site. To determine the type of foundation, the characteristics of the soil such as grain-size distribution and

compressibility are taken into consideration for the most economic choice. Though most of the samples are tested in the laboratory, there has been an increased use of in-situ testing which is investigating soils from their natural environment. However, offshore investigations require advanced tools in order to recover representative deepwater samples. If the tools are not available, estimates of geotechnical data can be extrapolated from the site information. To account for the absence of required soil properties based on laboratory tests, this thesis is devoted to providing guidelines for identifying engineering properties of U.S. coastal areas in part. The estimations consider critical parameters for anchor performance, and the properties in this paper collectively bring the knowledge of characteristics regarding moored lines, site, and soils. Then, these factors are used to influence the considerations for selecting an anchor type system within an interactive process.

Anchors for Floating Offshore Wind Turbines

This paper discusses three alternatives of anchor system. The first is piles that are designed to be driven into the ground for installation. The second are Direct-Embedment Anchors that are vertically inserted to a desired depth, then rotated to achieve higher pullout resistance. The third category are Drag-Embedment Anchors that are stabilized by dragging the fluke along the seabed surface. Regardless of these different foundation types, a conventional application of an anchor adapts a single attachment of mooring line.

However, the present thesis endeavors to encourage the use of the multiline anchor which significantly reduces the cost of stabilizing arrays of floating wind turbines. In the case of attaching additional lines to a single anchor, existing preference of the most suitable anchor design can be altered. Including a matter of multiline arrangement, this section assesses the performance of Piles, Direct Embedment Plate Anchors, and Drag Embedment Anchors. Considering a function of other crucial factors such as (1) mooring conditions, (2) site characteristics, and (3) soil properties, this study will score each type of anchor based on the performance. Moreover, collective assessments of three foundation types are produced for coastal area near central California. To that end, a suitable anchor type of each zone is identified alongside of the appropriate mooring system type.

2. VALIDATION OF AN ORCAFLEX PLATFORM MODEL

Construction of the OrcaFlex Model

In the analysis of floating wind turbines systems, OrcaFlex is a powerful program with many capabilities including model development based on graphical interface as well as rendering simulations. The major steps required to develop an OC4 floating wind turbine will be provided in the following. Main steps to be introduced include: incorporating dynamic effects, creating a floating platform, adding mooring lines in the model.

Once the inputs of the desired environmental conditions were defined, the integration method for time step was set to implicit to achieve unconditional simulation stability. To fully account for the primary motions of the platform, the calculation module included the effects of applied loads, wave load, added mass and damping, current load and wind load. These included effects are applied when computing the total six-component hydrodynamic and mooring loads after running the simulation.

After setting up an appropriate time step and containing dynamic effects, a floating structure was modeled to visualize the platform system. The vessel geometry was modified by adding and removing lines and vertices to represent the physical appearance of the floating body as shown in Figure 11. The combined mass of the rotor-nacelle assembly, tower, and platform columns was set so that the simulation begins at equilibrium.

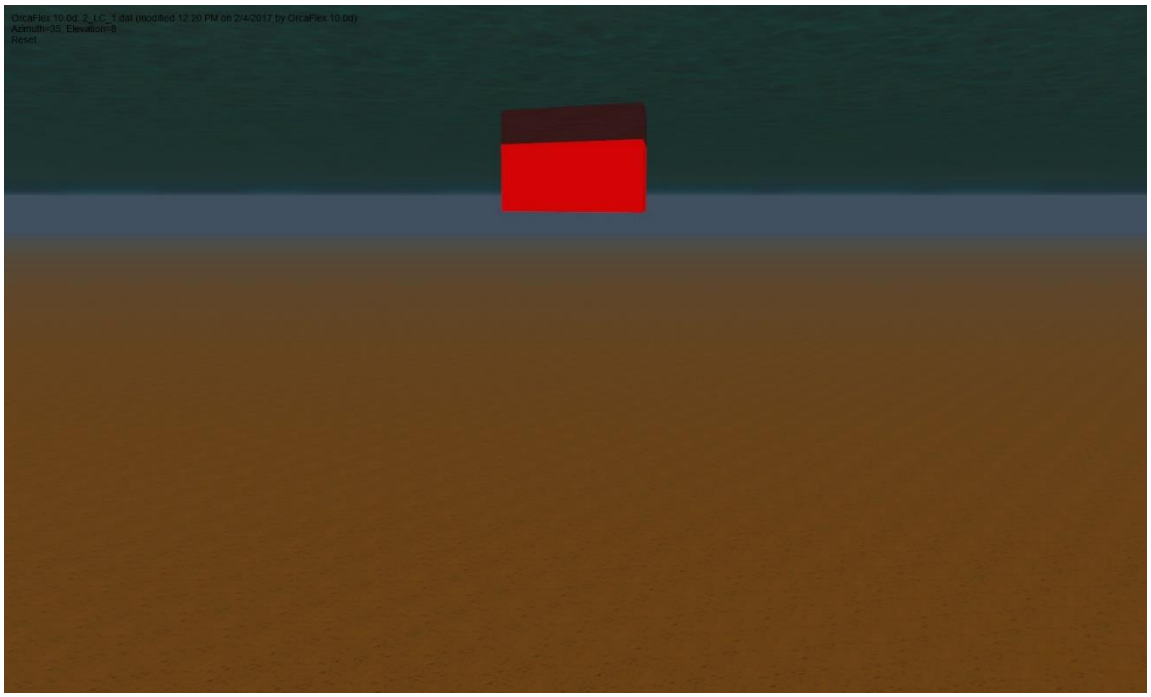

Figure 11: Platform body in the OrcaFlex model

The next step was adding bodies that account for quadratic drag forces on the platform. As shown in Figure 12, objects having all six degrees of freedom were attached to the assembly of the model. Since the platform columns are shaped as cylinders, the type of buoy was considered as spar buoy with the according drag, added mass and damping data. The platform bodies were discretized into smaller sub-cylinders which was done to allow sufficient drag along the body. The areas and drag coefficients were specified to compute more accurate drag force results.

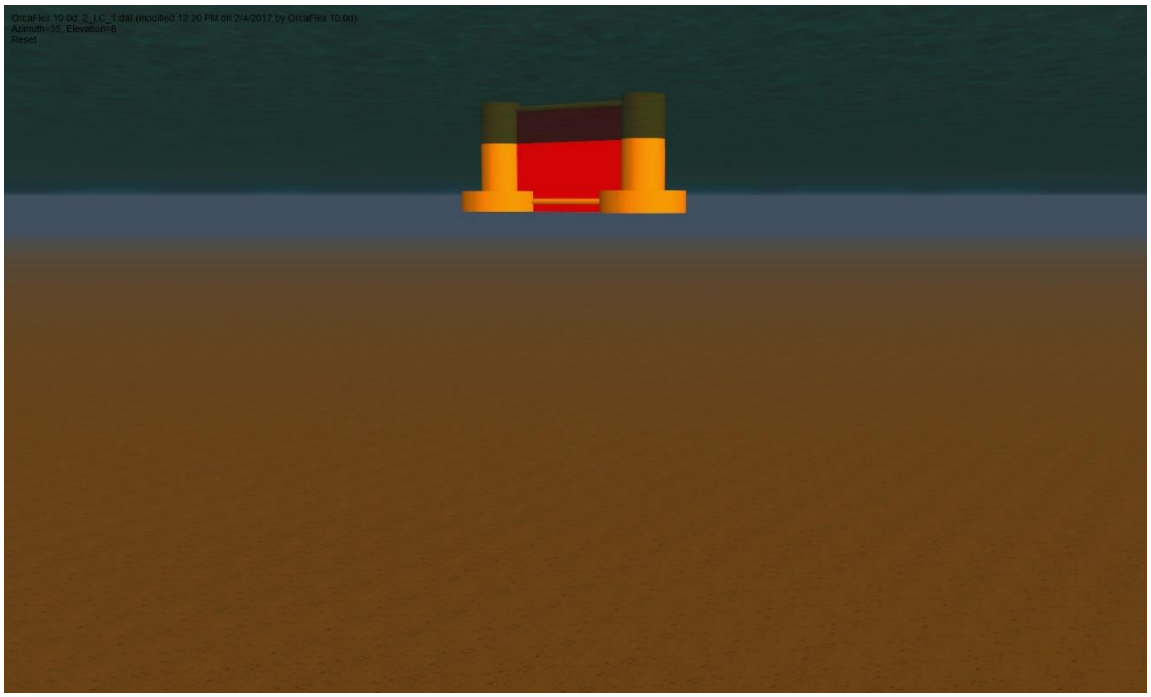

Figure 12: Assembly of the OrcaFlex model including 6D buoys

The final step needed was to present mooring lines in the model. A line model with one end fixed to the platform and the other anchored to the seabed was set to each base column at the desired position. The properties and attributes of the mooring were derived based on the material, diameter, and construction method of lines. A completed OrcaFlex model is found in Figure 13 in 3D view. It must be noted that additional adjustments were made to the model as the study went into looking at the effects of semi-taut shape as well as different water depths to meet the required safety factor of the system. However, simulations in this chapter were run with the essential parameters given by the study in Robertson and Jonkman (Robertson et al., 2014).

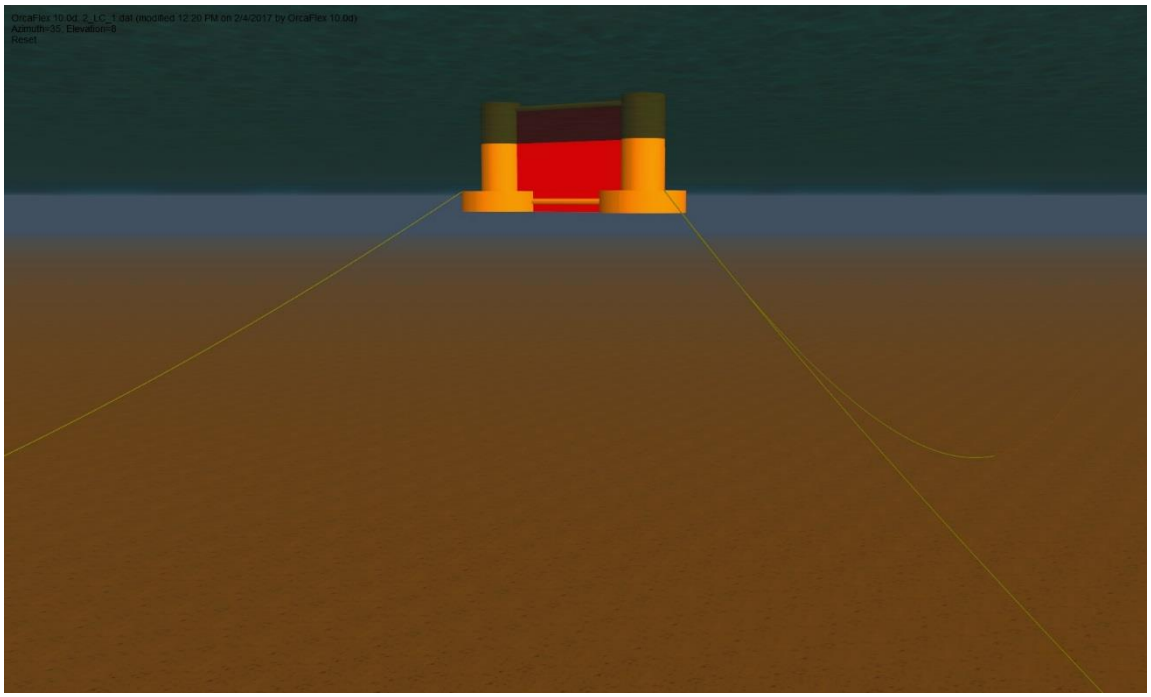

Figure 13: Final OrcaFlex model of the OC4 semi-submersible

OrcaFlex Program Model Verification Process

The hydrodynamic and mooring analysis codes used by FAST and OrcaFlex differ in simulation capabilities. In this chapter, a variety of conditions are examined to identify possible discrepancies between FAST and OrcaFlex simulation outputs. The comparison procedure is performed as follows. First, a set of waves only conditions are investigated to focus on the effects of wave excitations during simulations. Regular waves and irregular waves propagating in the direction of the +X-axis are introduced to test the platform behavior with waves. Next, the simulation is executed with the combination of wave excitation and wind excitation. In wind load cases, the turbine is facing a steady wind with uniform velocity profile. An irregular wave model is based on JONSWAP spectrum to look at response behavior in extreme conditions. Then, a current

with a power law profile is applied to the case under steady wind and regular wave to accommodate a full operation scenario in the offshore environment. In all cases, the results were generated to test consistency between the FAST and the OrcaFlex. Since the turbine is facing perpendicularly towards the environmental loads, the roll, yaw and sway motions were negligibly small and ignored in the analyses. Through this procedure, an understanding of differing theories behind each code is established.

Model Verification – Load Case 1

The first simulation investigates platform motion in regular sea state. The length of simulation was 500 seconds, and the outputs are all reported in time-series. The periodic waves with a height of 6 m and a period of 10 s are considered to evaluate the simulation consistency of the responses from the semisubmersible. The waves are aligned with the X-axis, propagating in a positive direction. The motions in sway and roll are not currently considered because the waves are acting along the surge motion.

Figure 14 shows the results of the coupled surge, heave and pitch motions respectively. A distinct color is assigned to the simulation results based on the type of modeling used as shown in the legend in the plots. For the heave and pitch results, all the plots are nearly identical throughout the whole simulation. In reference to both the heave plot and pitch plot, the data are oscillating with equal amplitudes, revealing satisfactory agreement between FAST and OrcaFlex. A strong consistency between the two models suggests a high degree of usability of OrcaFlex with the seas propagating when acquiring data for the degrees-of-freedom.

A larger difference is seen in the coupled surge motion, where a larger fluctuation in displacement appears in the FAST result, and this can be attributed to tether damping. A tether damping is a property present in the OrcaFlex for modelling simple elastic connections between objects. The stiffness of the connection link specifies a tether tension as follows:

$$T = \frac{k(L-L_o)}{L_o} \tag{7}$$

where k is the connection stiffness, L the stretched length between the two ends, and L_o the unstretched length. Because the FAST's default quasi-static model is lacking the ability to incorporate the elastic effects of connection points, the object relative position is higher than that of the OrcaFlex model. However, both the plots are showing that the system was positioned to its original state after an offset at the beginning of the simulation. Although the simulation results generated were not virtually identical for the surge motion, it is important to note that each program is decaying to its static equilibrium state. Since the release of the platform motion was observed in both FAST and the OrcaFlex simulations, the results for the surge displacement can be seen as an adequate agreement.

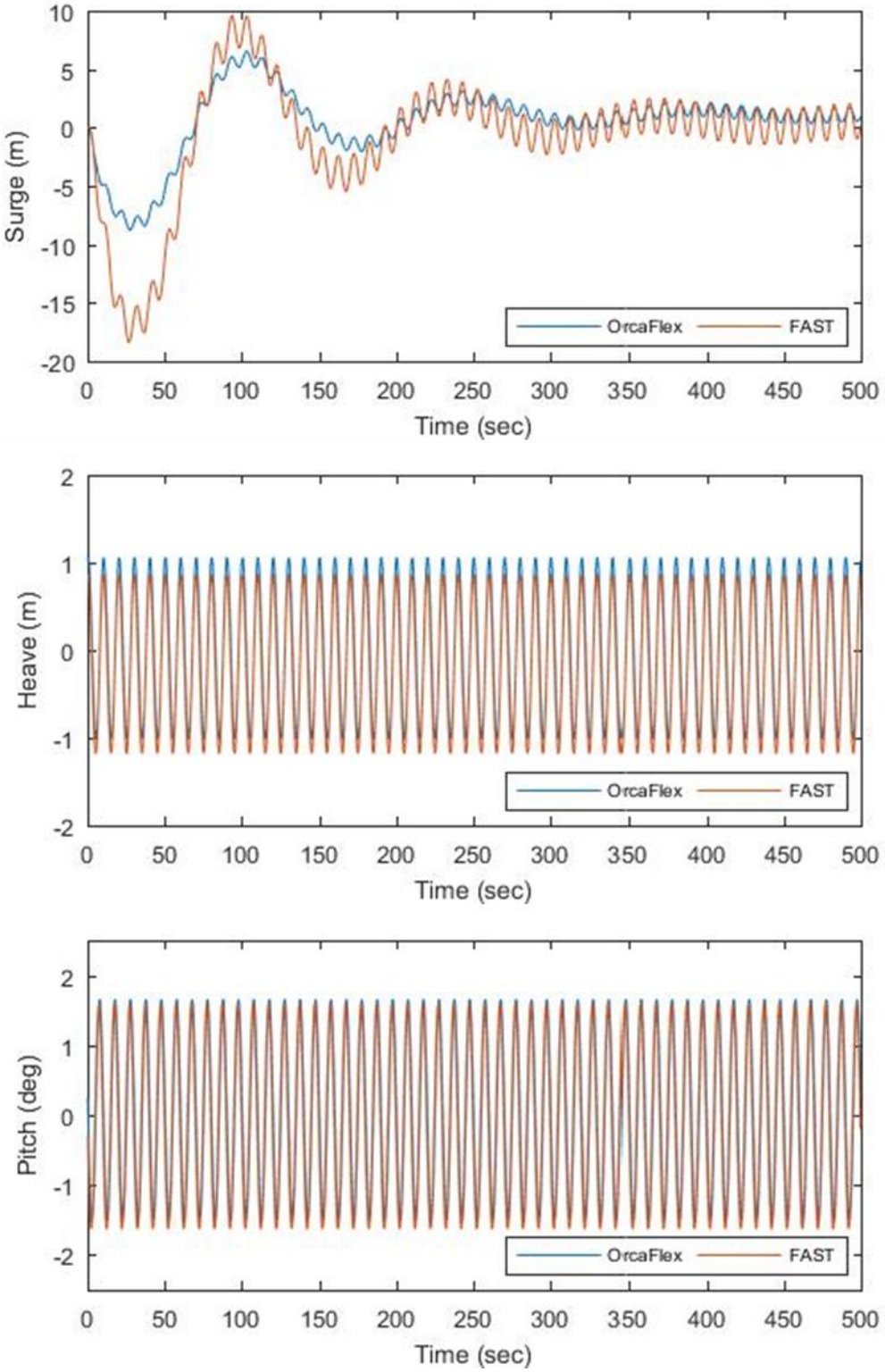

Figure 14: Platform motion responses (load case 1)

The different mooring line models are expected to demonstrate varying mooring tension values because of the distinct theories for hydrodynamic and mooring load calculations. For this reason, the line tension at fairleads and anchors are compared in Figure 15 and Figure 16, respectively. The degree of variance is within the realm of what modeling approach is employed by the code. The differentiation for anchor tension results is based on the hydrodynamic and mooring models that are noteworthy to break down the assumptions built into each code. The general technique shared by FAST and the OrcaFlex for including the hydrodynamic effects is the potential-flow theory. The potential-flow is used to capture loads originating from incident wave excitation and outgoing wave radiation. For approximating the viscous drag which results from flow separation, a quadratic drag matrix is derived in the FAST model while the Morison's equation is implemented in the OrcaFlex model. The equipped viscous drag model of the FAST is based on the following:

$$F_v^{FAST} = -B|\dot{q}|\dot{q} \tag{8}$$

where B is the drag matrix and $\dot{q}$ is the six degree-of-freedom platform velocity:

$$\dot{q} = \{\dot{X}, \dot{Y}, \dot{Z}, \dot{\phi}, \dot{\theta}, \dot{\psi}\} \tag{9}$$

The drag matrix B is based on the experimental study done by a physical model test (Masciola, 2011). Because the drag coefficients are driven based on a model-scale test, the formulation is not accounting for each of the multimember floating support columns. To avoid the mismatch between model-scale and full-scale derivation, the OrcaFlex model is featured with Morison's equation, which considers the platform as

discrete structural elements. The viscous drag models on each element are based on the formulation below:

$$F_v^{OrcaFlex} = \frac{1}{2}\rho C_D A_C |u - \dot{q}|(u - \dot{q}) \tag{10}$$

where C_D is the varying drag coefficient depending on the column member, A_C the cross sectional area of the column or the brace, and the $(u - \dot{q})$ is the relative velocity term. The idea of this enhanced viscous drag modelling is to reflect a full-scale system during the simulation by giving unique drag coefficients on each element of the platform. Moreover, the fluid velocity u from the Morison's equation is a varying viscous property that fluctuates due to the displaced positions of the body. The drag forces in the OrcaFlex formulation are therefore further refined for accounting for instantaneous platform position compared to those in FAST.

Besides the method of calculating the viscous drag, the difference between the mooring models used is another cause for a wide margin on the FAST and the OrcaFlex anchor tensions. The forces at the anchor in FAST are solved using a quasi-static approach, while those in the OrcaFlex model are derived with a dynamic cable model. In quasi-static models, a cable theory is employed by supposing the line is always in static equilibrium. The line solver accounts for the mass but it excludes the associated effects of fluid added mass, inertia, and drag. The simplified catenary equations used by quasi-static models are as follows:

$$x = \frac{T_o}{W_I} sinh^{-1}\left(\frac{W_I s}{T_o}\right) \tag{11}$$

$$z = \frac{T_o}{W_I}\left[cosh\left(\frac{W_I x}{T_o}\right) - 1\right] \tag{12}$$

$$s = \frac{T_o}{W_I} sinh\left(\frac{W_I x}{T_o}\right) \quad (13)$$

where x and z are the coordinates of a point along the cable, s the cable length, T_o the tension at the fairlead, and W_I the immersed weight of the cable. Hence, the accuracy of tension predictions made by FAST is based on the complexity of the simulation. OrcaFlex is well known for responding to the excitation loads that cannot be represented by FAST through the use of a dynamic cable model. The theory behind dynamic mooring line is based on the Newton's equation of motion:

$$(M + M_a)\ddot{X}(t) = F(t) - [B]\dot{X}(t) - [k]X(t) \quad (14)$$

where M is the mass, M_a the added mass, $\ddot{X}$(t) the acceleration vector, F(t) the external force vector such as fluid, wind and current induced loads, [B] the damping matrix, $\dot{X}$(t) the velocity vector, [k] the stiffness vector, and X(t) the displacement vector. In this last equation, an explicit integration approach is applied to solve for the derivative terms as below:

$$x(t + \Delta t) = x(t) + \frac{dx(t)}{dt}\Delta t \quad (15)$$

$$\frac{x(t+\Delta t)}{dt} = \frac{dx(t)}{dt} + \frac{d^2x(t)}{dt^2}\Delta t \quad (16)$$

Putting new position and velocity of a mass at every time step, Δt, varying effects due to mass, damping, and fluid acceleration are taken into consideration at the relative position of the mass. Therefore, as shown in Figure 15 and Figure 16, both viscous force and dynamic model methods resulted in differing mooring loads between FAST and the OrcaFlex. However, in reference to the average values as well as the equal phase of the data, satisfactory agreement is revealed between FAST and OrcaFlex in mooring loads.

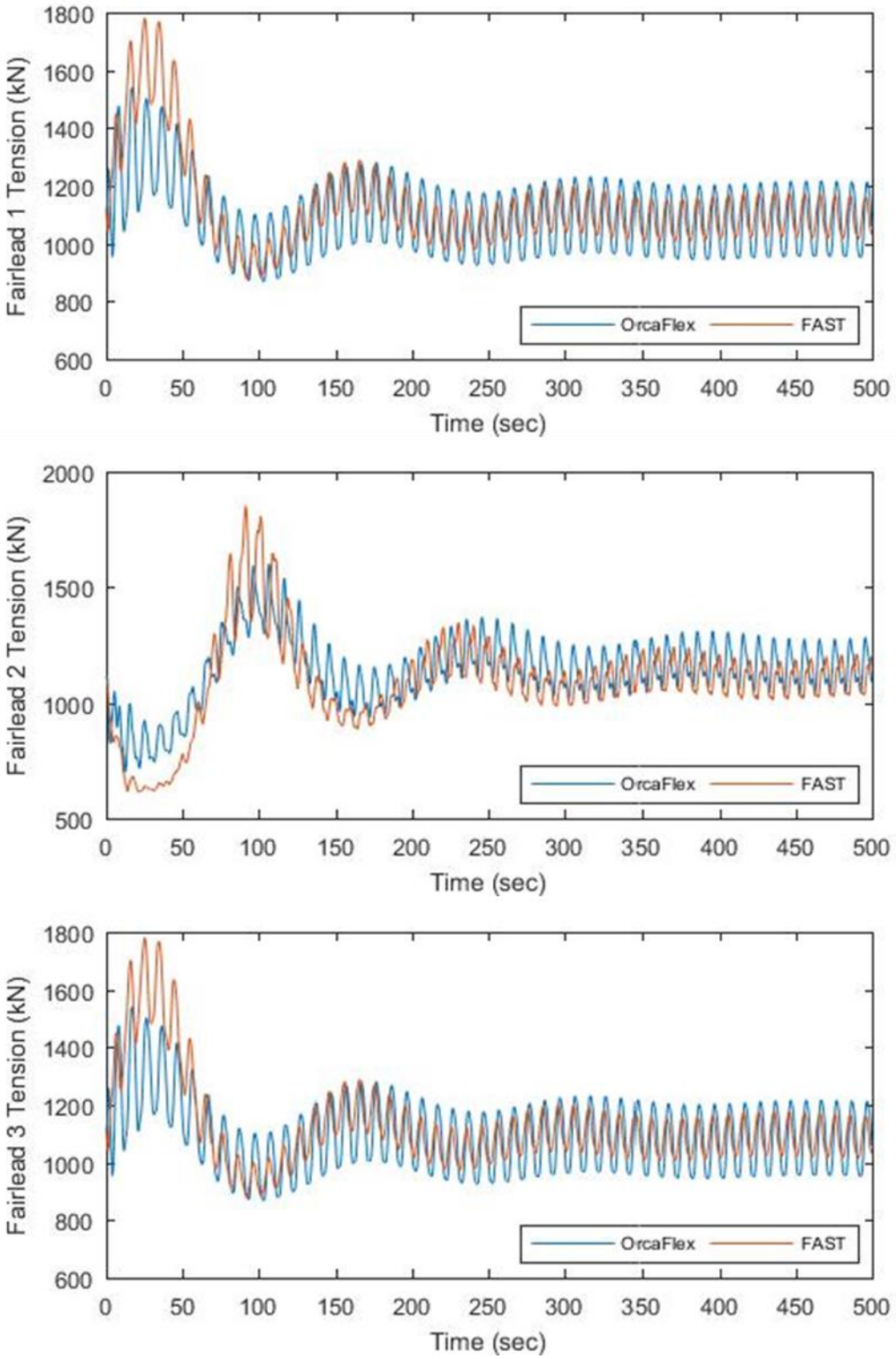

Figure 15: Time series of fairlead tensions (load case 1)

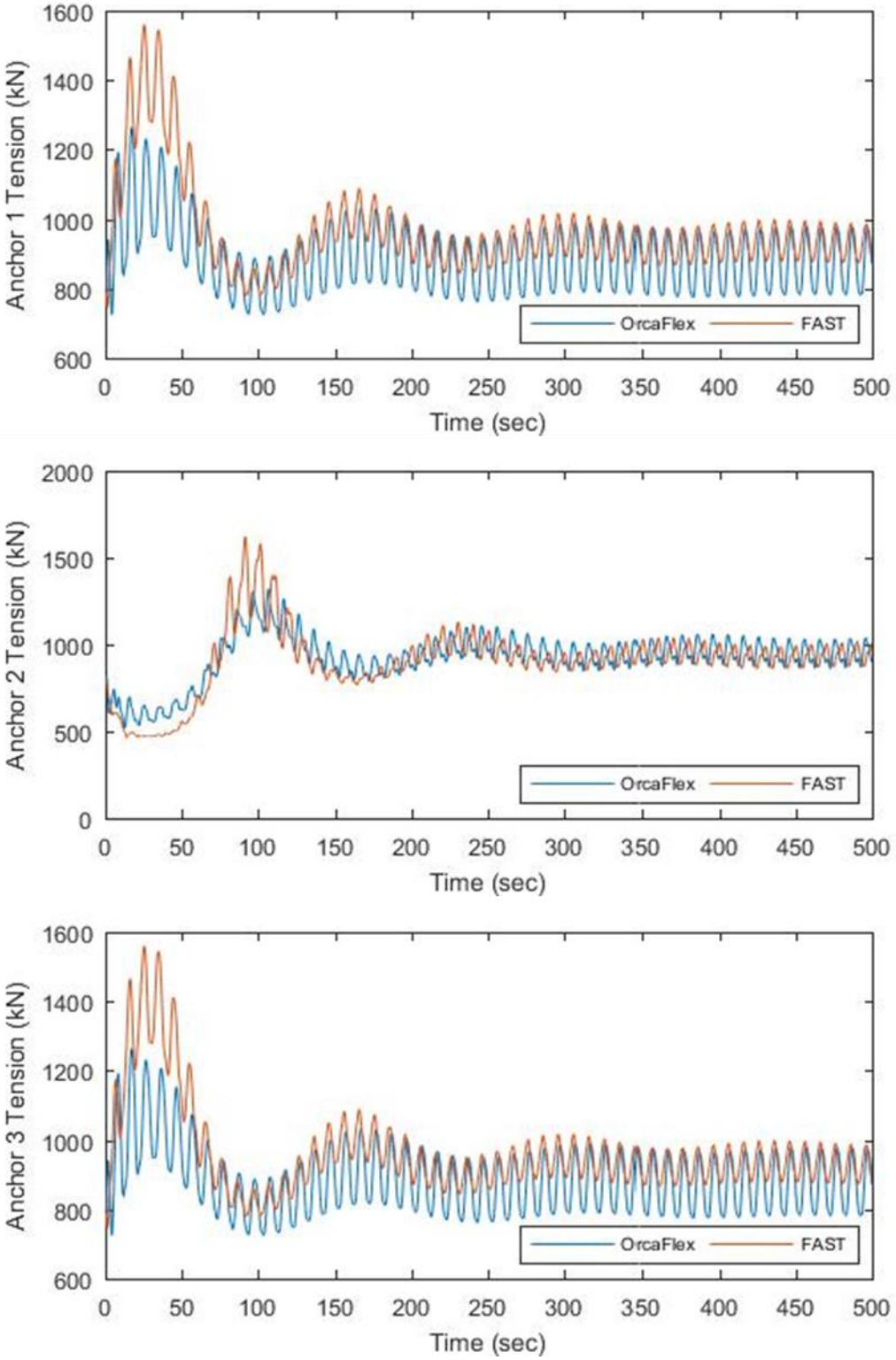

Figure 16: Time series of anchor tensions (load case 1)

Model Verification – Load Case 2

The case of irregular waves is considered in the next set. The sea conditions are considered by a significant wave height of 6 m, a peak-period of 10 s, and a peak enhancement factor of 2.87. These random waves were obtained from a JONSWAP spectrum. A JONSWAP model is expressed as:

$$S(f) = \left(\frac{\propto g^2}{16\pi^4 f^5}\right) exp\left(-\frac{5}{4\left[\frac{f}{fm}\right]^4}\right)\gamma^b \tag{17}$$

$$b = exp\left(\left(-\frac{1}{2\sigma^2}\right)\left(\frac{f}{f_m - 1}\right)^2\right) \tag{18}$$

$$\sigma = \begin{cases} 0.07\ for\ f \leq f_m \\ 0.09\ for\ f > f_m \end{cases} \tag{19}$$

where S(f) is the spectral density, α the constant that relates to the wind speed and fetch length, g the gravitational acceleration, f the frequency, f_m the peak frequency, and γ the peak enhancement factor. With the given input parameters, the JONSWAP spectrum allows a peaked spectra to represent sea state of an irregular wave model. The model was generated by the OrcaFlex as in Figure 17.

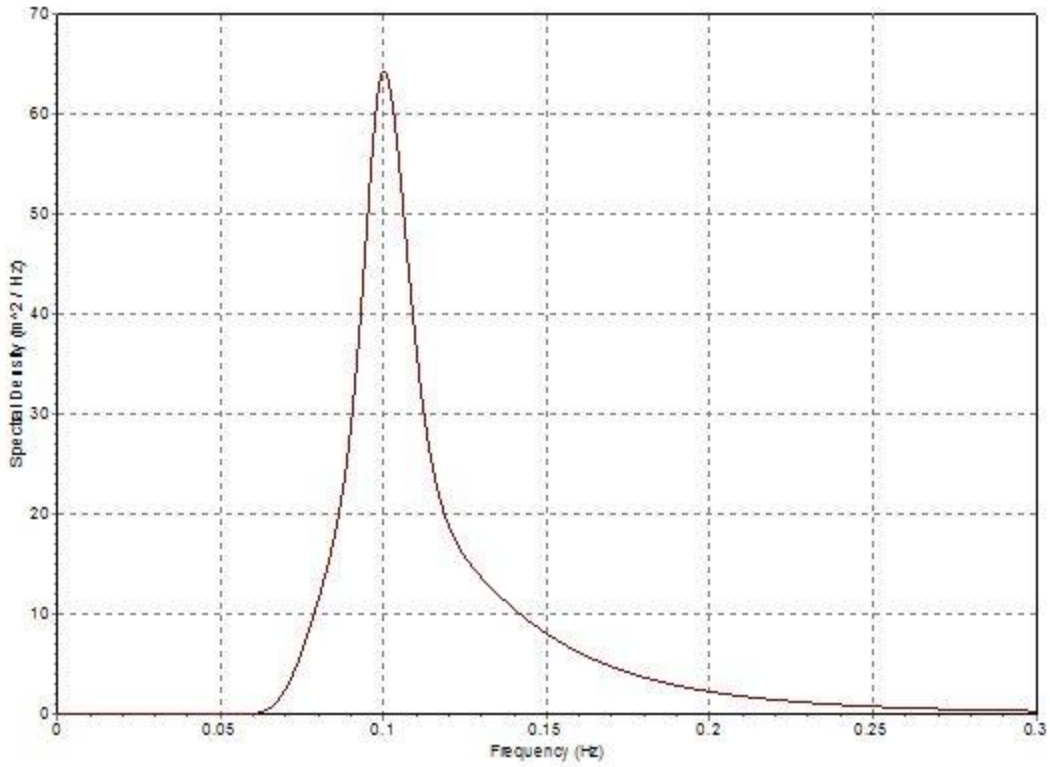

Figure 17: Spectral density in irregular water

Similar to the previous load case, the time series plots in Figure 18 support agreement in the surge, heave and pitch responses respectively. There is a slight difference among the tension plots, Figure 19 and Figure 20. This variation could be caused by the underlying mooring line theories that attribute to the inclusion of a dynamic mooring line representation, which is not presented in FAST. Yet, the tensions of the OrcaFlex are not significantly deviated from those of FAST. Consequently, the inclusion of irregular sea state does not appear to affect the consistency between FAST and OrcaFlex mooring tensions.

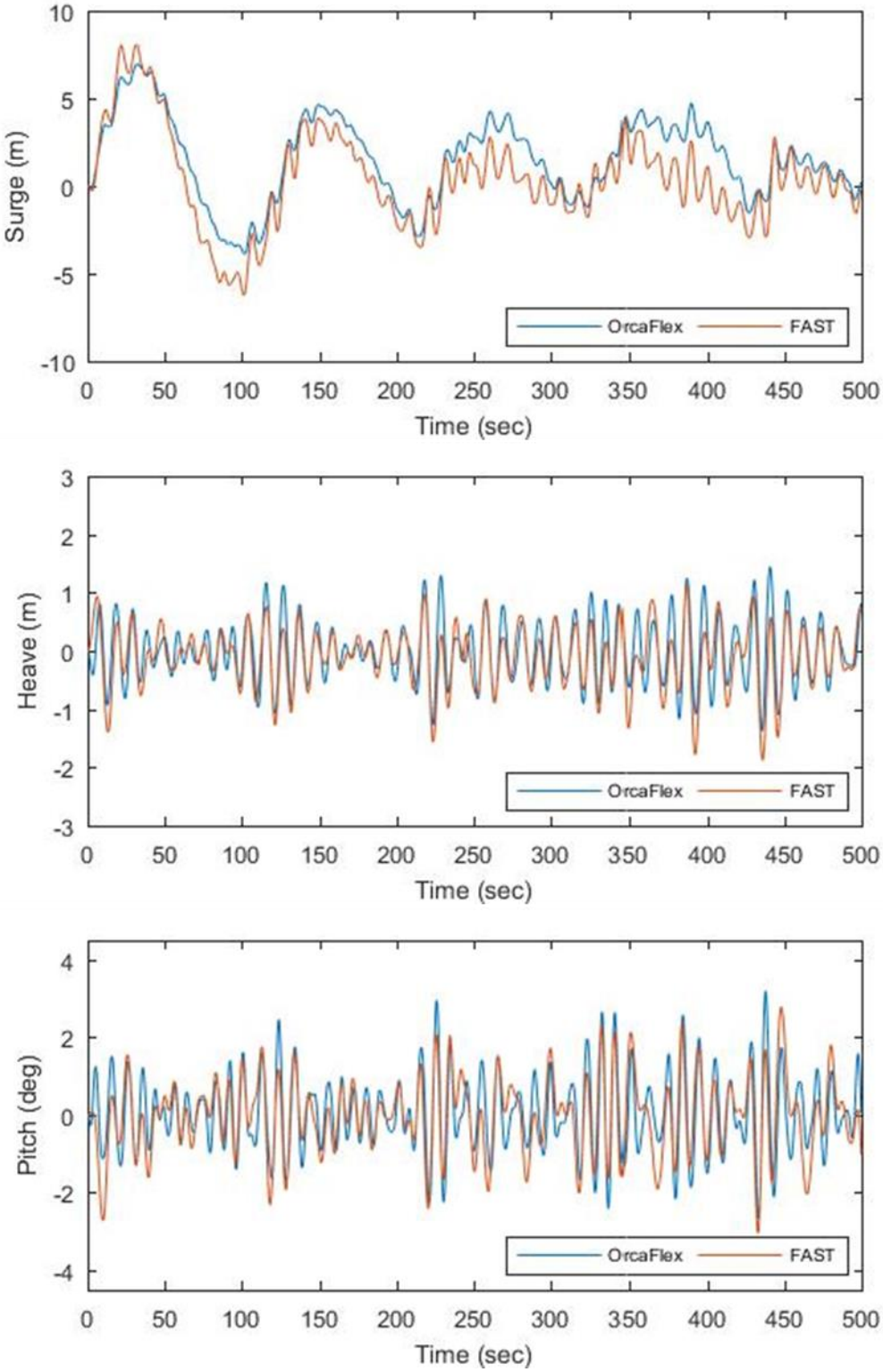

Figure 18: Platform motion responses (load case 2)

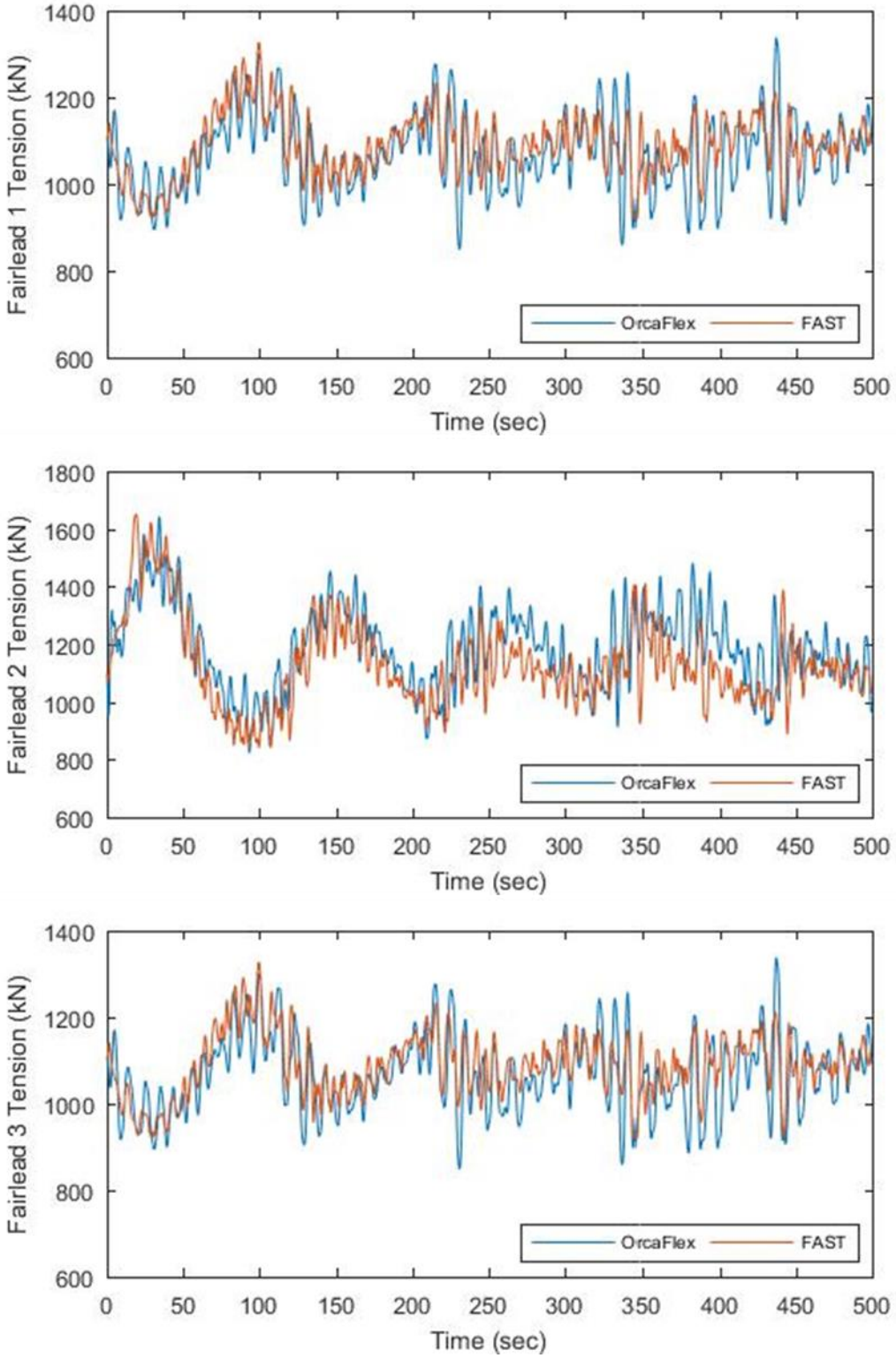

Figure 19: Time series of fairlead tensions (load case 2)

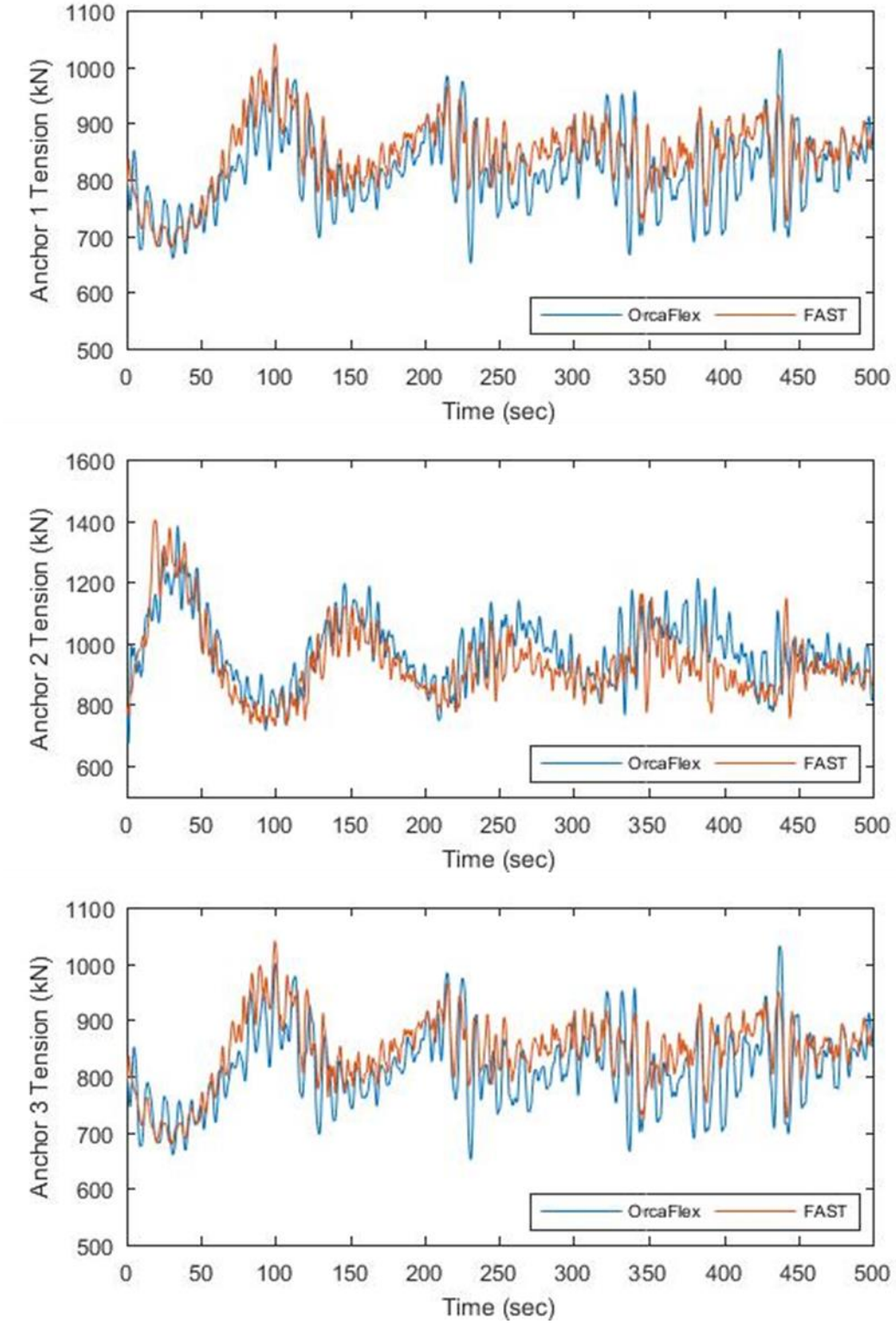

Figure 20: Time series of anchor tensions (load case 2)

Model Verification – Load Case 3

To this point, the results between FAST and the OrcaFlex have been compared under wave excitations only. This case is initiated to cover the aerodynamic loads by adding a $1/7^{th}$ power law wind at 10 meters above the Mean Water Level to the regular wave condition. This steady sheared wind is facing perfectly towards the positive global X-axis. Figure 21 shows the time series of surge, heave, and pitch plots. The results are fairly similar between FAST and the OrcaFlex, and the comparison suggests each program is executing its free-decay simulations correctly when regular wave and steady wind coexist. Figure 22 and Figure 23 then show the similar tensions for different codes, which is an indicator of strong agreement between FAST and the OrcaFlex. For the second mooring lines at fairlead and anchor that are aligned with zero-degree wind, the loads increased significantly compared to those in the case without wind. Such shift in tension values could be explained by the thrust force of the wind.

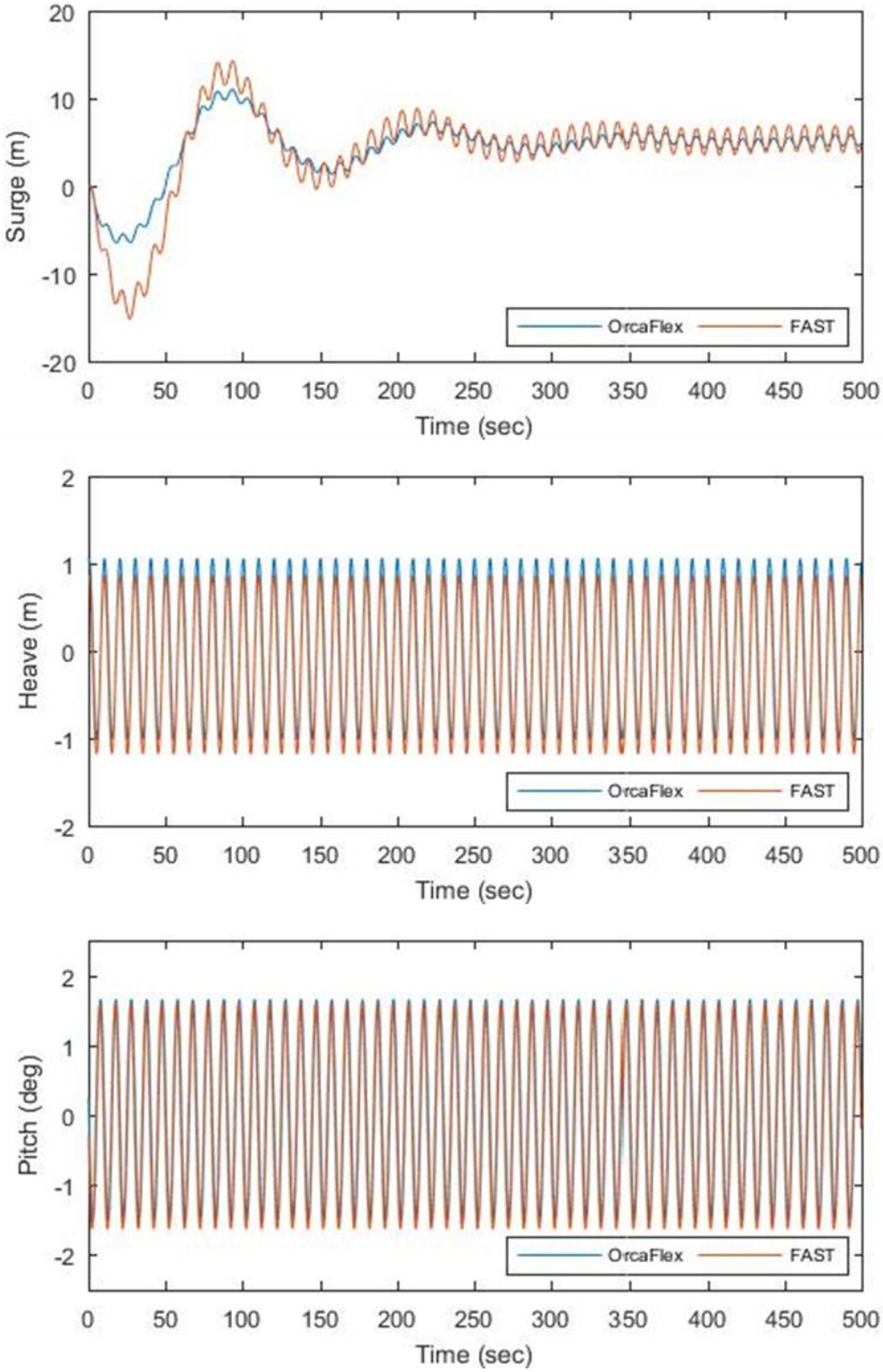

Figure 21: Platform motion responses (load case 3)

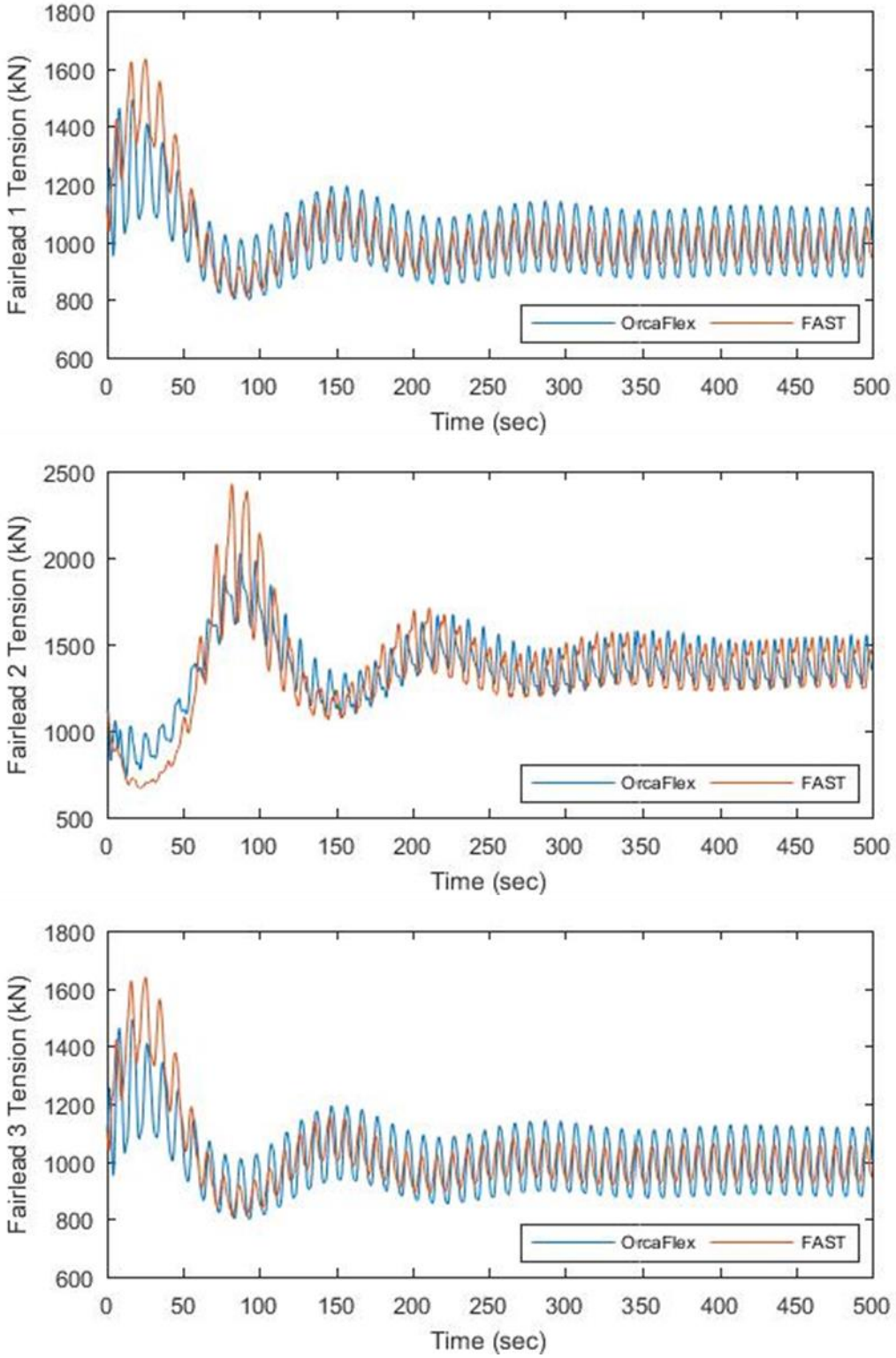

Figure 22: Time series of fairlead tensions (load case 3)

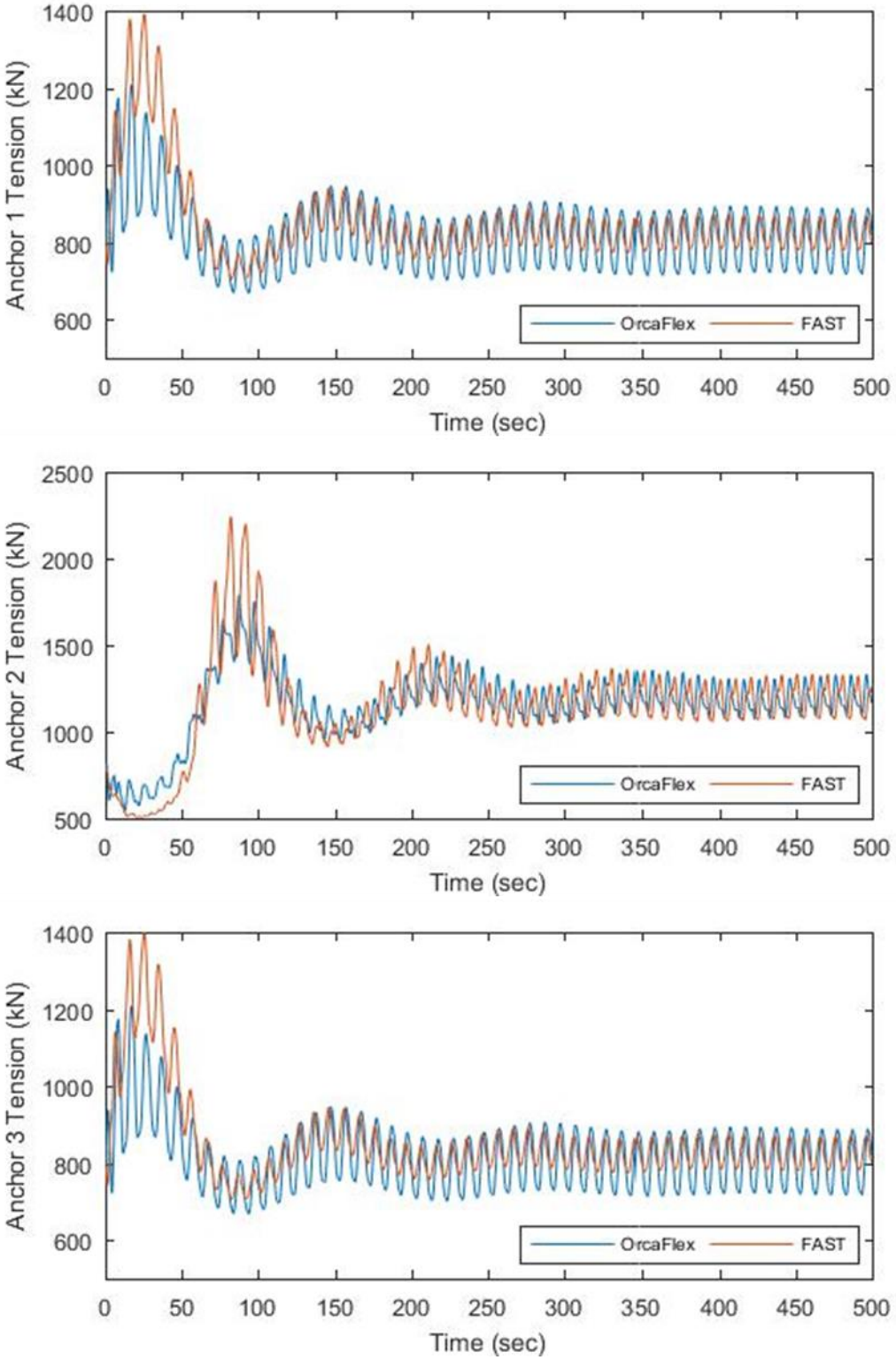

Figure 23: Time series of anchor tensions (load case 3)

Model Verification – Load Case 4

The survivability of a floating structure under extreme loads is an important issue to evaluate. This load case was examined to consider extreme event situations by subjecting the turbine to excitations of irregular waves and shear wind. The sea is defined based on a JONSWAP spectrum and the wind is a steady wind with the $1/7^{th}$ power law profile. As in Figure 24, an analysis of the simulation results shows similar trends for all free-decay responses. Moreover, differences between the two numerical models were negligible in tension plots, Figure 25 and Figure 26. A key finding in this load case is that the tensions in the second mooring line are higher those without the wind excitation. The noticeable increase is shown as the outcome of an extreme sea-state condition as well as the addition of sheared wind. The model-to-model comparison may suggest that the OrcaFlex solutions are reasonable tool for predicting the mooring response in harsh sea conditions.

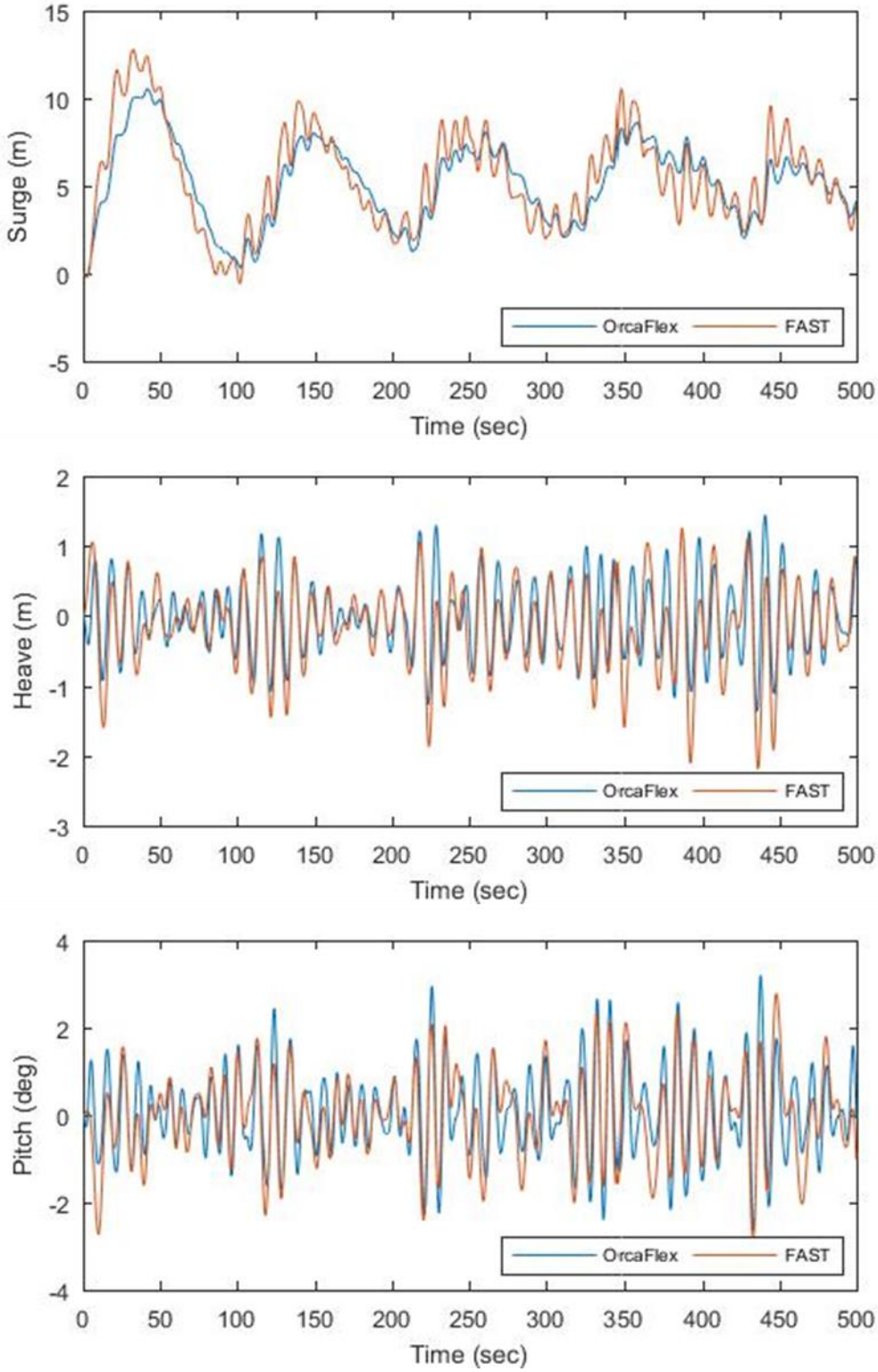

Figure 24: Platform motion responses (load case 4)

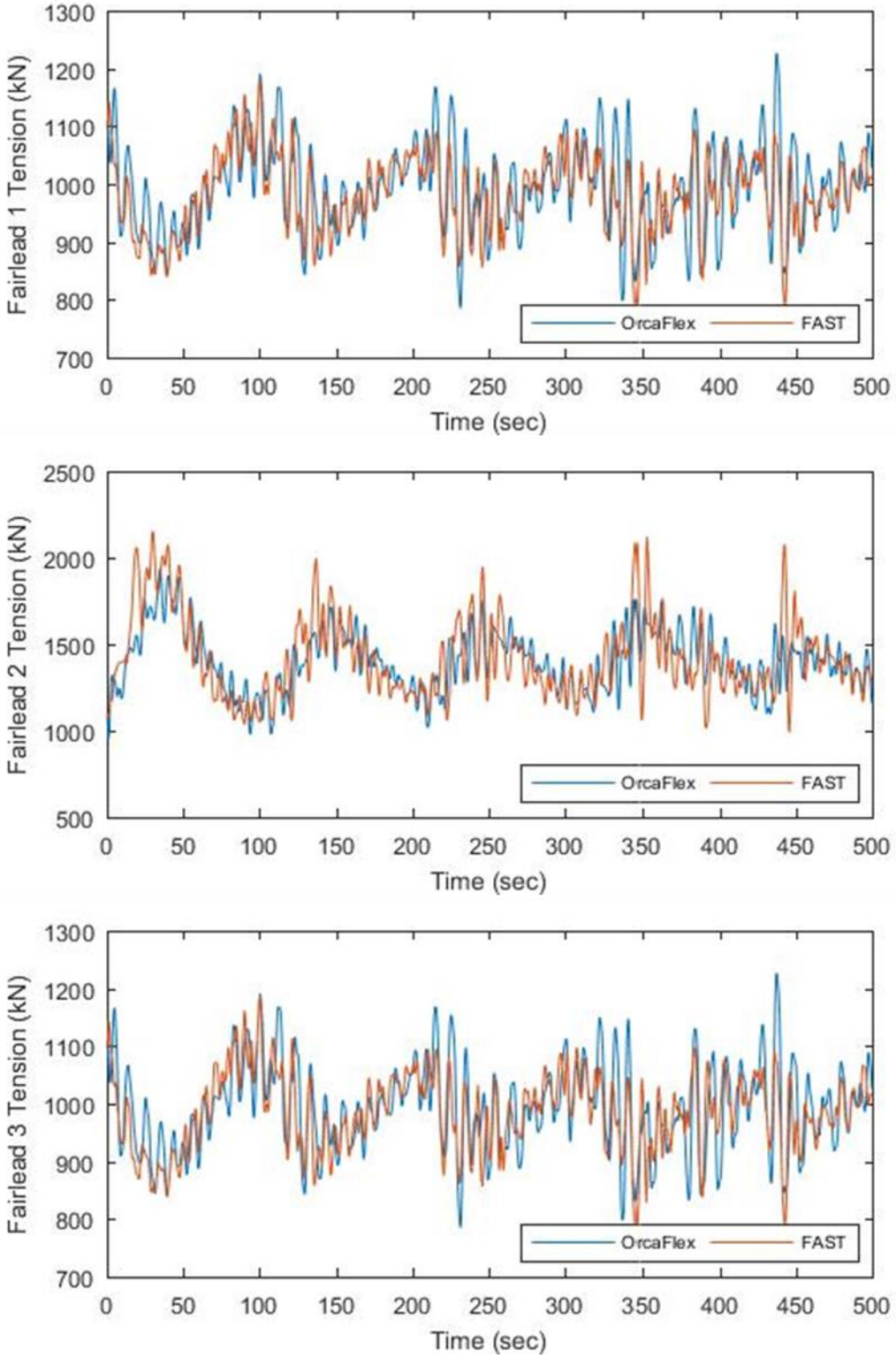

Figure 25: Time series of fairlead tensions (load case 4)

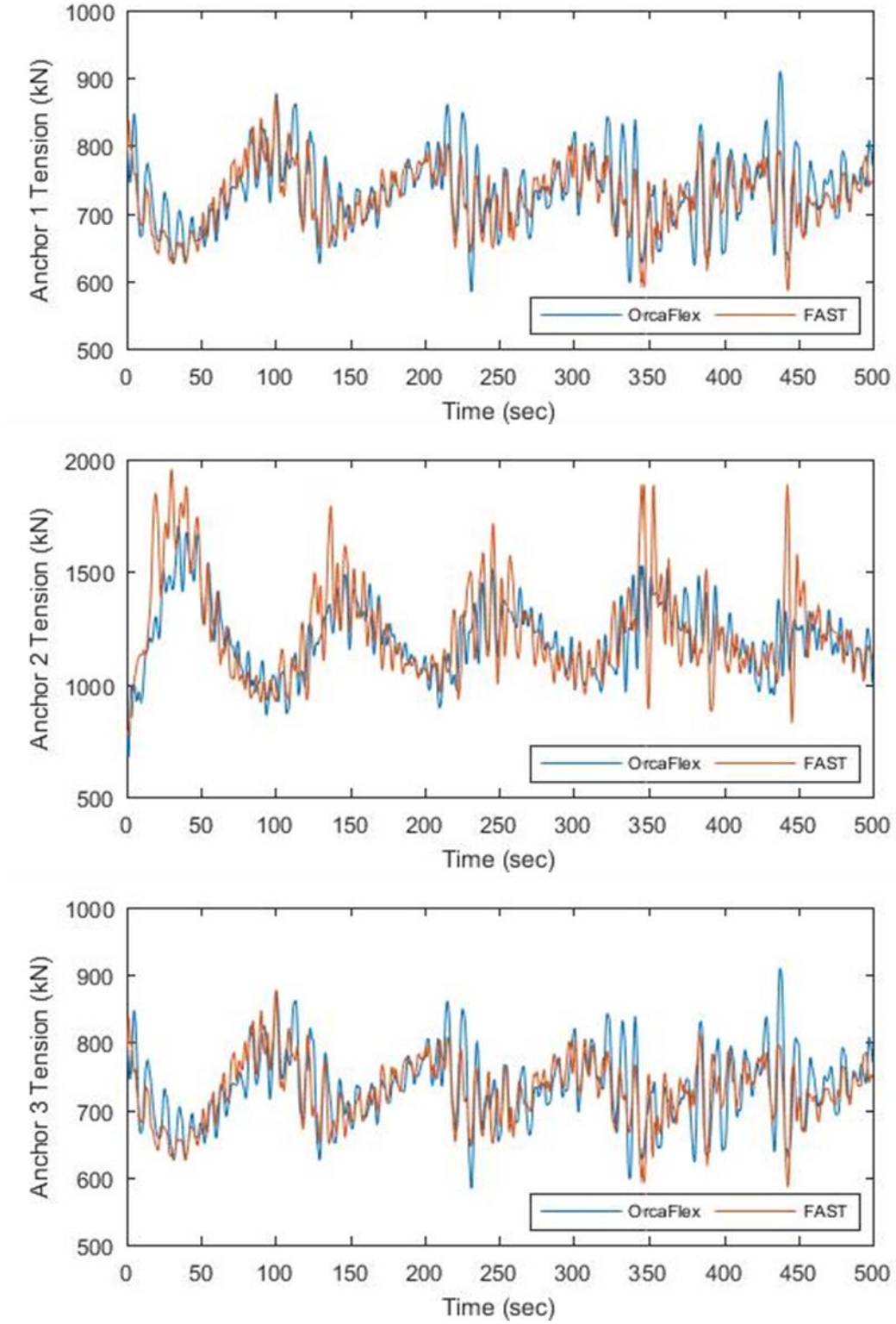

Figure 26: Time series of anchor tensions (load case 4)

Model Verification – Load Case 5

Load Case 5 examines the system with combined excitations including sheared wind, regular waves, and a current with a power law profile. The coupled heave and pitch motions appeared to be reasonable while difference was visible in surge, Figure 27. The offset difference between FAST and the OrcaFlex is based on whether the model includes the current induced viscous effect properly. In comparison to FAST, the results predicted by the OrcaFlex are decreased in the platform surge because the viscous-drag forces on platform columns are computed discretely based on the given unique drag coefficients. The representation of multi drag coefficients is omitted in FAST, and thus the subsequent results are returned with slightly higher platform displacements. Differences between FAST and the OrcaFlex supported same conclusions as previous load cases, Figure 28 and Figure 29. Variation seen is insignificant as both models are predicting the effects of currents with peak loads in lines parallel to the direction of environmental loads.

The model using FAST exploits the strength of bringing the tower motion, blade rotation, and aerodynamic forces into the platform motion. The comparisons performed suggest that the OrcaFlex modelling tool can also accurately predict the platform motions as well as the mooring loads under combined regular waves with currents.

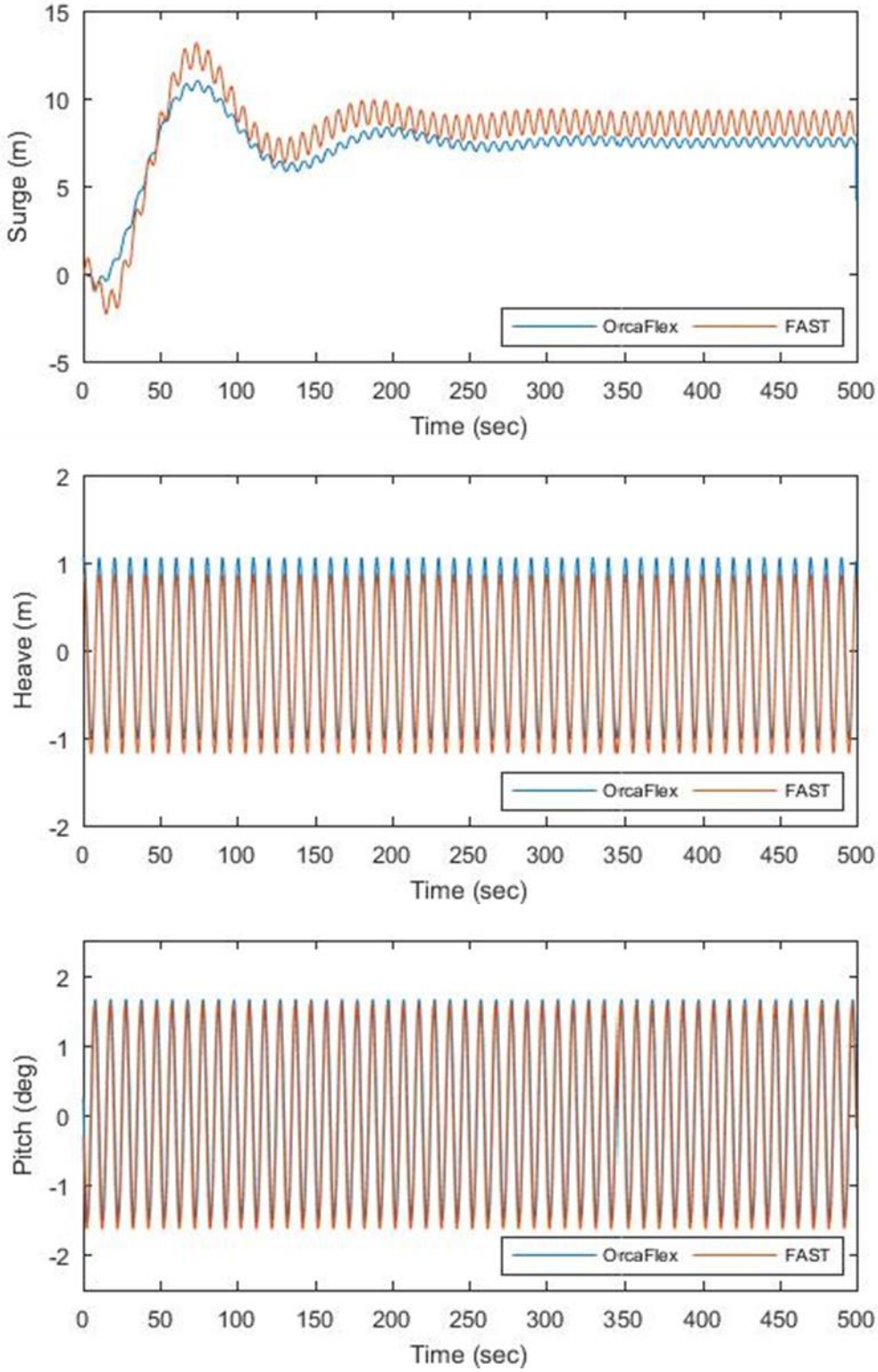

Figure 27: Platform motion responses (load case 5)

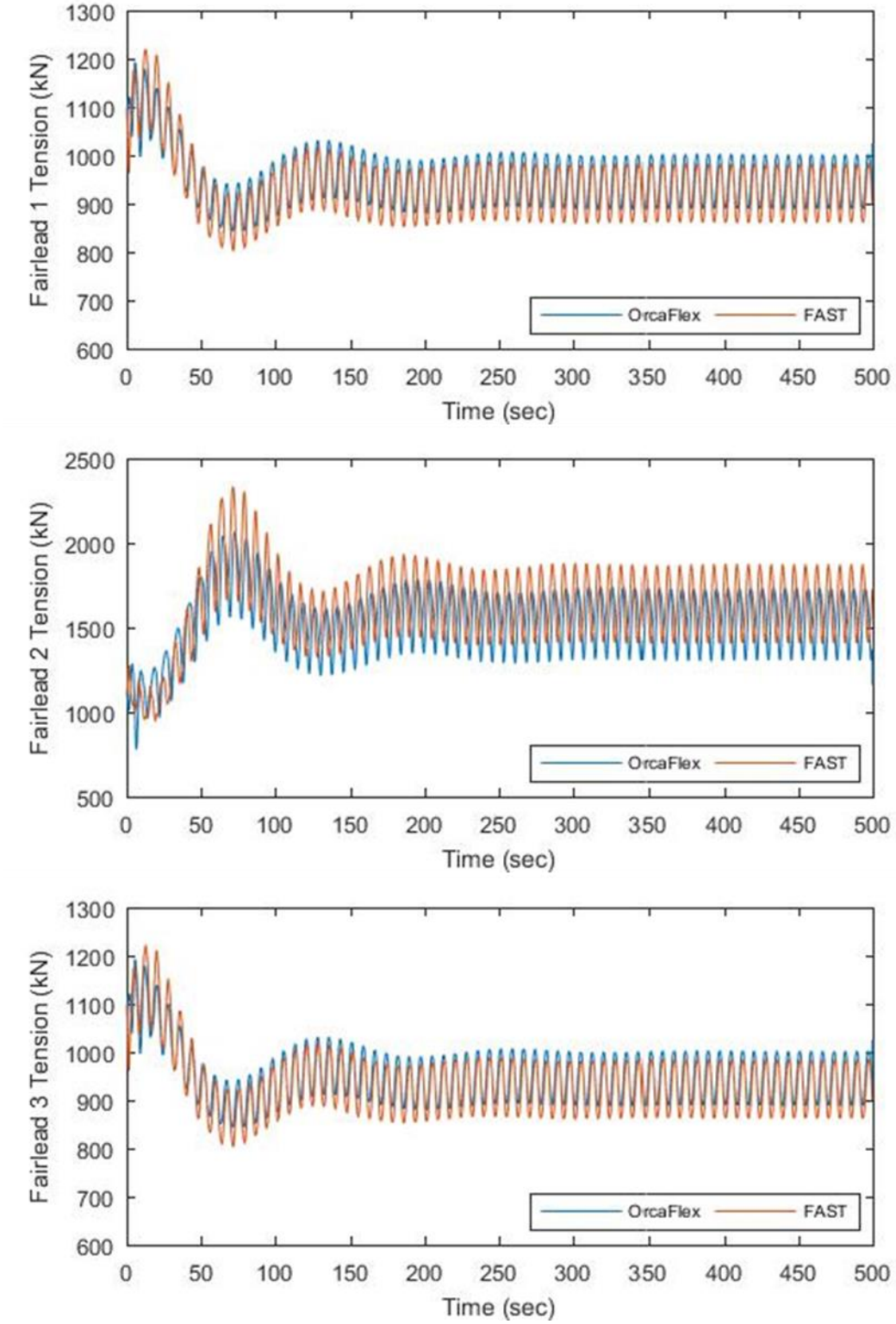

Figure 28: Time series of fairlead tensions (load case 5)

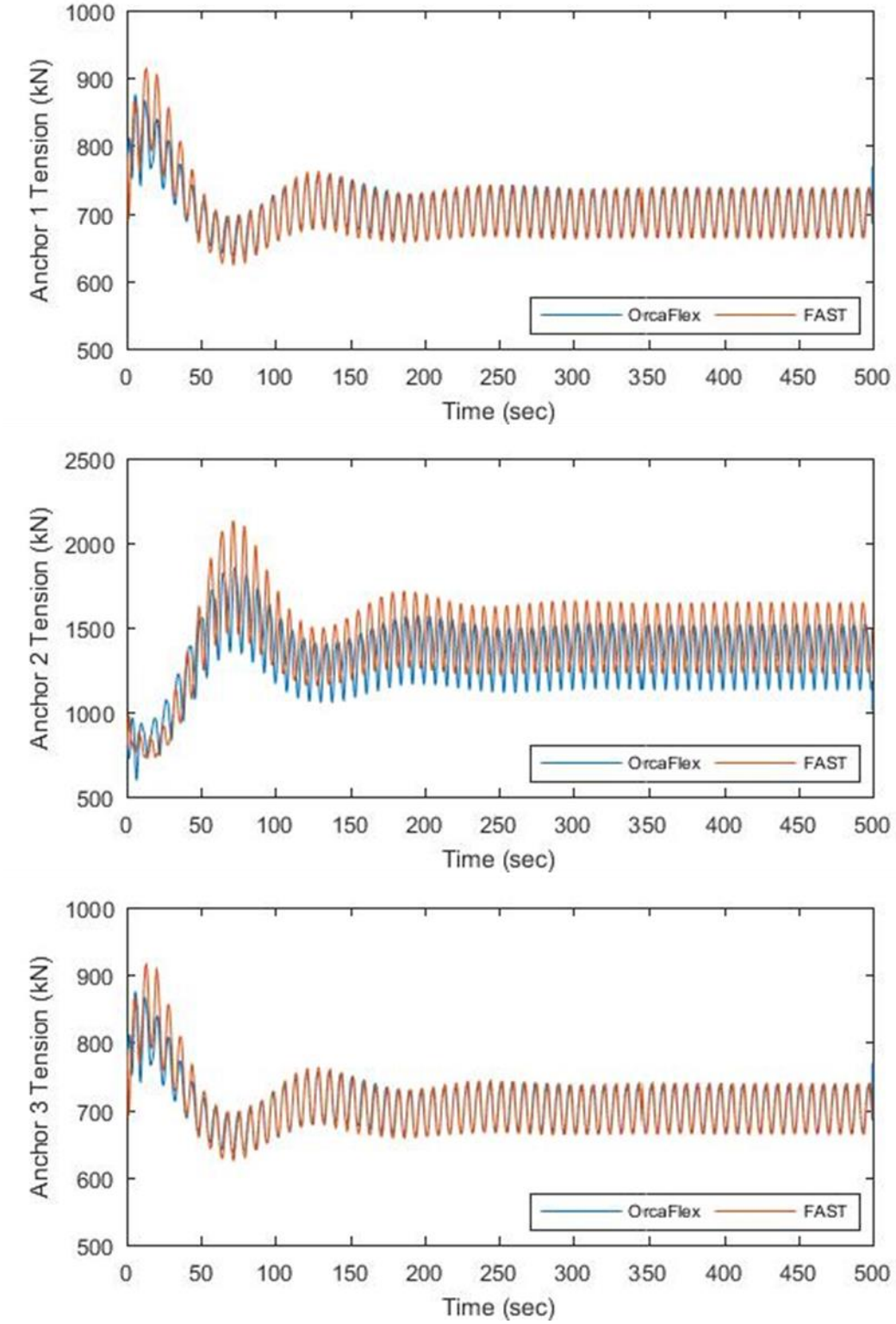

Figure 29: Time series of anchor tensions (load case 5)

Model Verification – Load Case 6

For the load case when prescribed by combined excitations including sheared wind, irregular waves, and a current with a power law profile, the results are consistent throughout the simulation. Through the model-to-model comparison, one can see that each program is operating correctly during response motions. The examined results are given in Figure 30 below.

The tension responses lacked differences as illustrated in Figure 31 and Figure 32. This led to a conclusion that FAST and the OrcaFlex simulations are both viable options for floating wind turbine simulations during the influence of extreme sea conditions. Recalling sophisticated hydrodynamic and mooring utilities for the OrcaFlex model, the applicability of such program suggests promising tool for offshore system design. For this reason, OrcaFlex is used as the main tool for anticipating the interested response behaviors of the OC4 semi-submersible wind turbine.

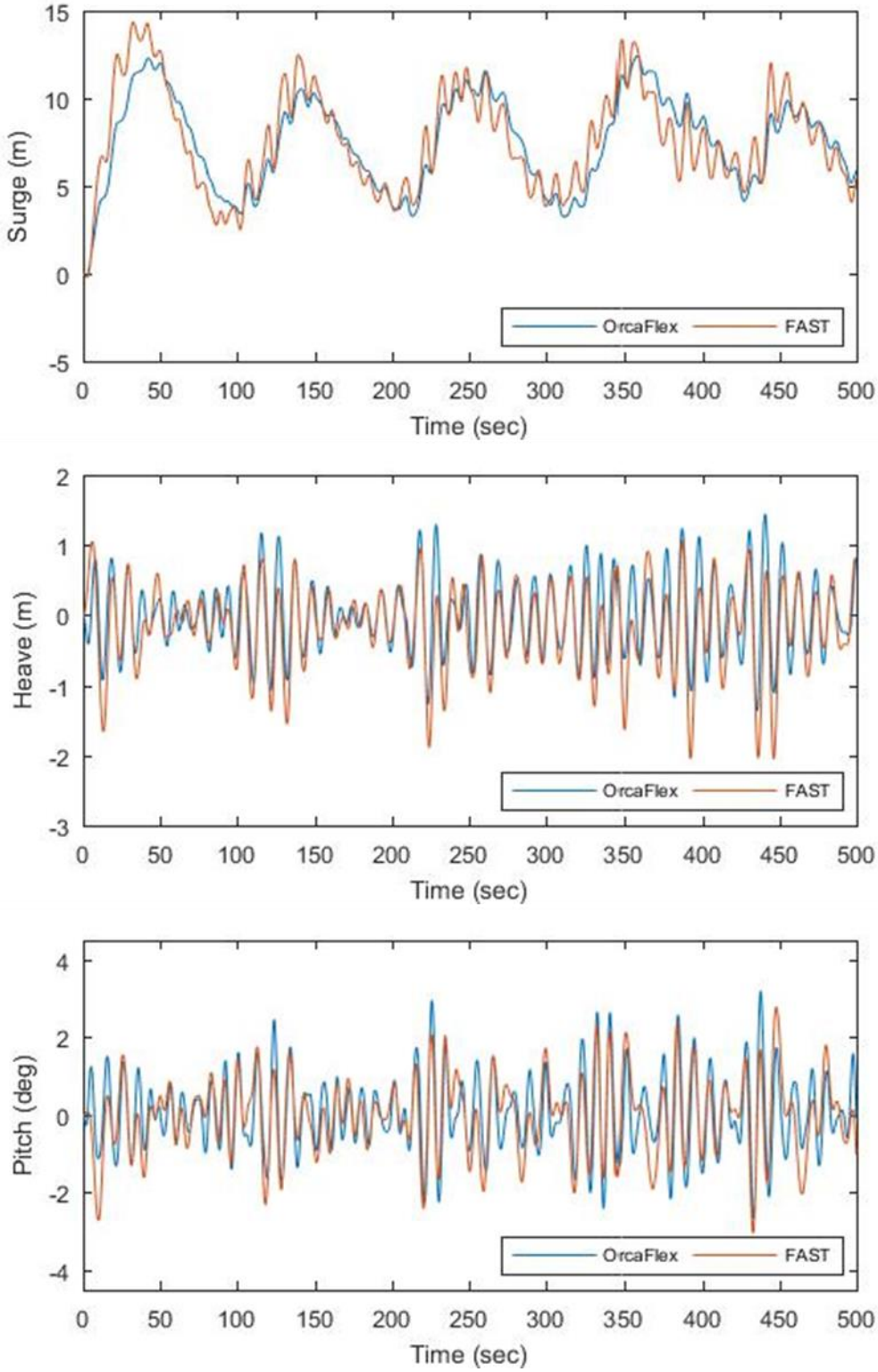

Figure 30: Platform motion responses (load case 6)

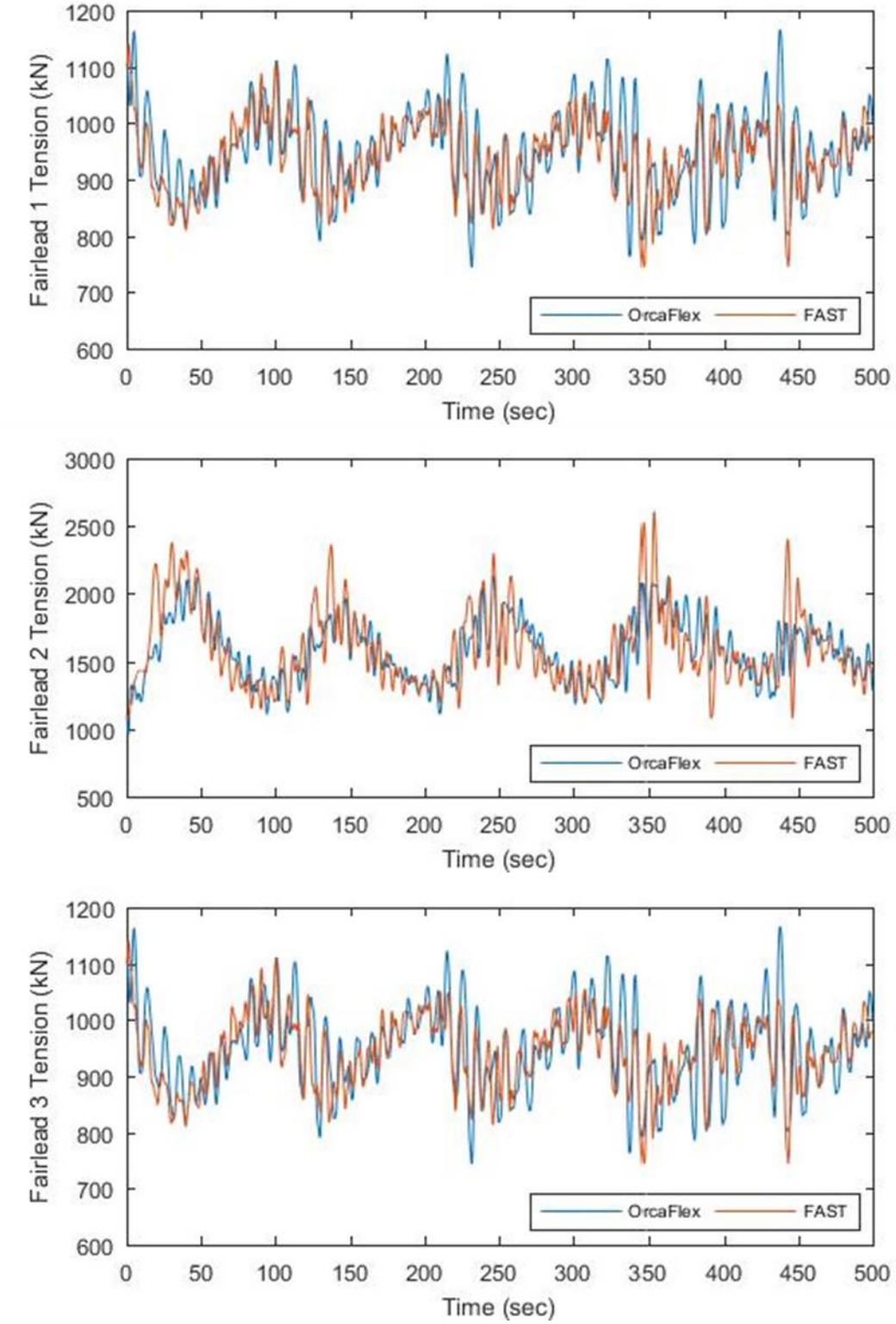

Figure 31: Time series of fairlead tensions (load case 6)

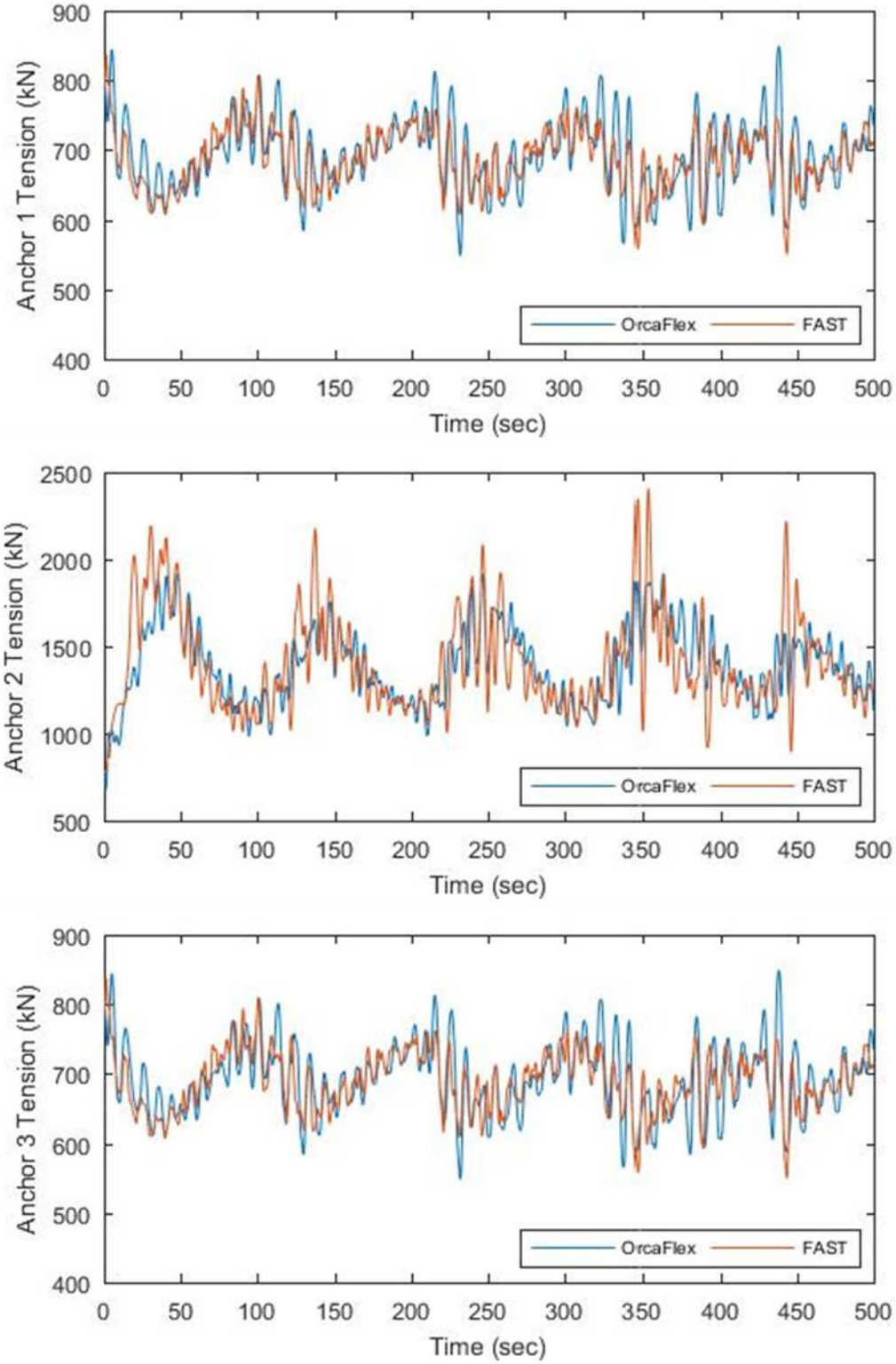

Figure 32: Time series of anchor tensions (load case 6)

3. COMPARISON OF CATENARY AND SEMI-TAUT MOORING SYSTEMS

Pretension

The study requires the design of a mooring configuration for a semi-submersible wind turbine off the coast of the United States. This chapter considers both a catenary and a semi-taut systems, under a total of six different environmental conditions. The environmental conditions are considered as listed in Table 2. Aiming to ensure the static-equilibrium position of the platform, the buoyancy from displaced water was taken into consideration to balance the weight of the system and the mooring lines, Figure 33. The platform has a 1.3989E8 N environmental load in the positive-z direction that accounts for the buoyancy force. This vertical force the weight of water before the displacement of the platform (Jonkman, 2007). The buoyancy force is defined in the equation below including the weight of the system as well as the mooring pretension:

$$\rho g V_0 - m_{Total} g = \sum T_{Mooring} \tag{20}$$

where ρ is the water density, g the gravity, V_0 the displaced volume of the floating platform, m_{Total} the total mass of the system, and $T_{Mooring}$ the mooring pretension. The study is focused on stress utilization at the anchor point, hence the reason for considering the mooring pretension. The analysis tool, OrcaFlex, specifies the system needs stabilize the floating platform under still-water conditions by adjusting the mooring system pretension. The hang-off points from the semi-submersible and the anchor positions are given as the default catenary mooring arrangement.

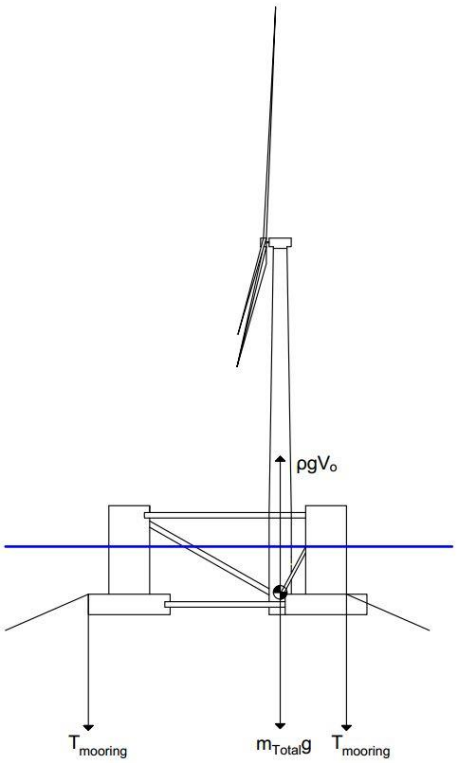

Figure 33: Side profile of the OC4 semisubmersible platform

where ρ is the water density, g the gravity, V_0 the undisplaced volume of the floating platform, m_{Total} the total mass of the system, and $T_{Mooring}$ the mooring pretension. The study is focused on stress utilization at the anchor point, hence the reason for considering the mooring pretension. The analysis tool, OrcaFlex, specifies the system needs to maintain the vertical position of the floating platform under still-water conditions by adjusting the mooring system pretension. The hang-off points from the semi-submersible and the anchor positions are given as the default catenary mooring arrangement.

Mooring Positioning Arrangements

The mooring system is separated by 120-degree spacing with three lines. The arrangement of the anchors is to help station-keeping of the semisubmersible platform, and one of the lines is oriented along the x-axis, in order to maximize the effectiveness of the mooring line. This is because the loads on the platform are all acting in the negative-x direction. The water depth below the fairleads is equal to 186 m with the top of the base columns located at a depth of 14 m below the surface water level. Through optimizing the duplicated mooring design of the OC4 semisubmersible, the semi-taut mooring configuration is determined as shown in Table 3. In addition, the properties of both types of mooring system are given in the previous Table 2. A complete redesign of the mooring system was warranted to ensure that the system stayed within the load envelope.

Table 3: Mooring line (chain) properties

	Length (m)	Diameter (m)	Mass Density (kg/m)	Axial Stiffness (kN)
Catenary	835.5	0.06	71.64	307.44E6
Semi-taut	550	0.06	71.64	307.44E6

Catenary Line Construction

As in the document of OC4 description, the semisubmersible platform was modeled with 3 mooring lines, and each of which line has a length of 835.5 m and a submerged mass per unit length of 108.63 kg/m (Robertson et al., 2014). A static

analysis was performed to locate anchors by the code MoorDyn from FAST. The anchor position is identified by considering the suspended mooring line length to be defined as

$$L_s = \frac{V}{w} \tag{21}$$

where V is the vertical tension in the mooring cable determined from equation above, w the submerged weight of the line per unit length, and L_s the length of the suspended mooring line. The horizontal tension at the top is found by

$$H = \frac{w\left(L_s{}^2 - D^2\right)}{2D} \tag{22}$$

where H is the horizontal force at the top, and D the vertical distance between the fairlead and the sea bottom. If the horizontal coordinate of the suspended mooring line length is expressed as

$$x = \frac{H}{w} cosh^{-1}\left(\frac{wD}{H} + 1\right) \tag{23}$$

The distance to the anchor from the origin is given by

$$x_A = L - L_s + x \tag{24}$$

where L is the unstretched mooring line length. By inserting the given length of unstretched mooring line, the location of a single anchor along the horizontal axis is obtained. Then, the shape of a single catenary mooring line at the static equilibrium state is depicted as in Figure 34 and Figure 35.

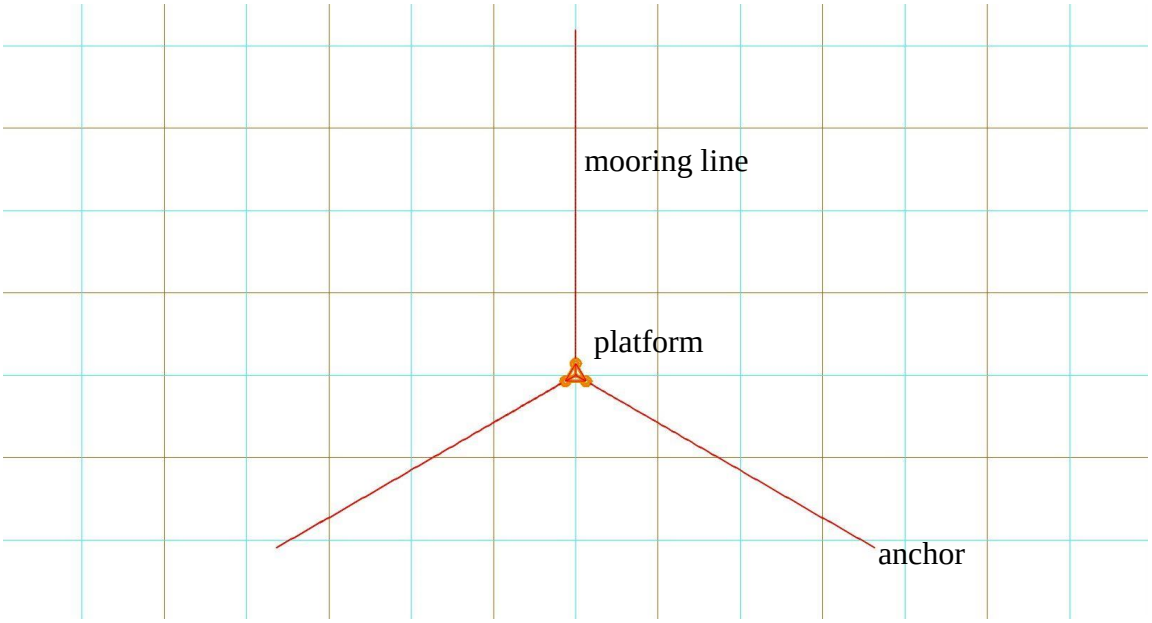

Figure 34: Plan view of catenary mooring line layout from OrcaFlex

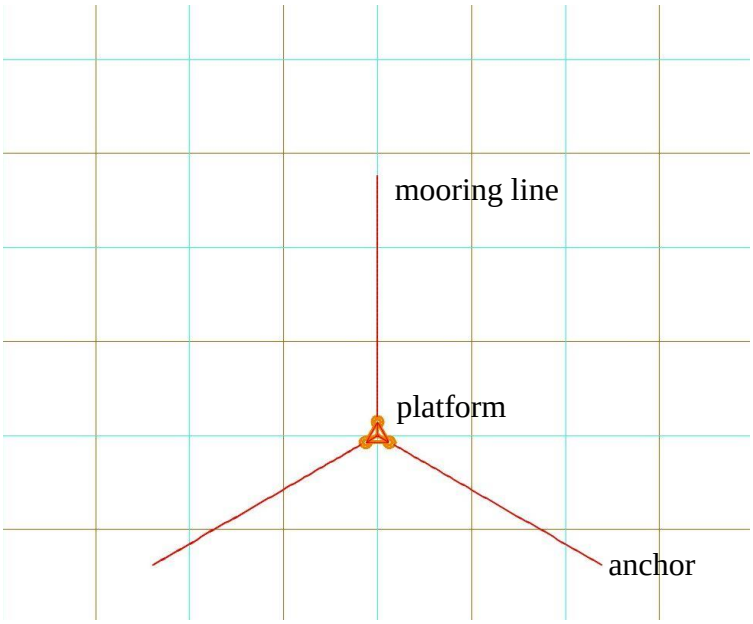

Figure 35: Plan view of semi-taut mooring line layout from OrcaFlex

Semi-Taut Line Construction

Given the water depth information and dimensions of the semisubmersible, several iterations were performed to determine the best angle of the mooring line with respect to the seafloor. A 20° angle was the optimum tradeoff between reducing platform motion and minimizing the amount of anchor tension. Each anchor position was calculated, using trigonometry rules, with the results shown in Table 4. The final calculation of anchor positions provided the initial layout of the mooring configuration. The initial calculations for anchor positions considered the mooring line length as the hypotenuse of a right triangle. However, to avoid excessive tensions, the mooring shape was combined with slack. While minimizing the length of the grounded mooring line, several different mooring lengths were tried to optimize the semi-taut shape of the line, and determined that a mooring line length of 550 m was optimal. The line composition used a chain but had different properties to lessen the tension of the line. Table 3 summarizes the lengths and line types used for semi-taut mooring line.

Table 4: Mooring line endpoint construction results

Catenary	Fairlead 1	Anchor 1	Fairlead 2	Anchor 2	Fairlead 3	Anchor 3
x (m)	20	419	-41	-838	20	419
y (m)	35	725	0	0	-35	-725
z (m)	-14	0	-14	0	-14	0
Semi-taut	Fairlead 1	Anchor 1	Fairlead 2	Anchor 2	Fairlead 3	Anchor 3
x (m)	20	276	-41	-552	20	276
y (m)	35	478	0	0	-35	-478
z (m)	-14	0	-14	0	-14	0

Figure 36 and Figure 37 provide the plan and elevation views for the catenary and semi-taut system respectively, from the OrcaFlex post-analysis. In this work, motion responses for a platform as well as the anchor tensions using catenary and semi-taut mooring system are calculated. Based on the results, a conclusion of which mooring arrangement is more beneficial for station-keeping the OC4 model is made. The load cases consider factors such as wave conditions, wind conditions, and current effects.

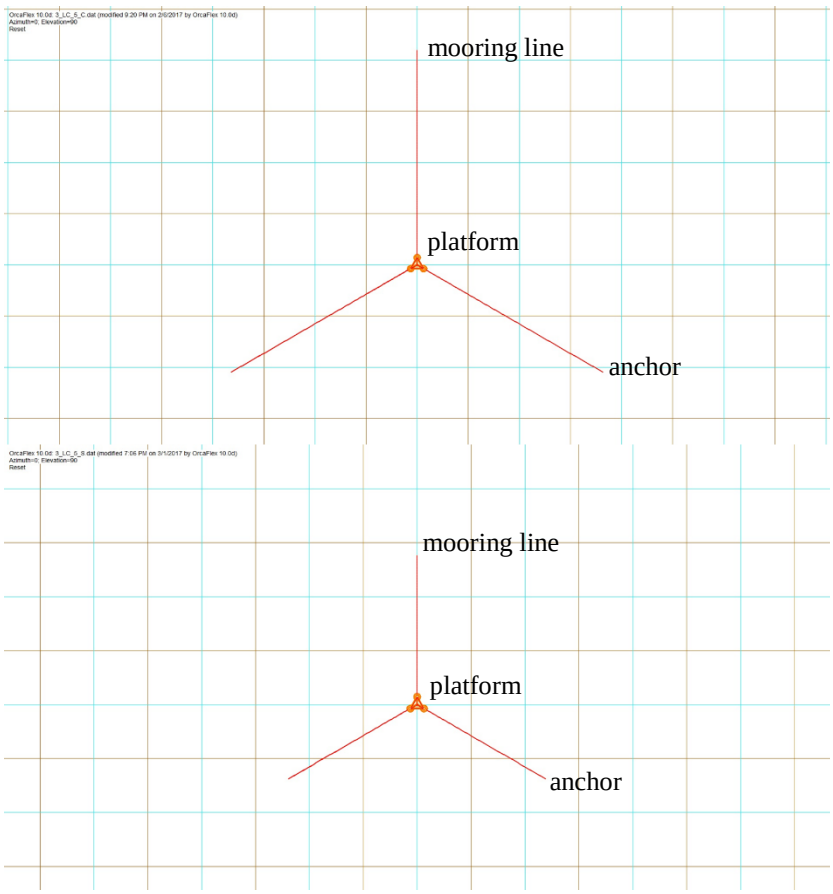

Figure 36: Plan views of catenary (top) and semi-taut (bottom) system from OrcaFlex

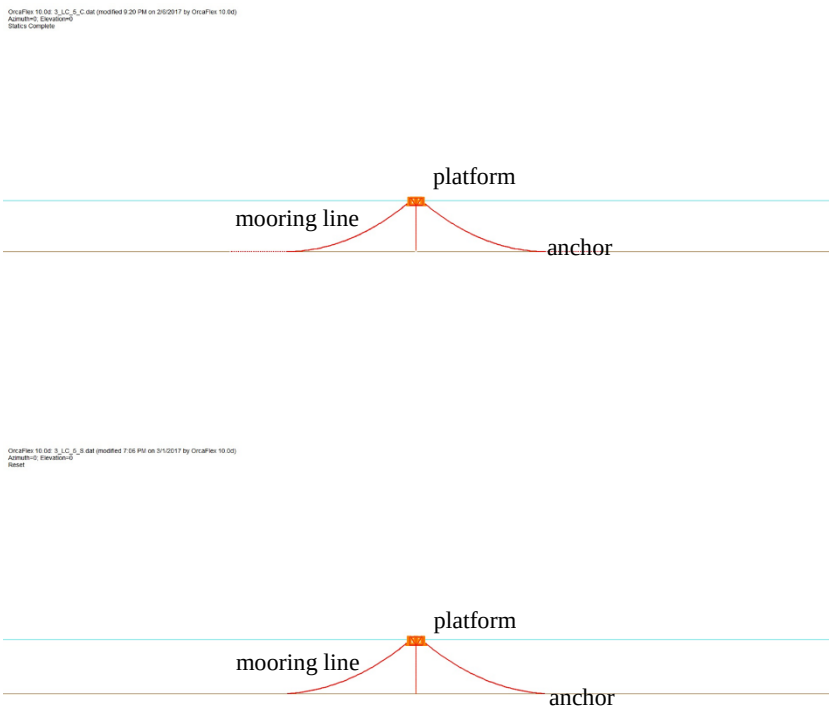

Figure 37: Side views of catenary (top) and semi-taut (bottom) system from OrcaFlex

Redundancy in Mooring System Design

In the case of a line failure, providing redundancy exhibits a promising reliability of the mooring system. When there is no redundancy, a single line failure can potentially cause an anchor to lose 3 usable turbines. For this reason, each turbine was secured by six mooring lines with two lines from each anchor. This redundancy for a six-leg fixed platform showed reduction in mooring loads when compared to those with only three lines.

Comparison of Mooring Systems – Load Case 1

The regular waves are basic conditions for testing the performance of the mooring system. A condition of regular waves with a height of 6 m and a period of 10 s is numerically simulated respectively using catenary and semi-taut mooring systems. As found in Figure 38, the range of the surge for both systems is from -3 to 1m, which is a reasonable offset for a floating platform. the heave and pitch time series are also plotted and the motions are respectively similar. The average surge motion for two types of mooring configurations is almost identical. It can be seen that in the catenary mooring length is larger than that of the semi-taut mooring, and thus the efficient line length is lower than that for semi-taut system (Wang et al., 2013). Figure 39 and Figure 40 show the comparison of the dynamic tensions for the catenary mooring and the semi-taut mooring. The average mooring line tension is semi-taut > catenary. It can be seen that the two different mooring setups may cause radical changes to the mooring line tensions but not the coupled motions of the semisubmersible.

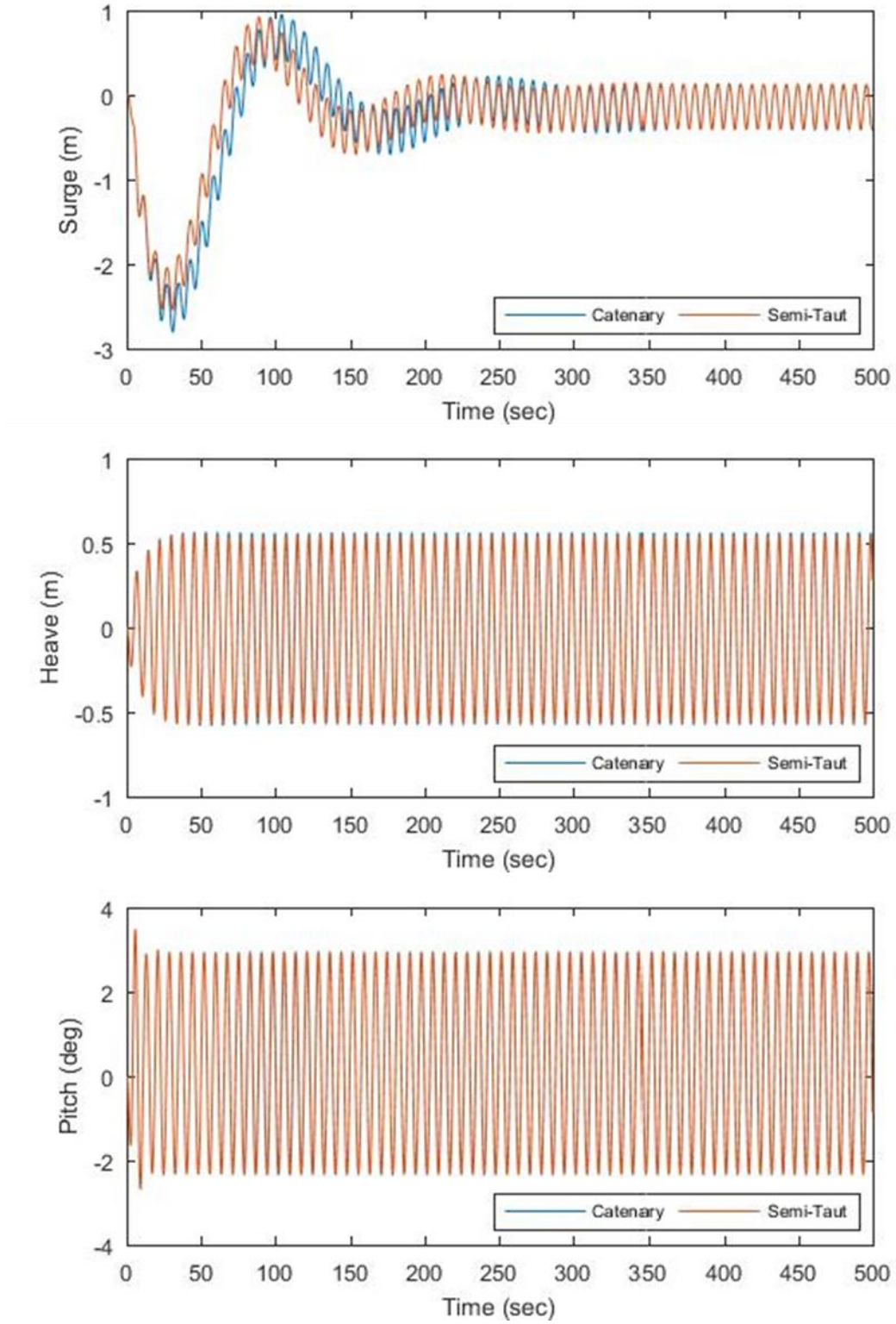

Figure 38: Platform motion responses of mooring system (load case 1)

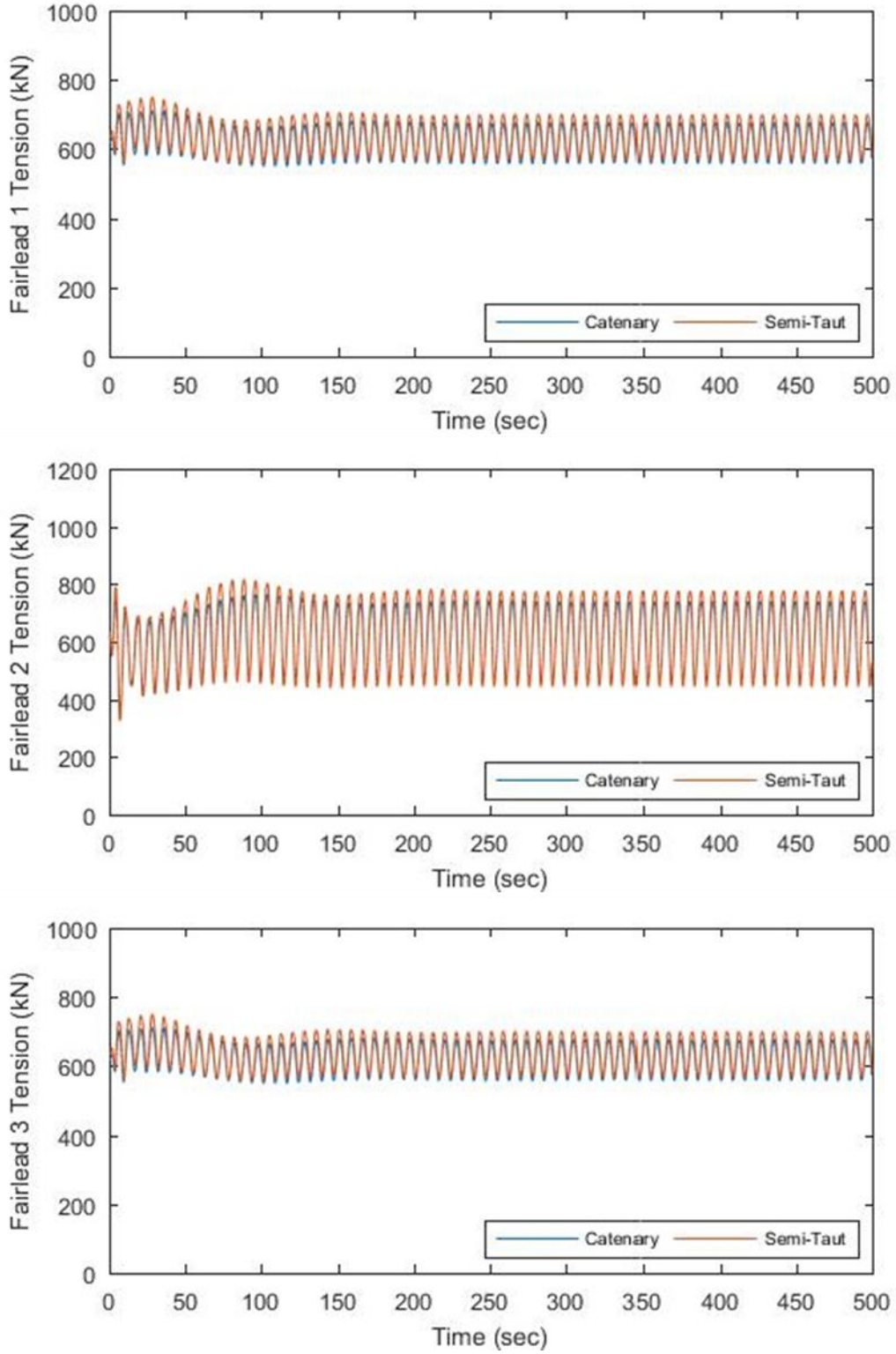

Figure 39: Fairlead loads of mooring system (load case 1)

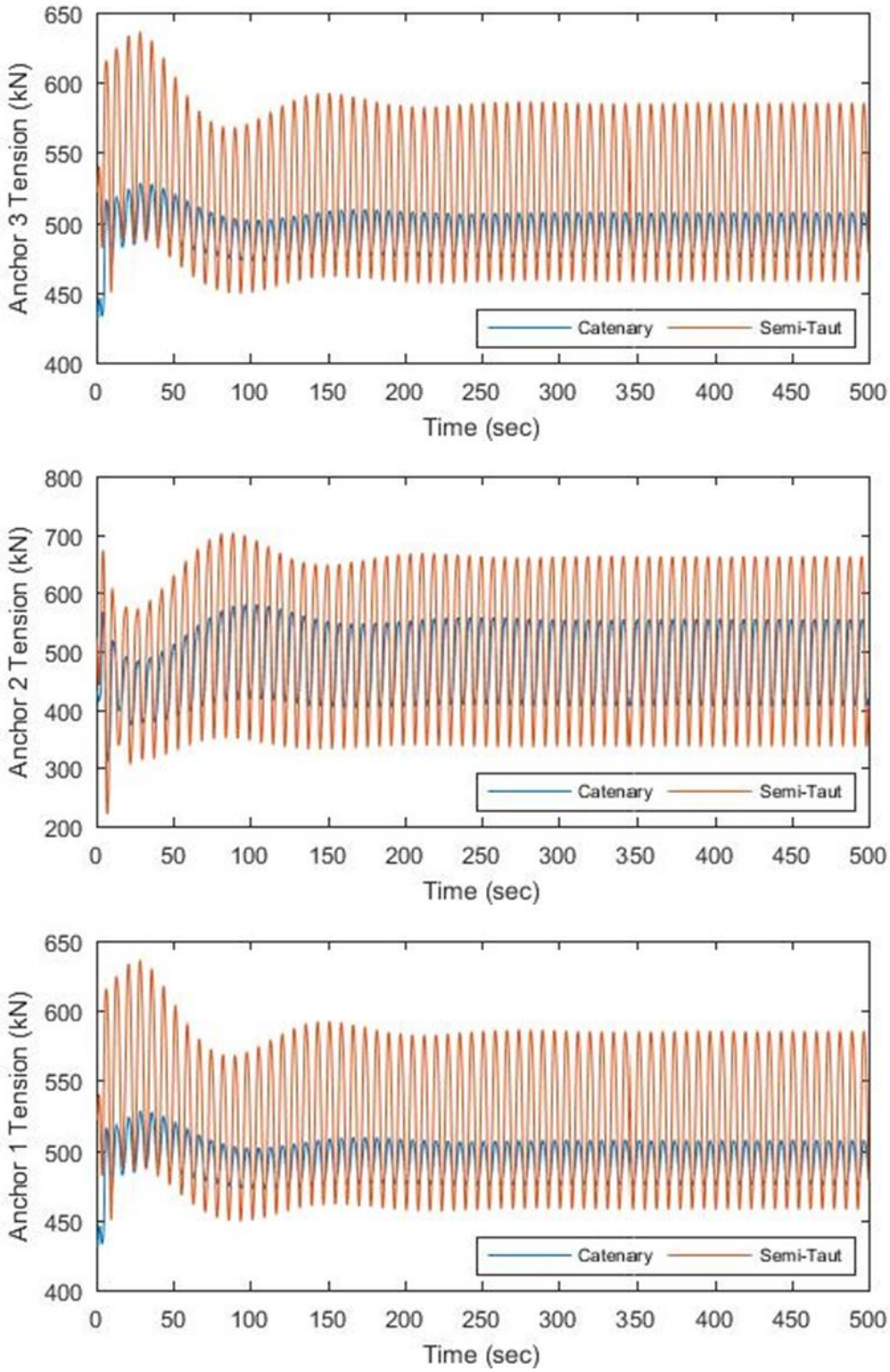

Figure 40: Anchor loads of mooring system (load case 1)

Comparison of Mooring Systems – Load Case 2

The aim of evaluating the effect of irregular waves on the mooring dynamics is to examine the survivability of the system. Simulation results of extreme waves are plotted in Figure 41, Figure 42 and Figure 43. The motion responses are almost identical except for the surge. The surge response is in less agreement between the two mooring systems as the corresponding surge in the catenary mooring is greater than that of the semi-taut mooring. It can be deduced that the elastic component of the semi-taut mooring allows the platform to achieve large stiffness of mooring system. As a result of larger wave excitation, the mooring loads are higher than those in the regular waves, and the semi-taut system has higher loads than those of the catenary mooring. The reason is that the higher stiffness of the semi-taut mooring line responds more dynamically to the wave excitation motion. The phenomenon suggests that the catenary setup under extreme conditions may have a negative impact on the fatigue issues with severe loads, and further analyses are needed.

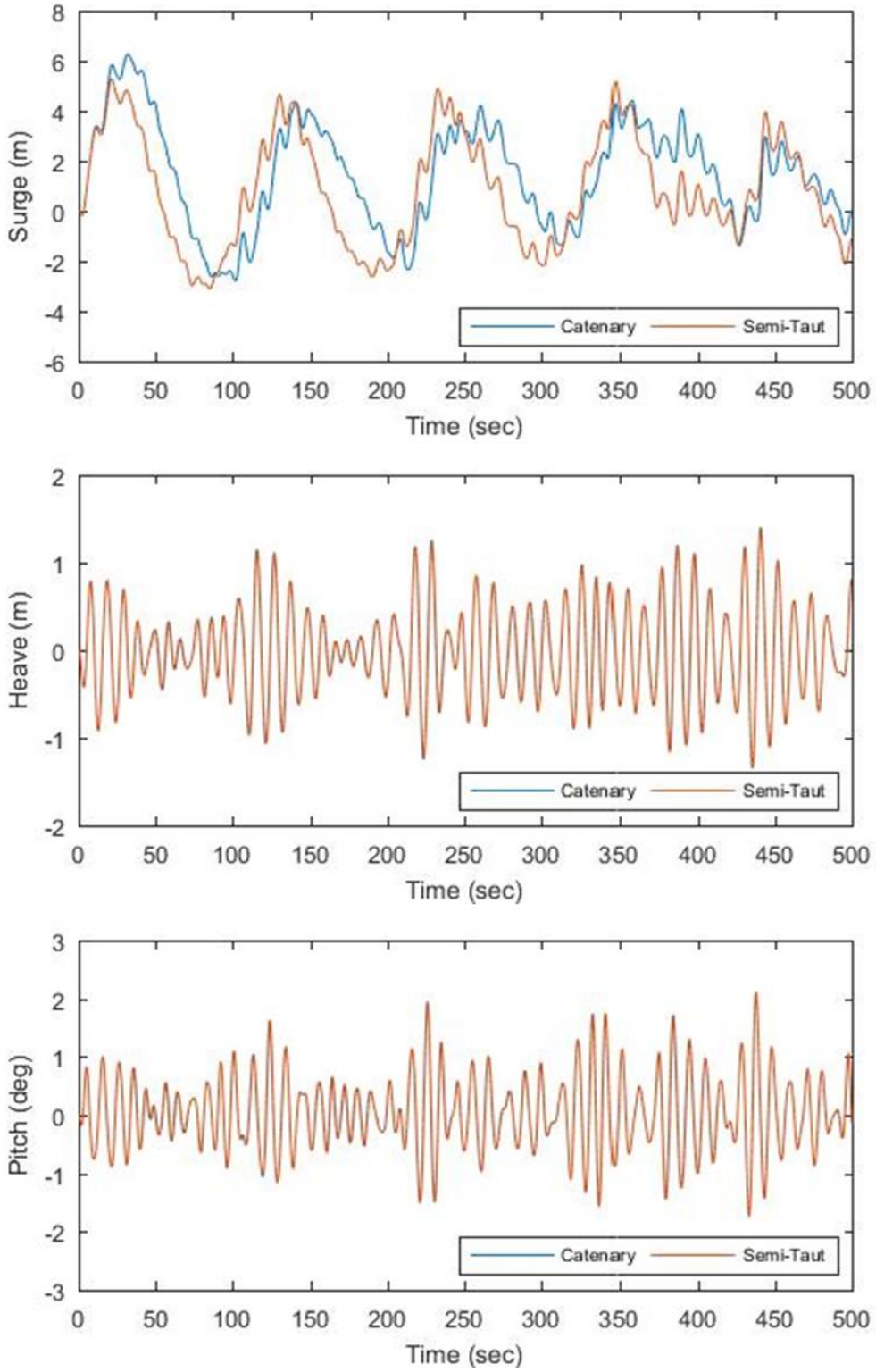

Figure 41: Platform motion responses of mooring system (load case 2)

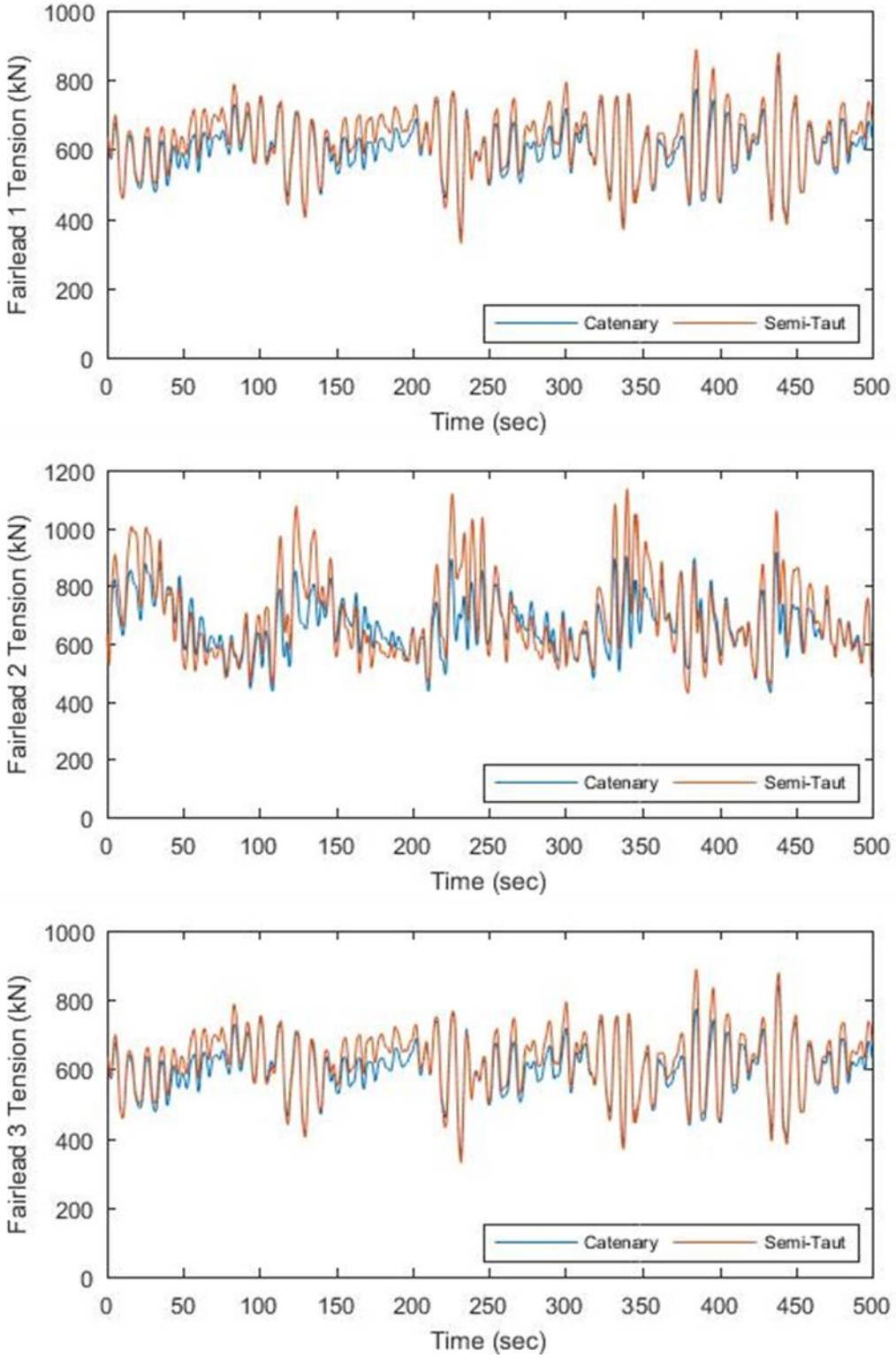

Figure 42: Fairlead loads of mooring system (load case 2)

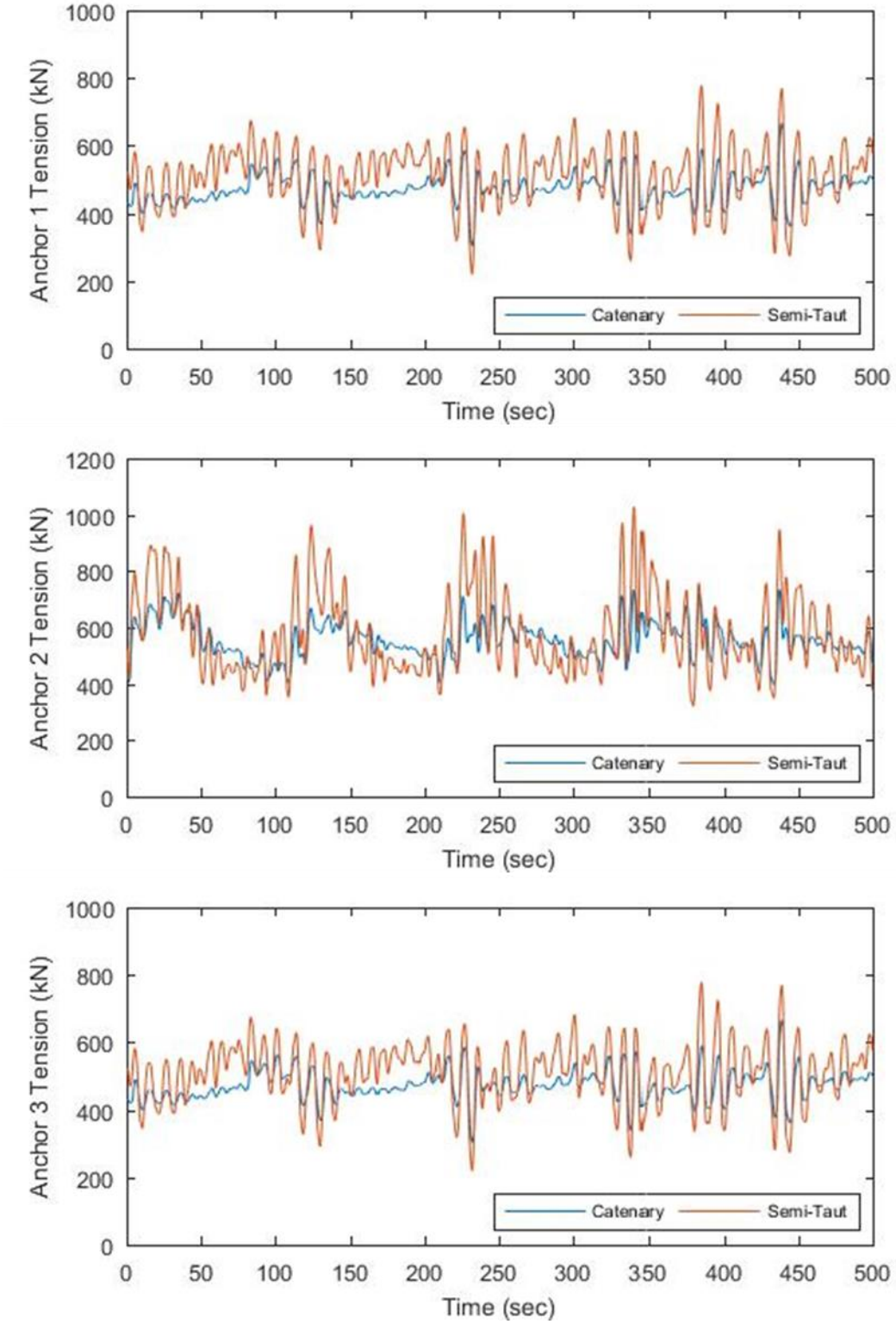

Figure 43: Anchor loads of mooring system (load case 2)

Comparison of Mooring Systems – Load Case 3

Tests on regular waves with a prescribed uniform sheared wind were performed to compare the loads and motions under wind excitation. Figure 44 shows the curves of surge, heave, and pitch motions respectively. Based on the results of surge motions under steady wind condition, the average surge motion for catenary is greater than the semi-taut mooring system. Again, the results of heave and pitch motions for two types of mooring system are similar. Through comparisons of mooring line tensions using catenary and semi-taut system in Figure 45 and Figure 46, the influences to the transfers of line tension are observed to be almost identical for waves only conditions. For the most loaded mooring line #2, it is noteworthy to see the tension is increased by the wind excitation in both catenary and semi-taut mooring systems. Furthermore, the wind excitation loads added on the mooring tension for semi-taut system are significantly larger than those in the catenary system. According to the most loaded mooring line, the phenomenon may suggest that the semi-taut mooring system could be exposed to fatigue problems due to large amplitude changes.

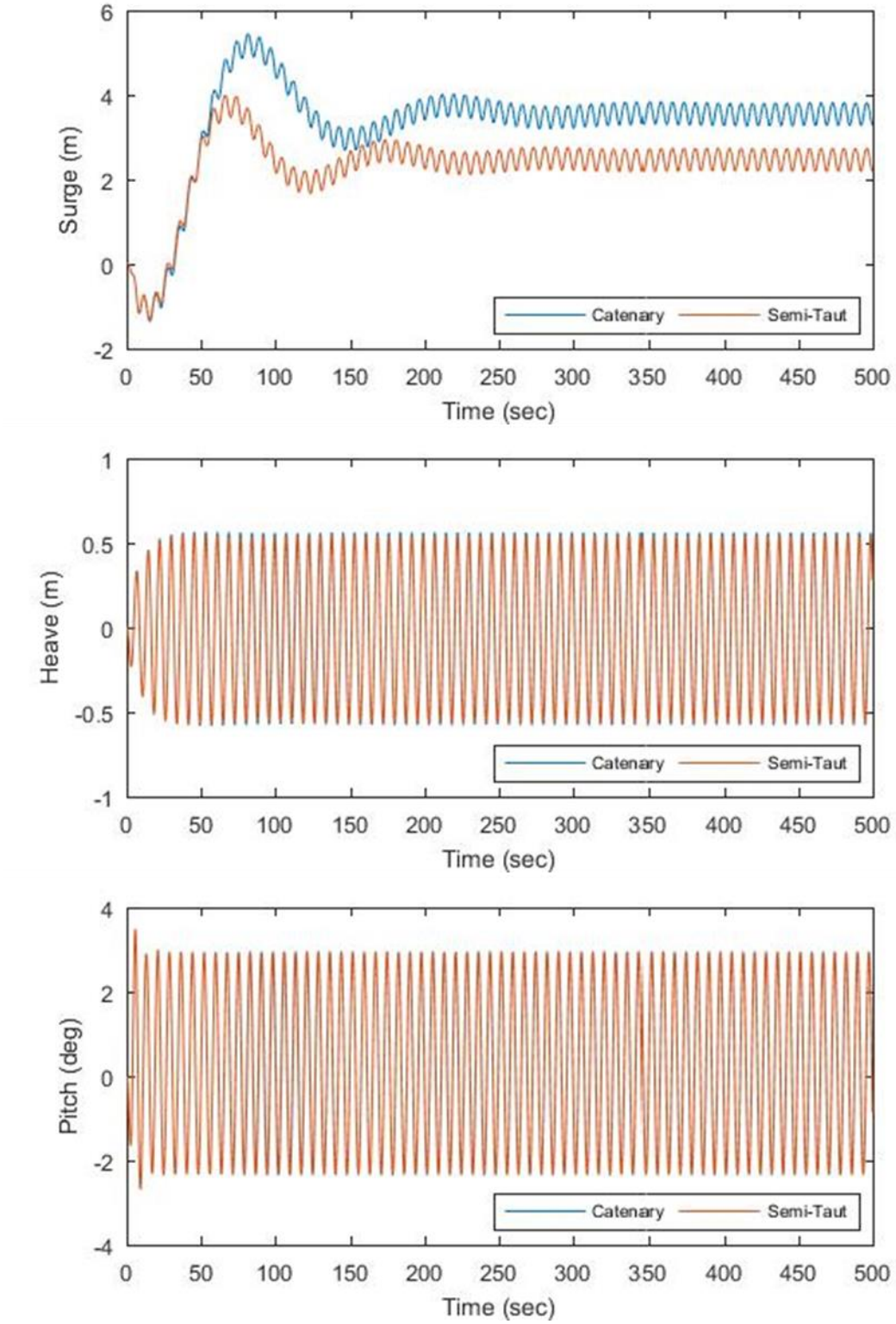

Figure 44: Platform motion responses of mooring system (load case 3)

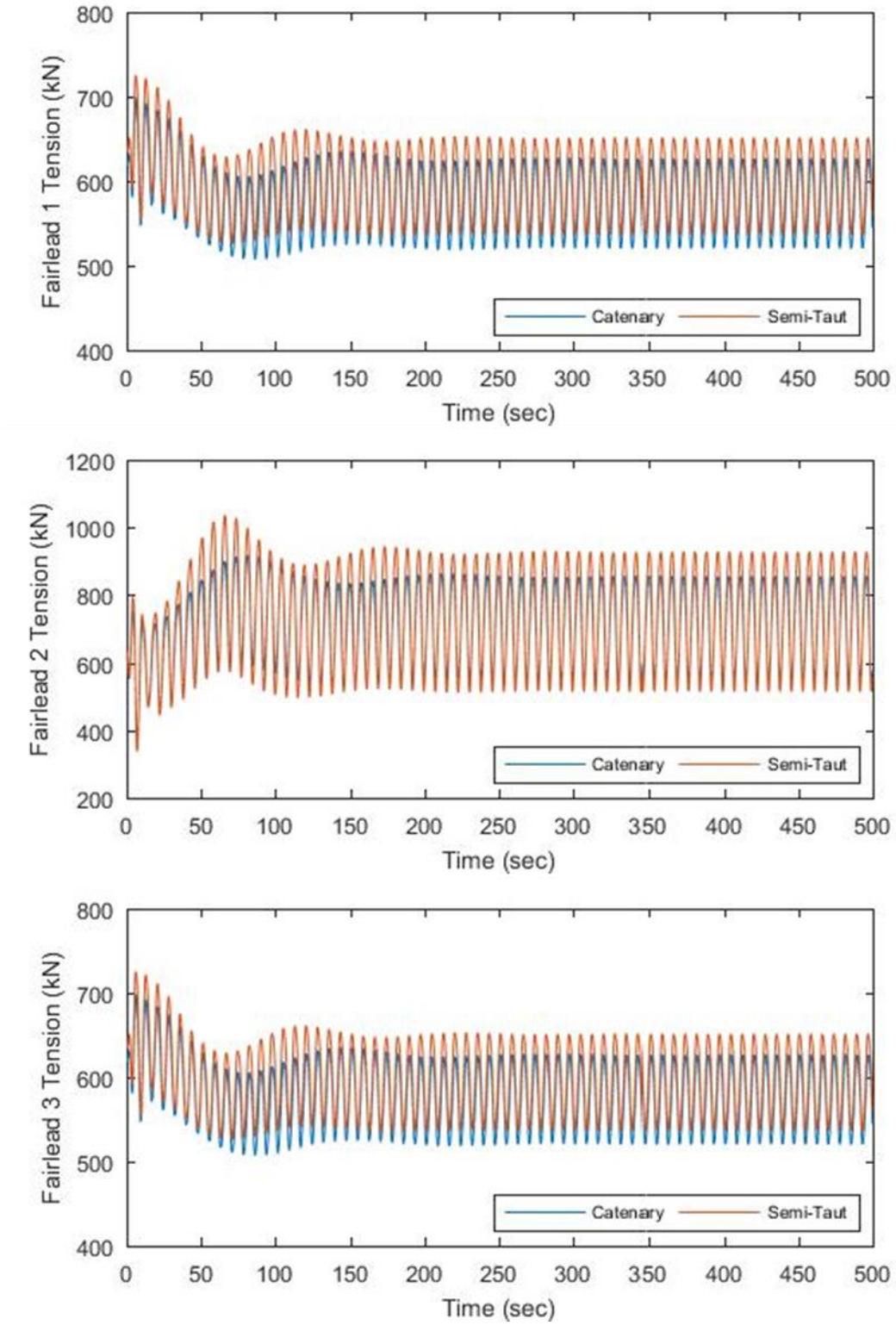

Figure 45: Fairlead loads of mooring system (load case 3)

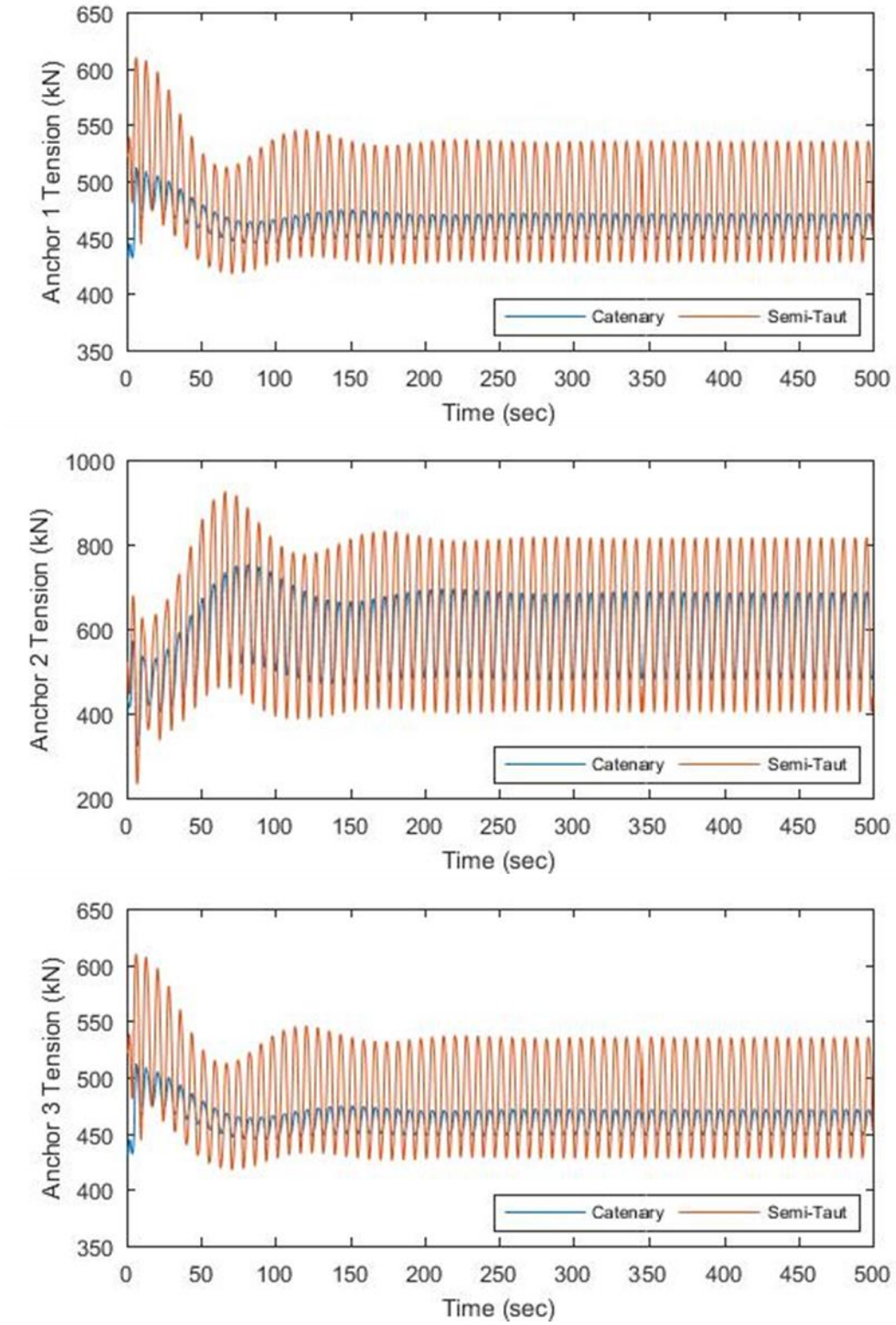

Figure 46: Anchor loads of mooring system (load case 3)

Comparison of Mooring Systems – Load Case 4

The results now show the case of irregular sea conditions combined with sheared wind model. Figure 47 shows the coupled motions of a semi-submersible platform supported by catenary and semi-taut system. The results of heave and pitch motions are fairly similar, but the higher surge responses are found in the catenary mooring curve. Figure 48 and Figure 49 then show the dynamic tension results, and the tension curve of the second mooring line suggests the wave and wind excitation loads are captured more in the semi-taut system with larger variation in mooring loads. For the unloaded mooring lines, the simulations showed that the catenary mooring system experienced less change in amplitudes of line tensions.

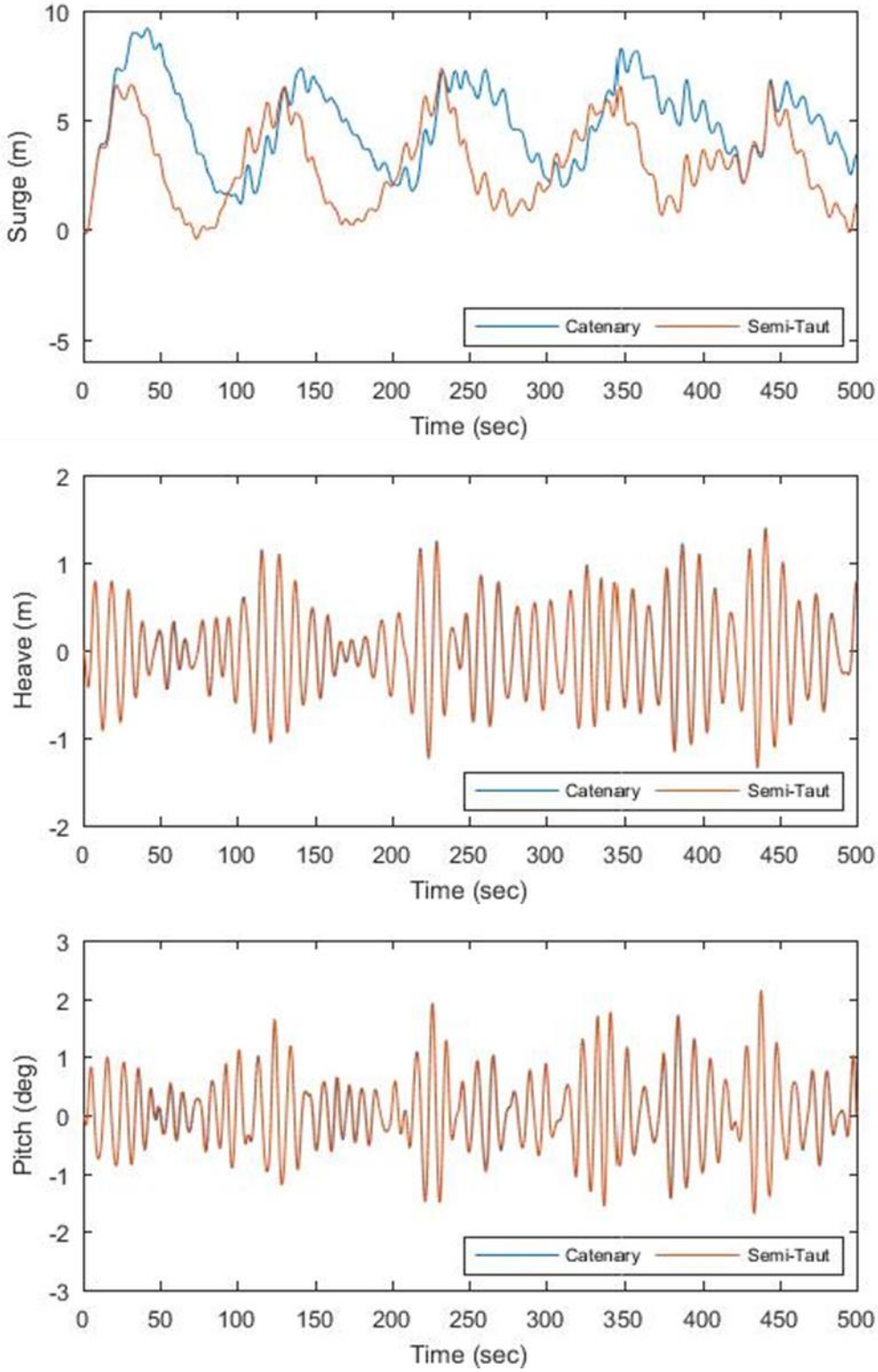

Figure 47: Platform motion responses of mooring system (load case 4)

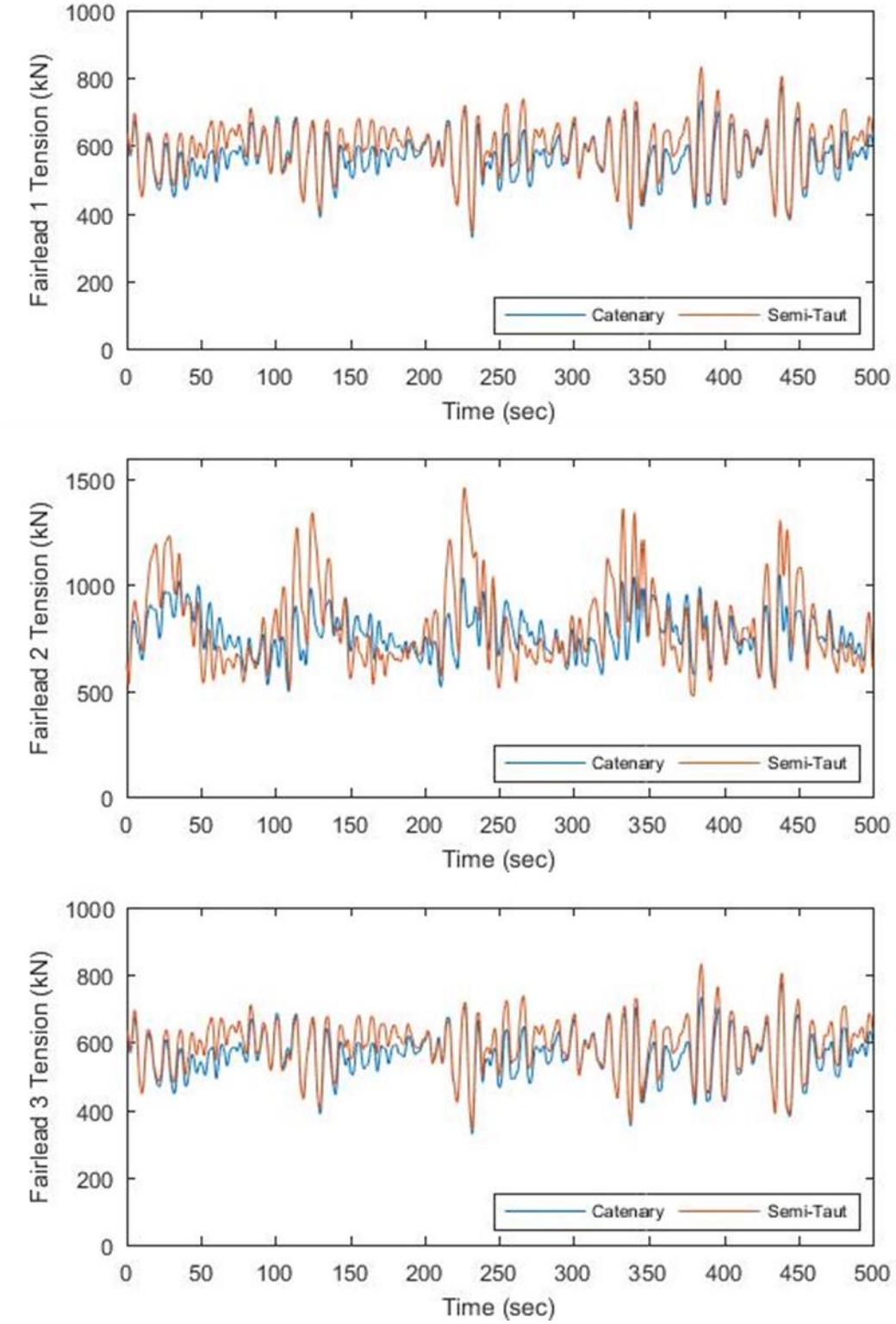

Figure 48: Fairlead loads of mooring system (load case 4)

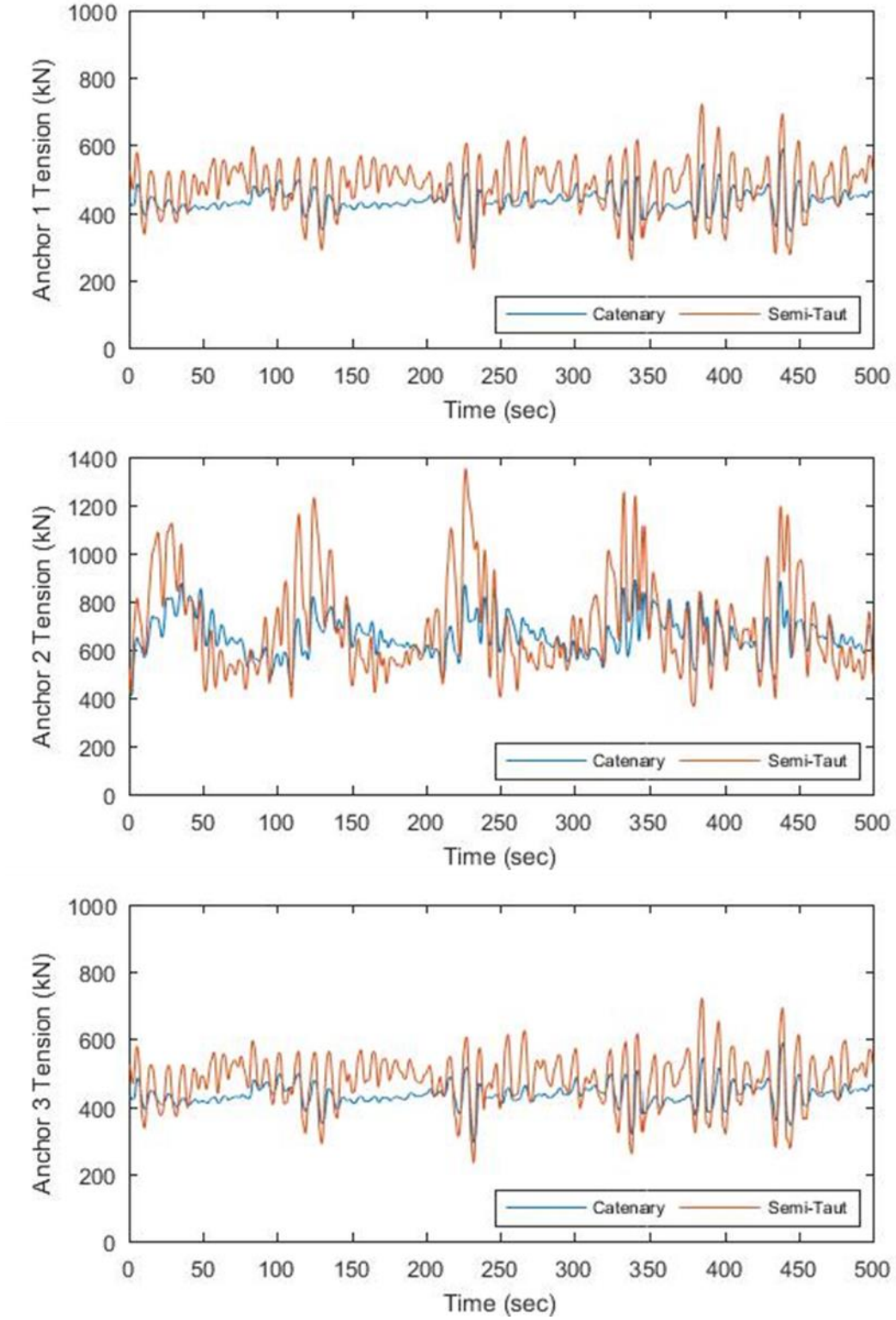

Figure 49: Anchor loads of mooring system (load case 4)

Comparison of Mooring Systems – Load Case 5

A condition of regular waves with a height of 6 m and a period of 10 s is combined with both sheared wind and current to examine the survivability under an actual sea condition. Simulation results of extreme waves are plotted in Figure 50, Figure 51 and Figure 52. A difference is seen in the surge, as the corresponding surge in the catenary mooring is greater than that of the semi-taut mooring. Based on the results of surge motions under steady wind condition, the average surge motion for catenary is greater than the semi-taut mooring system, but the results of heave and pitch motions are identical. The maximum horizontal offset is observed among the simulations with regular waves since this case involves both current and wind. The loads on fairleads and anchors are much higher than those in the regular waves without the current because of the current excitation loads. Mooring system requires optimization under the extreme waves combined with wind and current, and thus the last load case extended the scope of comparison by considering irregular waves.

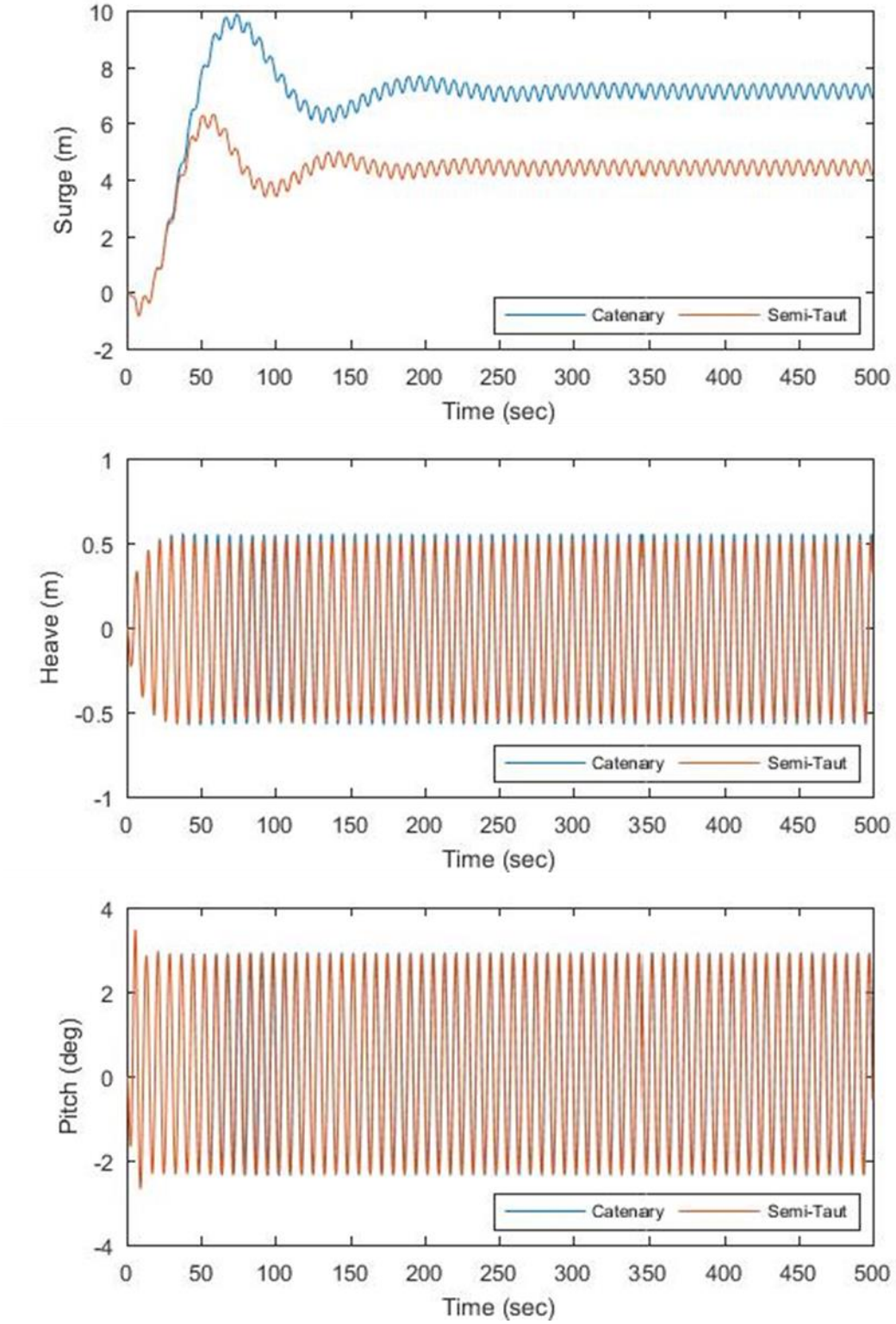

Figure 50: Platform motion responses of mooring system (load case 5)

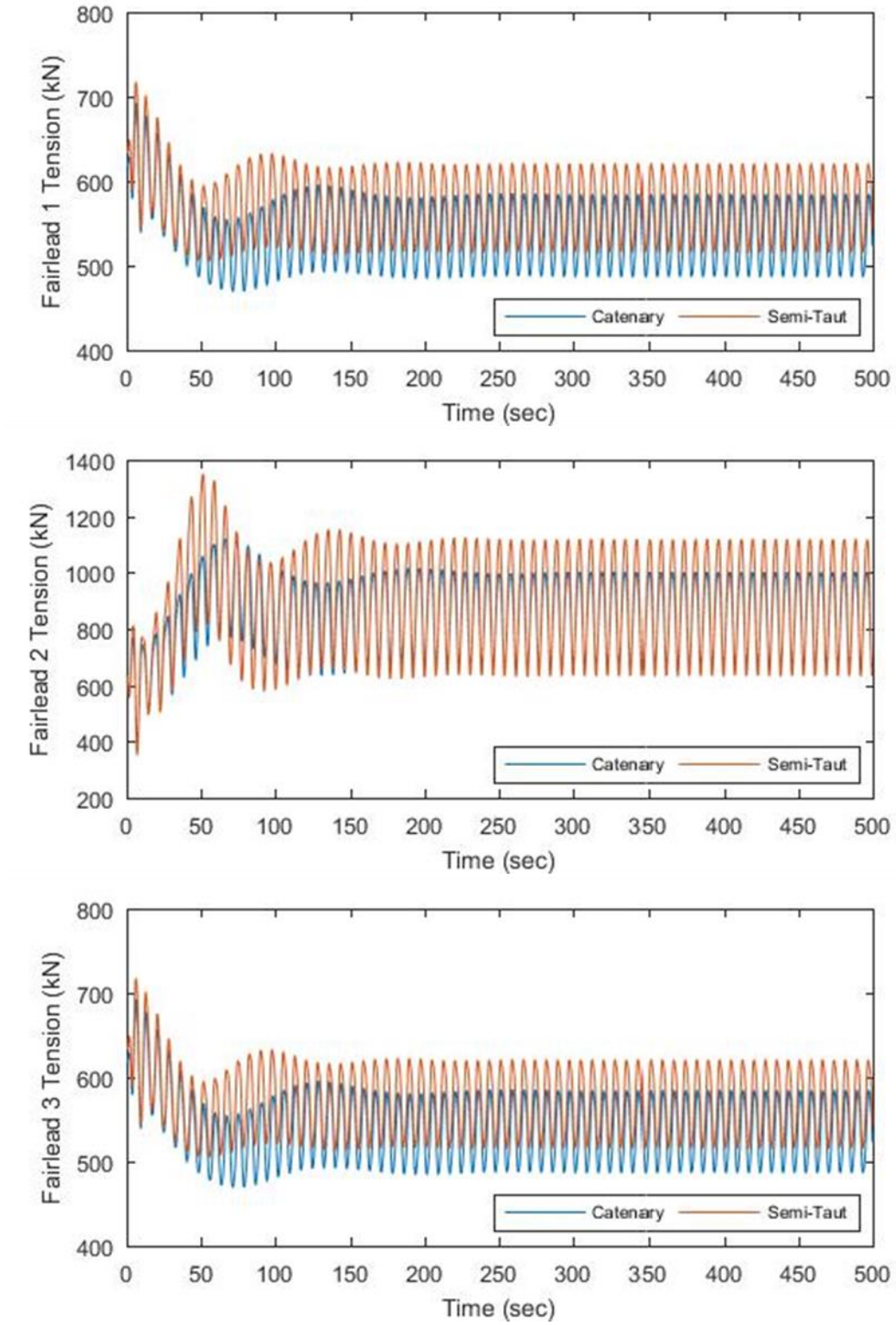

Figure 51: Fairlead loads of mooring system (load case 5)

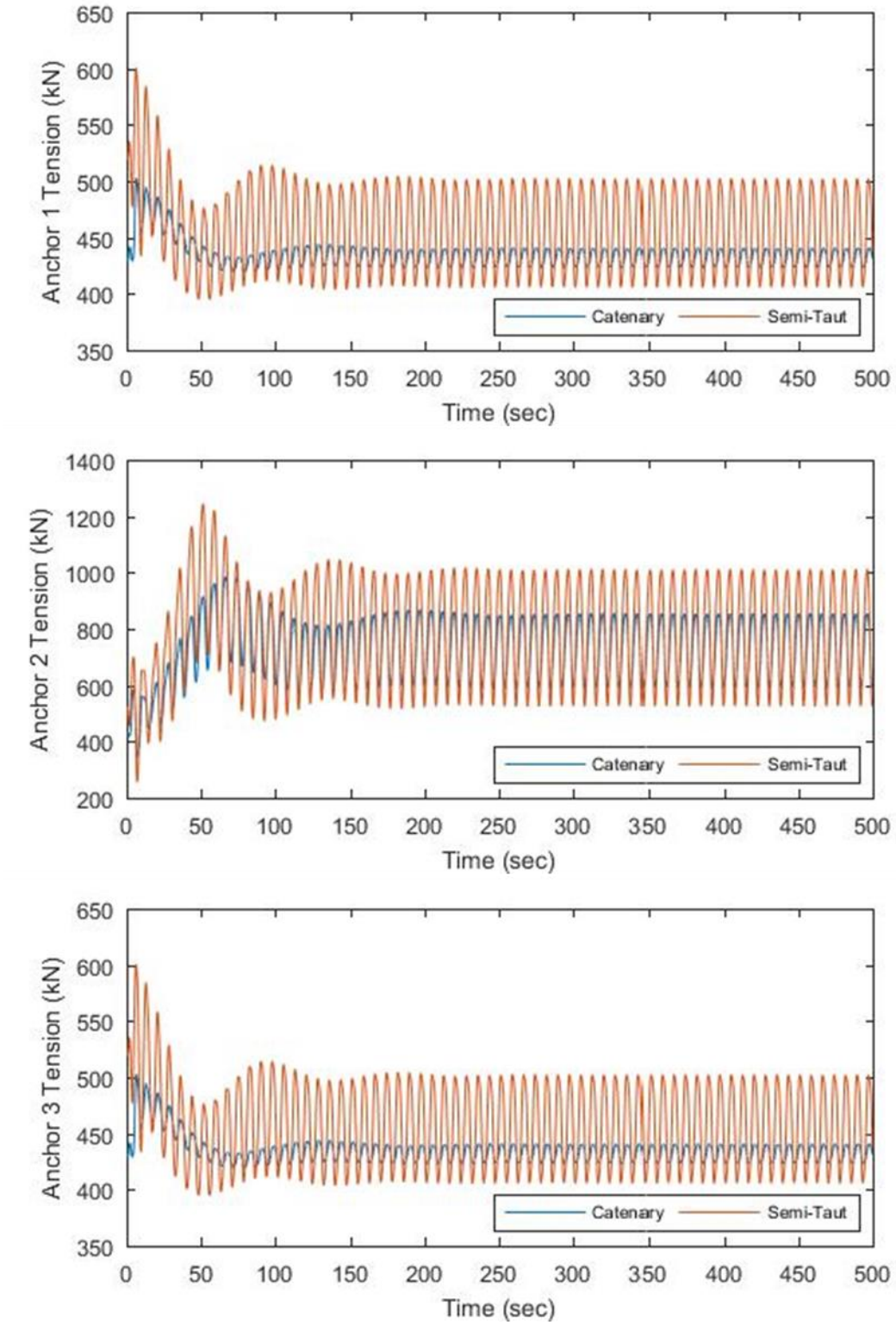

Figure 52: Anchor loads of mooring system (load case 5)

Comparison of Mooring Systems – Load Case 6

The comparison also considered extreme sea conditions in combination with a current. The current speed at surface is 0.5 m/sec and a power law profile with the exponent of 1/7 was applied. The curves in Figure 53 are comparing the system response in surge, heave, and pitch for two types of mooring system. The results show the same trend as the previous cases as the average surge motion for the semi-taut system is less than the catenary system. It can be seen that the catenary system is affected by the current velocity more than the semi-taut lines are. The reason is that the effect of current on catenary mooring line increases the induced damping of the cable. The simulation shows an effect on drag force by damping under the influence of current. As a result, the horizontal offset of the platform in the catenary system is larger than that of the semi-taut system. Figure 54 and Figure 55 show the mooring tension plots in time series in regard to selected mooring systems. By comparing the results of mooring tensions of previous case and current case, it can also be concluded that the increase in the fairlead tensions are most on the second line, which is oriented along the direction of the current velocity. The anchor tension values are similar to those at the fairlead.

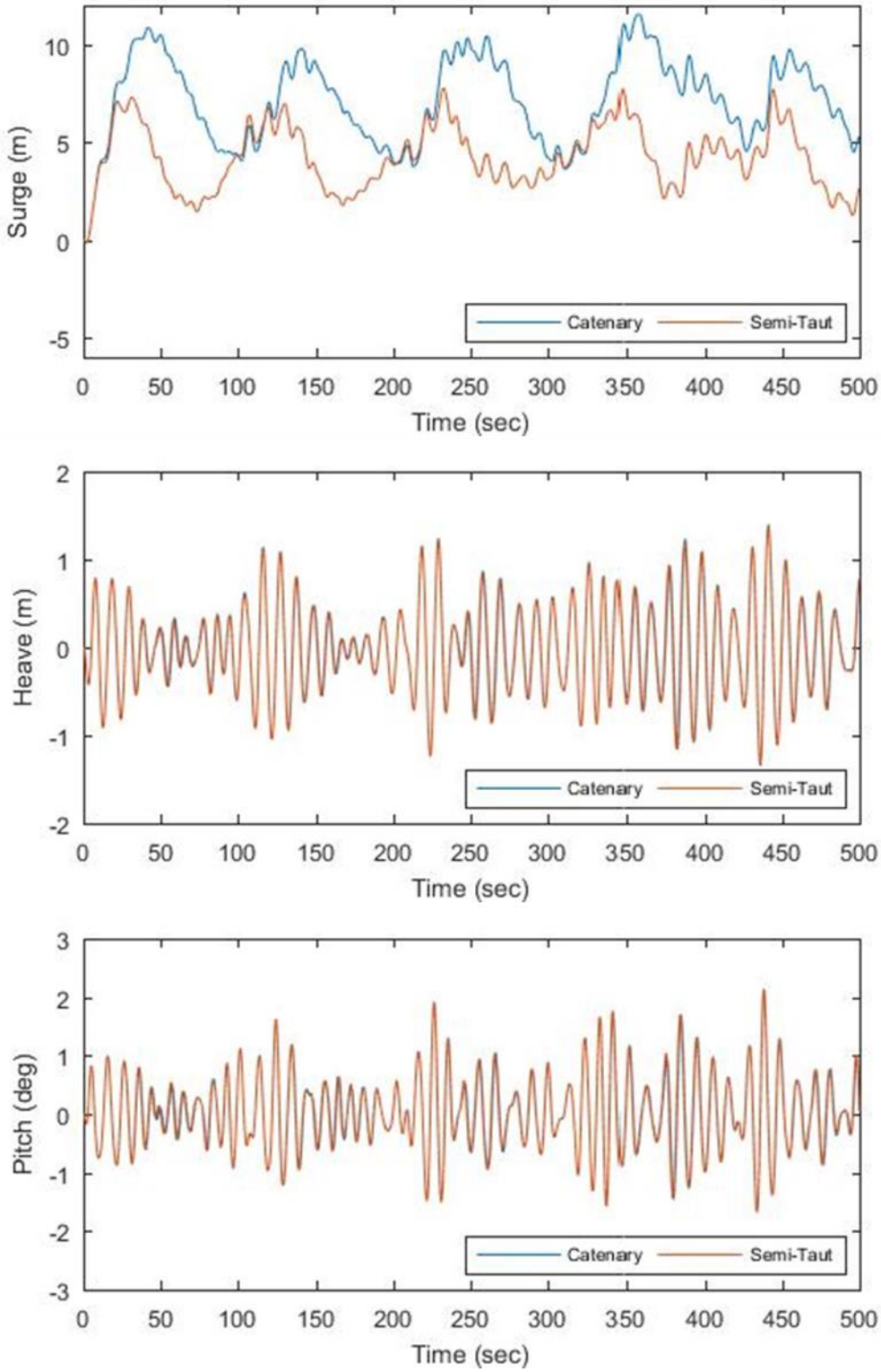

Figure 53: Platform motion responses of mooring system (load case 6)

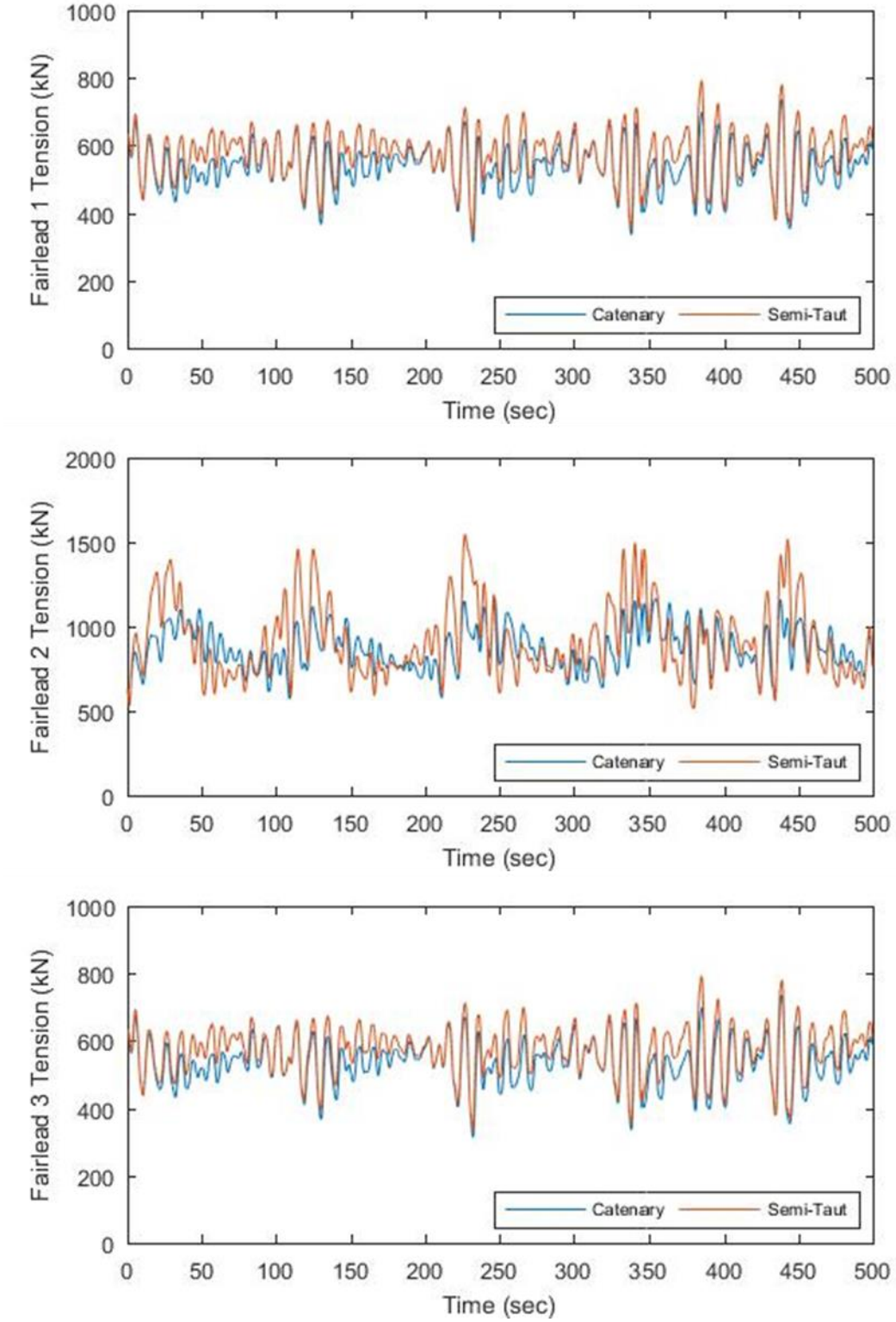

Figure 54: Fairlead loads of mooring system (load case 6)

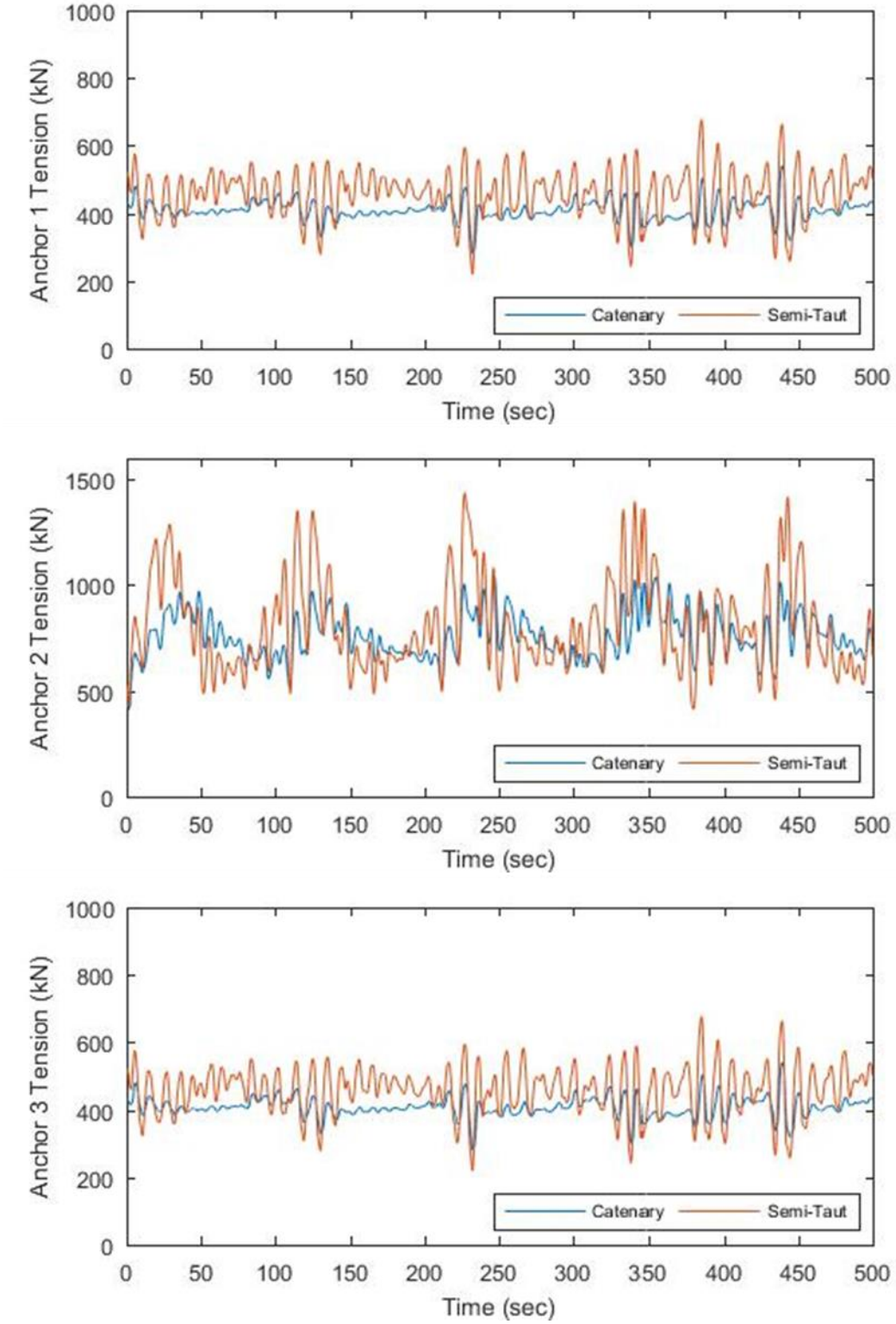

Figure 55: Anchor loads of mooring system (load case 6)

4. WATER DEPTH SENSITIVITY

The effect of water depth on the OC4 Semisubmersible Floating Offshore Wind Turbine because the environmental conditions can vary in water depth, it is appropriate to examine the operation of the floating wind turbine as the water depth changes. In this chapter, the behavior of two types of mooring system are studied at 3 different water depths, 150 m, 200 m, and 250 m. In the offshore industry, a water depth is considered as one of the key design parameters that affects the motion response of the floating body. For larger water depths, it is generally assumed that the weight of the mooring system is increased and the effects of deeper water installation are visible on the values for platform motions and mooring line tensions. The shallow water effect is another area of study in this study to quantify the effects of water depth variation. In order to check the main difference among various vertical distances between fairlead and seafloor, a method of comparing mooring systems at particular water depth was undertaken. As seen in the previous chapter, the mooring systems used in this analysis are catenary and semi-taut system with the OC4-Semisubmersible platform. Results from the studies will present dynamic responses of the OC4 floating wind turbine including degrees of freedom and anchor tensions. In this comparison, the previously mentioned load cases have been considered. From the comparison it can be expected that the details regarding the different environmental conditions will offer guidance on how to prepare for moored floating platform designs under specific water depth. The simulations are performed for a range of 50 m water depth between the nominal value of 200 m. The preliminary

design procedure of the selected mooring systems at particular water depths are described below.

Description of Catenary Modeling

With change in water depth, an appropriate mooring configuration for the according catenary system requires a redesign of the catenary shape. A new static model for the cable manipulates a mathematical solver to execute the iterative process of mooring analysis. In this paper, Matlab, a computer software, was used to develop a coordinate system of a single line. The fundamentals are discussed below and the equations are coded in Appendix A.

Figure 56 illustrates a concept of a mooring line for the purpose of determining the horizontal and vertical position of the anchor. A cable is divided into multi nodes, and the weight of submerged line is assigned to each nodal section.

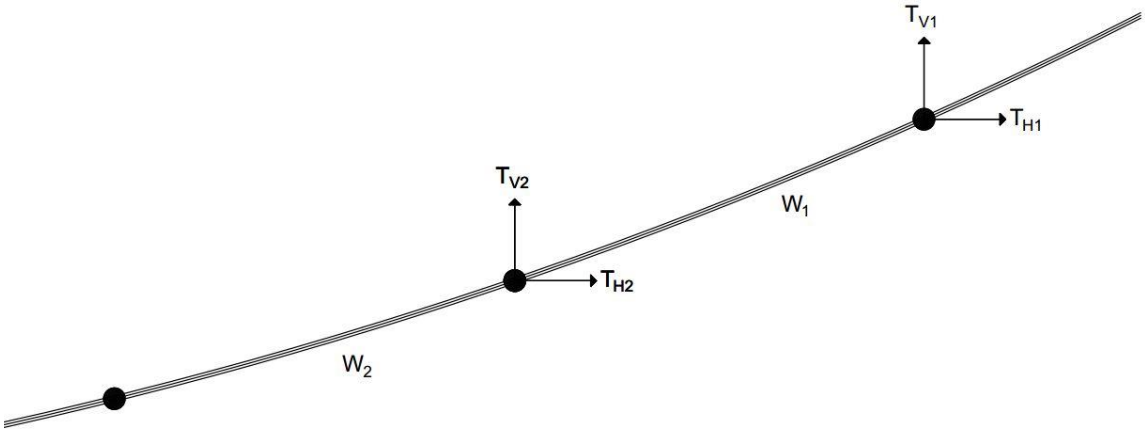

Figure 56: Segment division of the cable

The horizontal component of the tension force for each node is considered as a constant, and it can be written as

$$T_{H1} = T_{H2} = T_{H3} = T_{H4} \ldots . T_{Hn} \tag{25}$$

Thus, the subsequent nodes have the vertical component of tension as a reduced load by the gravity force of each nodal section. The equation for the vertical component of tension at the depth of each node is given as

$$T_{V2} = T_{V1} - W_1 \tag{26}$$

$$T_{V3} = T_{V2} - W_2 = T_{V1} - W_1 - W_2 \tag{27}$$

$$T_{V4} = T_{V3} - W_3 = T_{V1} - W_1 - W_2 = W_3 \tag{28}$$

$$T_{Vn} = T_{Vn-1} - W_{n-1} = T_{V1} - W_1 - W_2 \ldots W_{n-1} \tag{29}$$

After obtaining the components of tension, the angle between the nodes is

$$\theta_1 = tan^{-1}\left(\frac{T_{V1}}{T_{H1}}\right) \ldots . \theta_n = tan^{-1}\left(\frac{T_{Vn}}{T_{Hn}}\right) \tag{30}$$

Alongside of the given water depth, a zero anchor uplift angle will be another input parameter to plot the ideal catenary shape. The output of the solver includes the coordinate of each node from the anchor as well as the amount of mooring line on the seafloor. This grounded length is dictated by the friction between the line section and the seafloor, and the friction force is determined as

$$T_{H2} = T_{H1} - \mu W_1 \ldots . T_{Hn} = T_{Hn-1} - \mu W_{n-1} \tag{31}$$

where μ is the friction coefficient for the cable material where it is 1.2 for chain and 0.5 for wire or rope in general. The results of the software are tabulated in Appendix A, and the location of each anchor is found in Table 5: Mooring endpoint results.

Table 5: Mooring endpoint results for 150m (top) and 250m (bottom) water depths

Water Depth = 150 m						
Catenary	Fairlead 1	Anchor 1	Fairlead 2	Anchor 2	Fairlead 3	Anchor 3
x (m)	20	361	-41	-722	20	361
y (m)	35	626	0	0	-35	-626
z (m)	-14	0	-14	0	-14	0
Semi-taut	Fairlead 1	Anchor 1	Fairlead 2	Anchor 2	Fairlead 3	Anchor 3
x (m)	20	207	-41	-415	20	207
y (m)	35	359	0	0	-35	-359
z (m)	-14	0	-14	0	-14	0
Water Depth = 250 m						
Catenary	Fairlead 1	Anchor 1	Fairlead 2	Anchor 2	Fairlead 3	Anchor 3
x (m)	20	470	-41	-940	20	470
y (m)	35	814	0	0	-35	-814
z (m)	-14	0	-14	0	-14	0
Semi-taut	Fairlead 1	Anchor 1	Fairlead 2	Anchor 2	Fairlead 3	Anchor 3
x (m)	20	345	-41	-689	20	345
y (m)	35	597	0	0	-35	-597
z (m)	-14	0	-14	0	-14	0

Description of Semi-Taut Modeling

Figure 57 shows the arrangements of both the catenary system and the semi-taut system considered in water depths of 150m, 200m, and 250m respectively. The length of the ground chain is minimized as shown in the semi-taut arrangements. Since the catenary design is mainly dictated by the submerged weight of the lines, converting to a semi-taut system required some adjustment to the mooring properties to maintain the stability of the floating platform. With the semi-taut mooring line type, the mooring line has been replaced by a material used for the semi-taut system from the previous chapter to provide elasticity. Changing the vertical distance between the fairlead and the seafloor along with the length of mooring line caused variation to the load envelope of the

floating platform. To obtain the desired response characteristics, the vertical position of the floating platform was adjusted to the surface water level by varying the volume of the ballast. Table 5 and Table 6 show the calculated anchor positions and the properties of the mooring line in different water depths of 150 m, 200 m, and 250 m respectively.

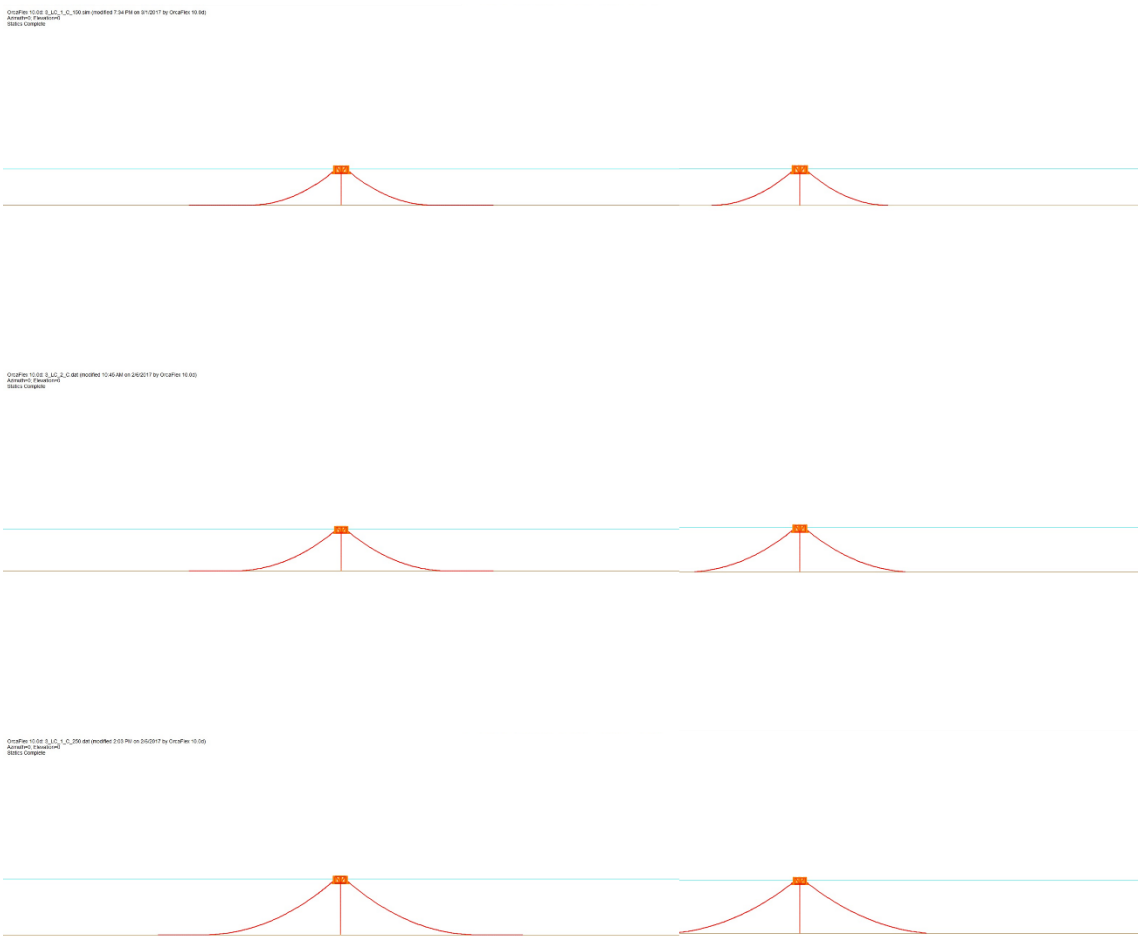

Figure 57: From top-bottom, comparison of elevation veiws at 150m, 200, and 250m

Table 6: Properties of studied mooring lines

Parameters	Catenary			Semi-taut		
Water depth (m)	150	200	250	150	200	250
Length of mooring line (m)	710	835.5	950	404	550	696
Mass per unit length (kg/m)	71.64	71.64	71.64	71.64	71.64	71.64
Mooring radius (m)	626	797	814	374	511	648

Influence of Water Depth Variation – Load Case 1

Three water depths, 150 m 200 m and 250 m were investigated to study the variation of dynamic response of the OC4 semisubmersible. The same load cases were considered as found in Table 2. The translational motions and rotational motions of the platform using catenary and semi-taut system are shown in Figure 58 and Figure 61 respectively. As far as the obtained values for both types of systems, the plots show that responses in water depth of 150 m, 200 and 250 m are very close. The motions of surge, heave and pitch are independent of water depth with similar graphs for all the water depths for both types of system. The dynamic mooring tensions using the two types of mooring systems in 150 m, 200 m and 250 m water depths are plotted in Figure 59, Figure 60, Figure 62 and Figure 63. Looking at the trends of the figures, it is clear how mooring line tension increases for both catenary line and semi-taut line with the increase in water depth. This highlights the importance of water depth variation as the tensions are varied by the correspondingly changing mooring stiffness.

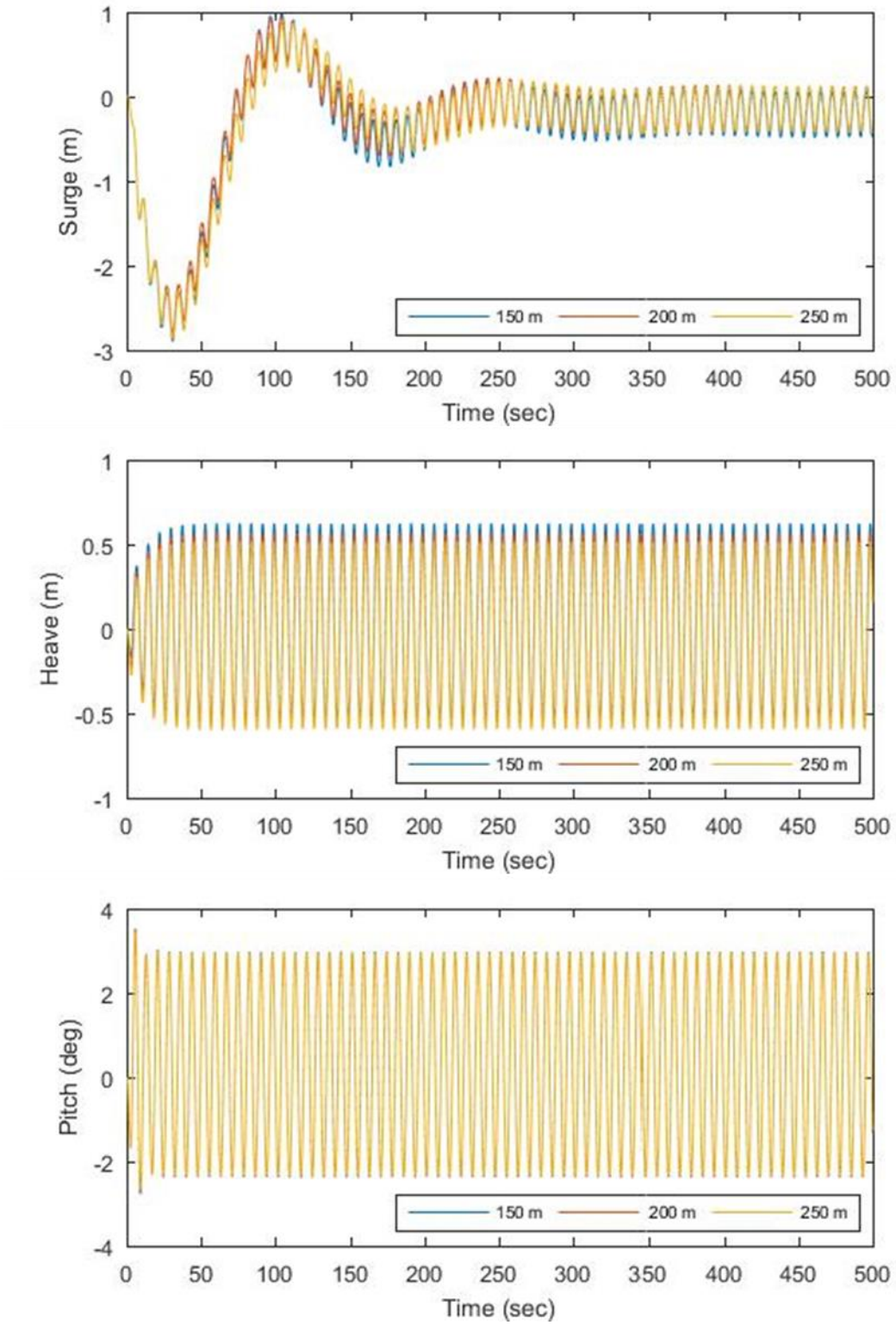

Figure 58: Motions of catenary system for examined water depths (case 1)

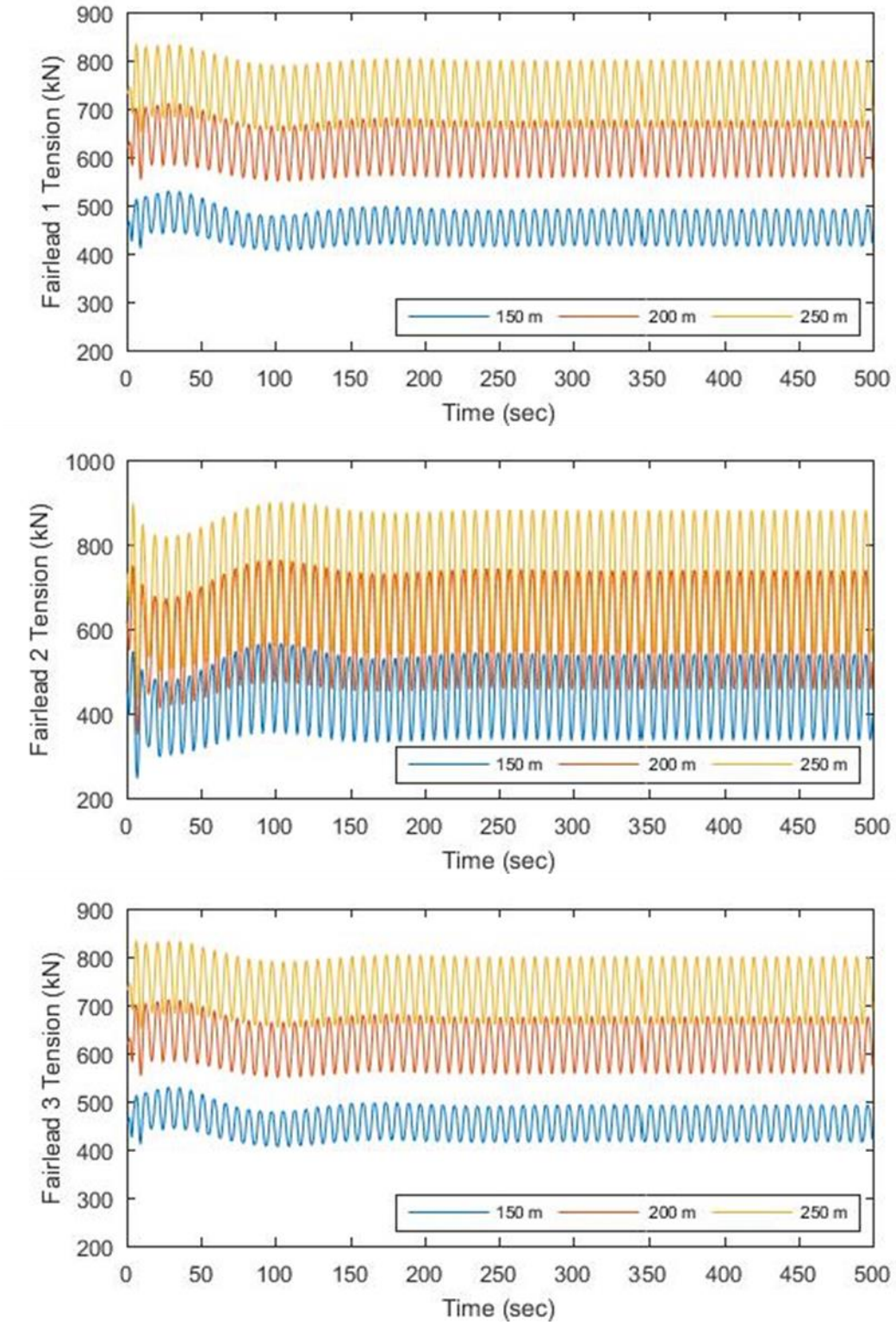

Figure 59: Fairlead tensions of catenary system for examined water depths (case 1)

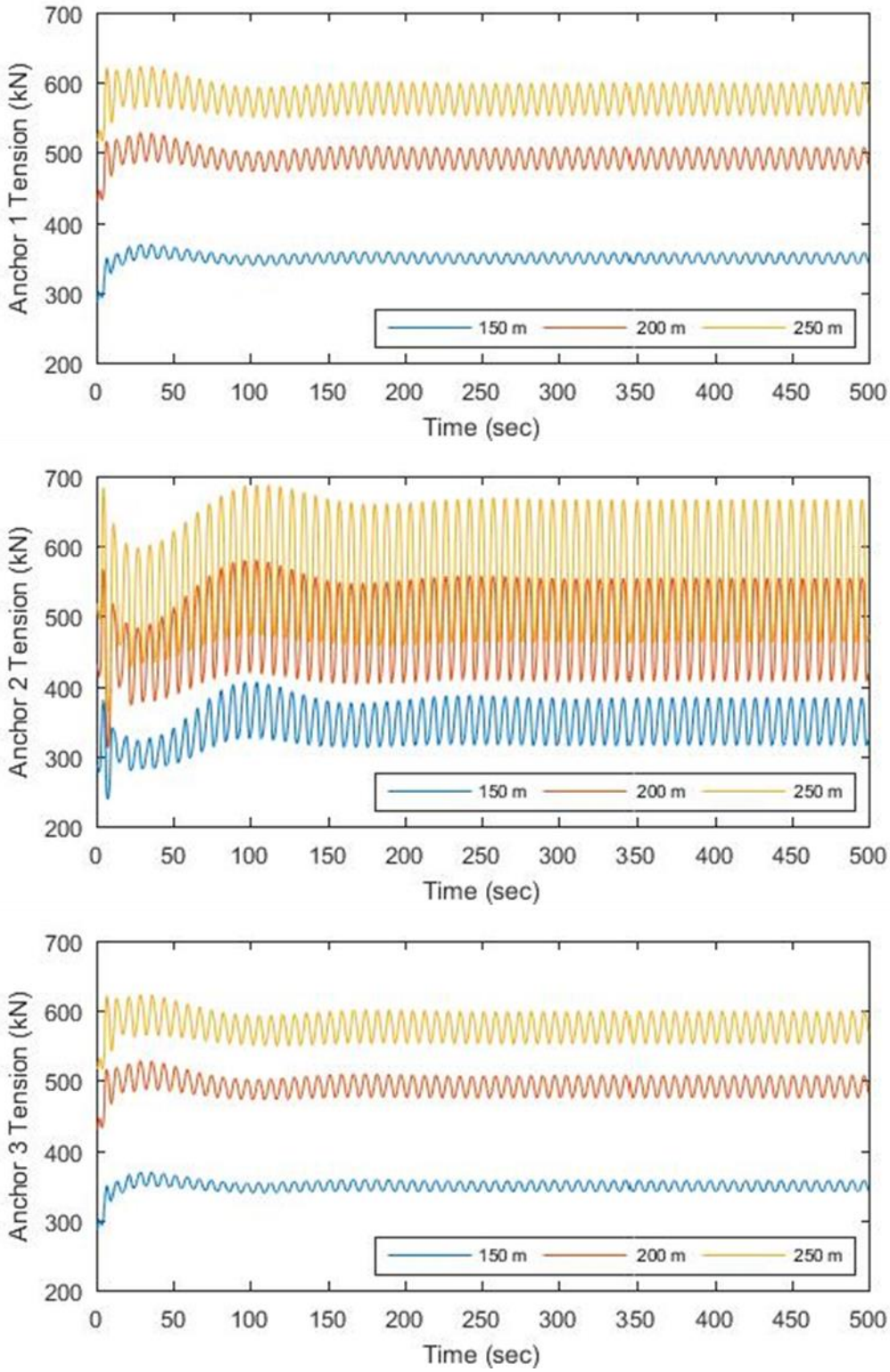

Figure 60: Anchor tensions of catenary system for examined water depths (case 1)

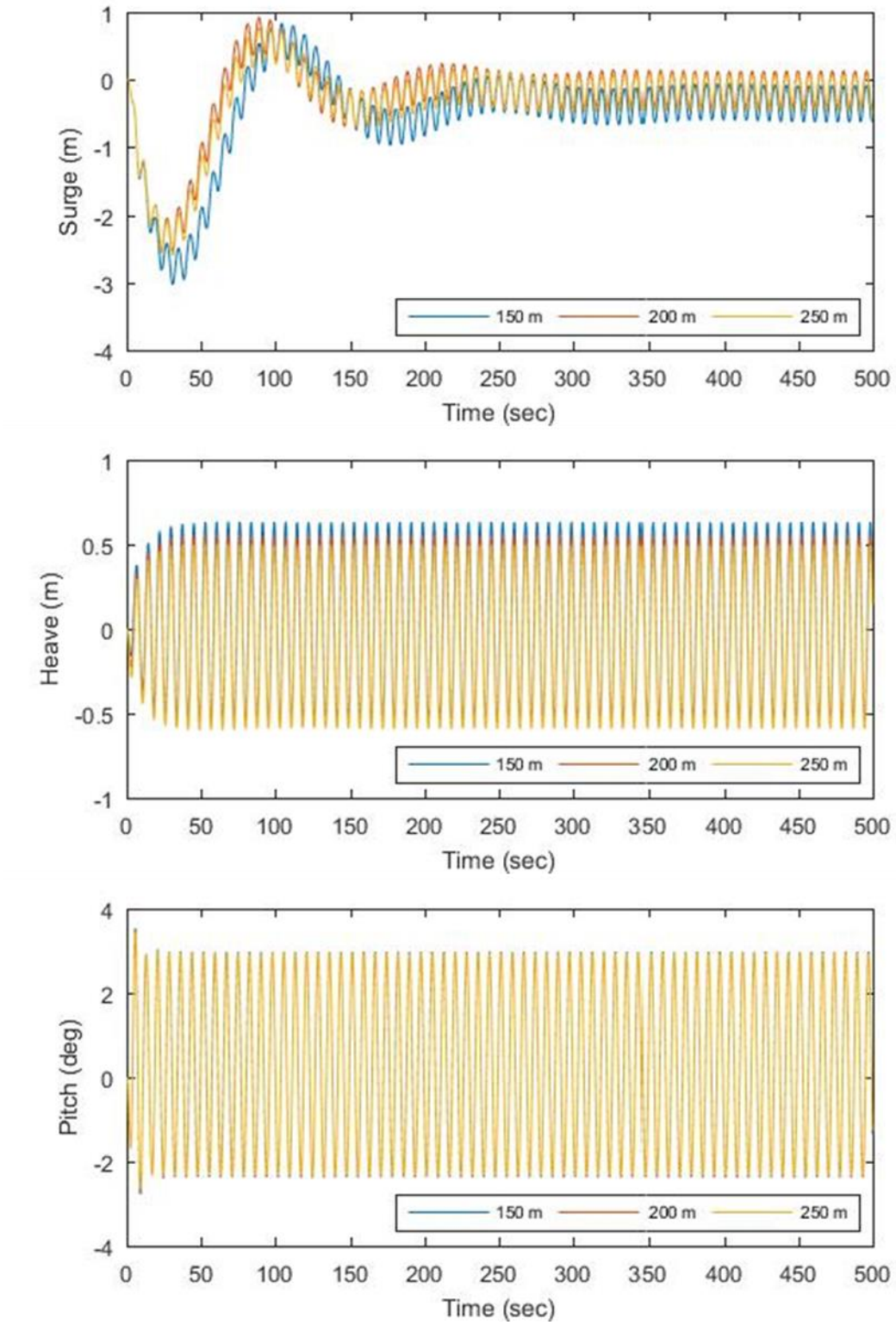

Figure 61: Motions of semi-taut system for examined water depths (case 1)

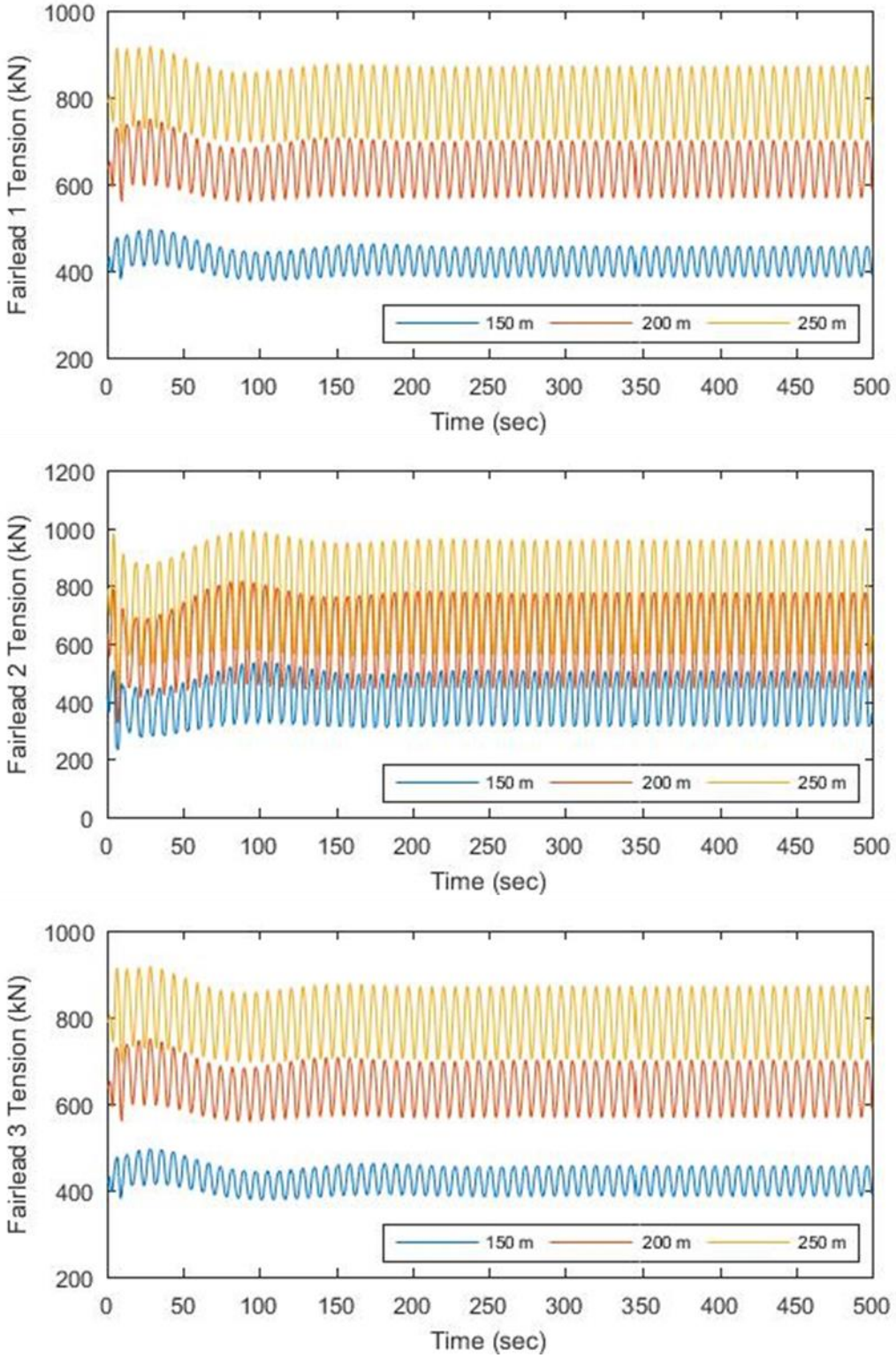

Figure 62: Fairlead tensions of semi-taut system for examined water depths (case 1)

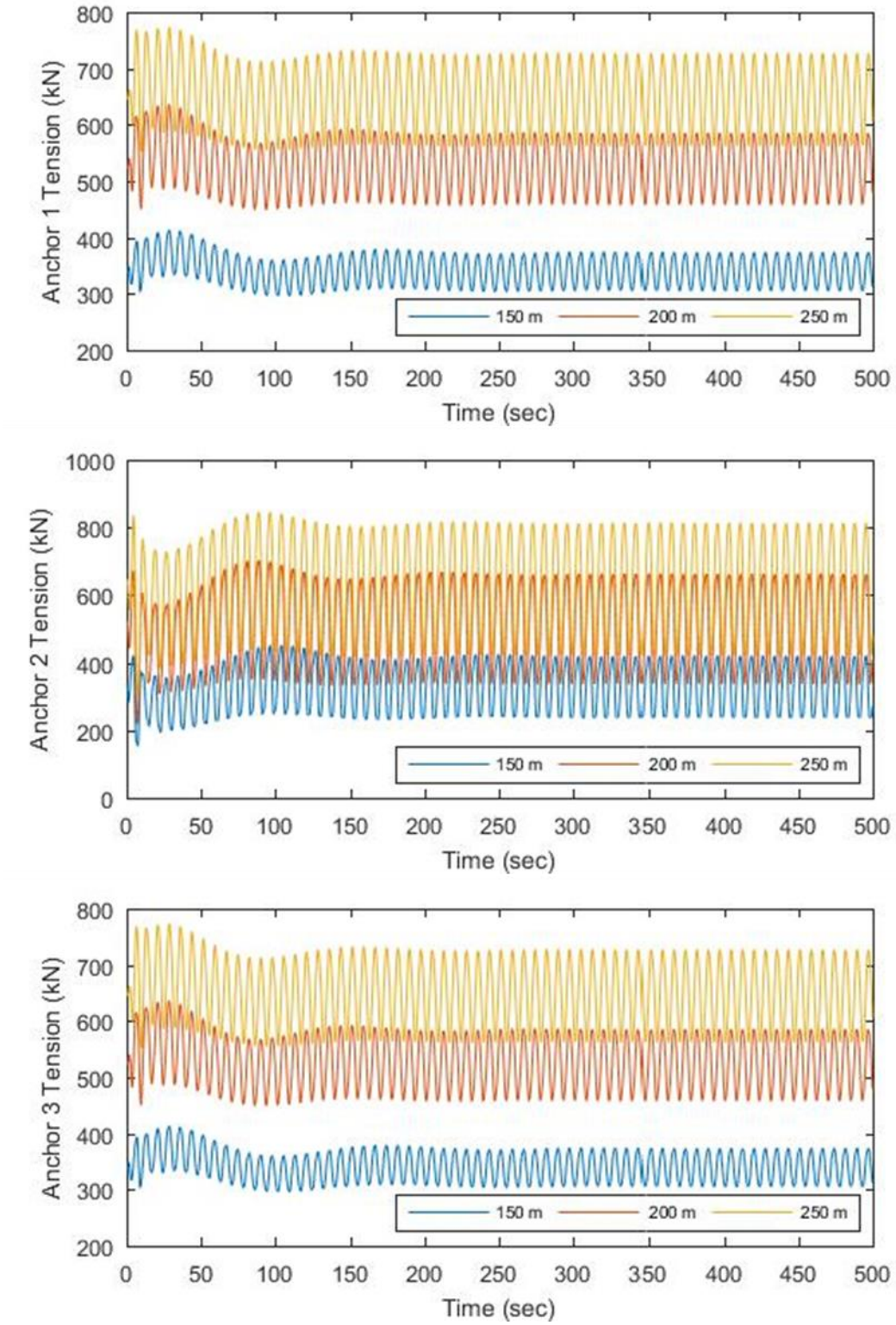

Figure 63: Anchor tensions of semi-taut system for examined water depths (case 1)

Influence of Water Depth Variation – Load Case 2

The water depth variation was also considered with regard to extreme conditions where the platform is subjected to irregular wave excitation loads. The degrees of freedom surge, heave, and pitch for different water depths using catenary and semi-taut mooring are plotted in time series as in Figure 64 and Figure 67 respectively. The motion responses are similar despite of the little difference due to influence of mooring length. It should be noted that the motions of the platform in translational and rotational field are not affected the different water depth. From the results of mooring responses in Figure 65, Figure 66, Figure 68 and Figure 69, the trends of the graphs are almost identical to those under regular wave condition. The largest tension values were obtained in 250 m water depth for both catenary and semi-taut system.

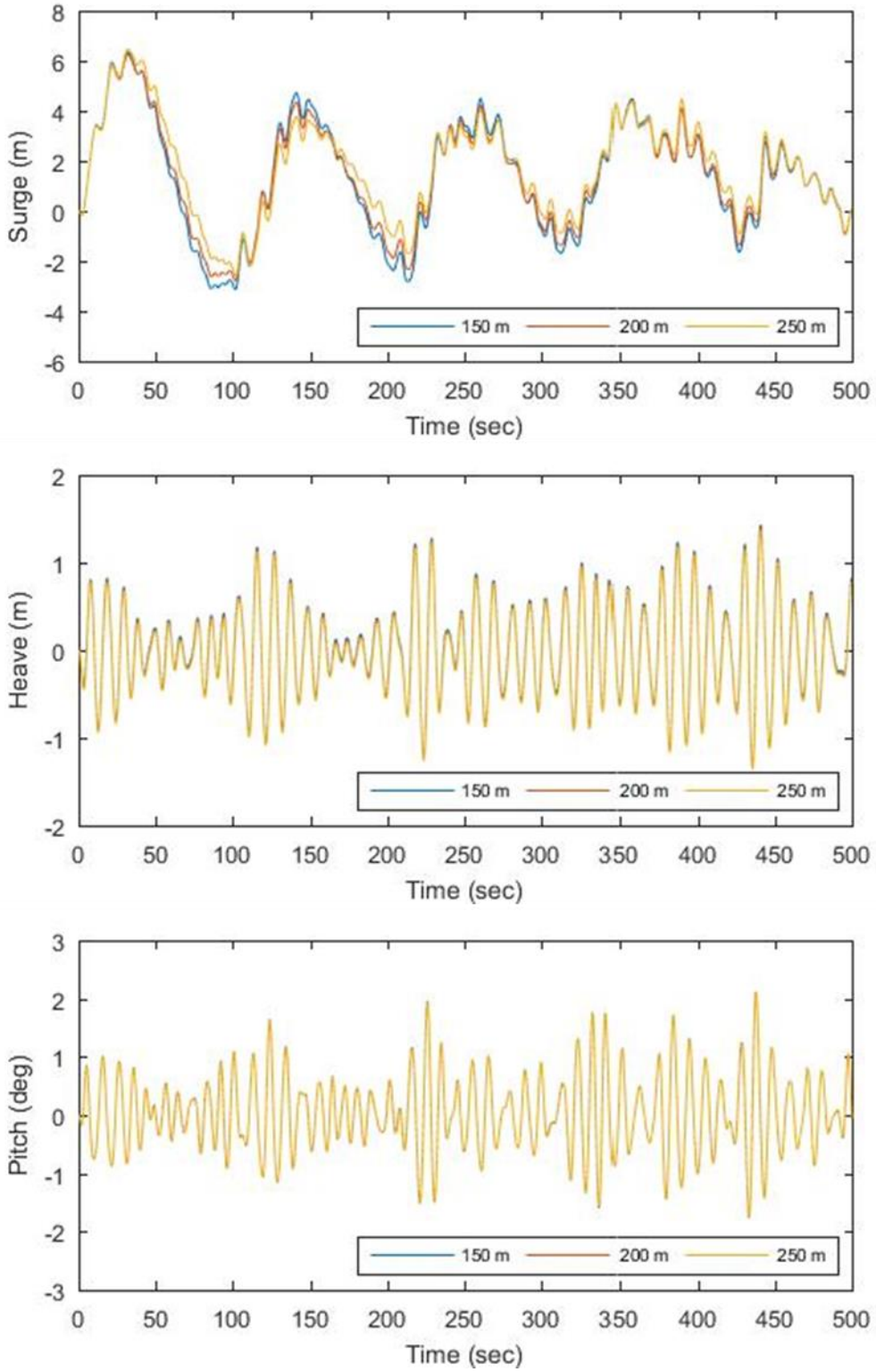

Figure 64: Motions of catenary system for examined water depths (load case 2)

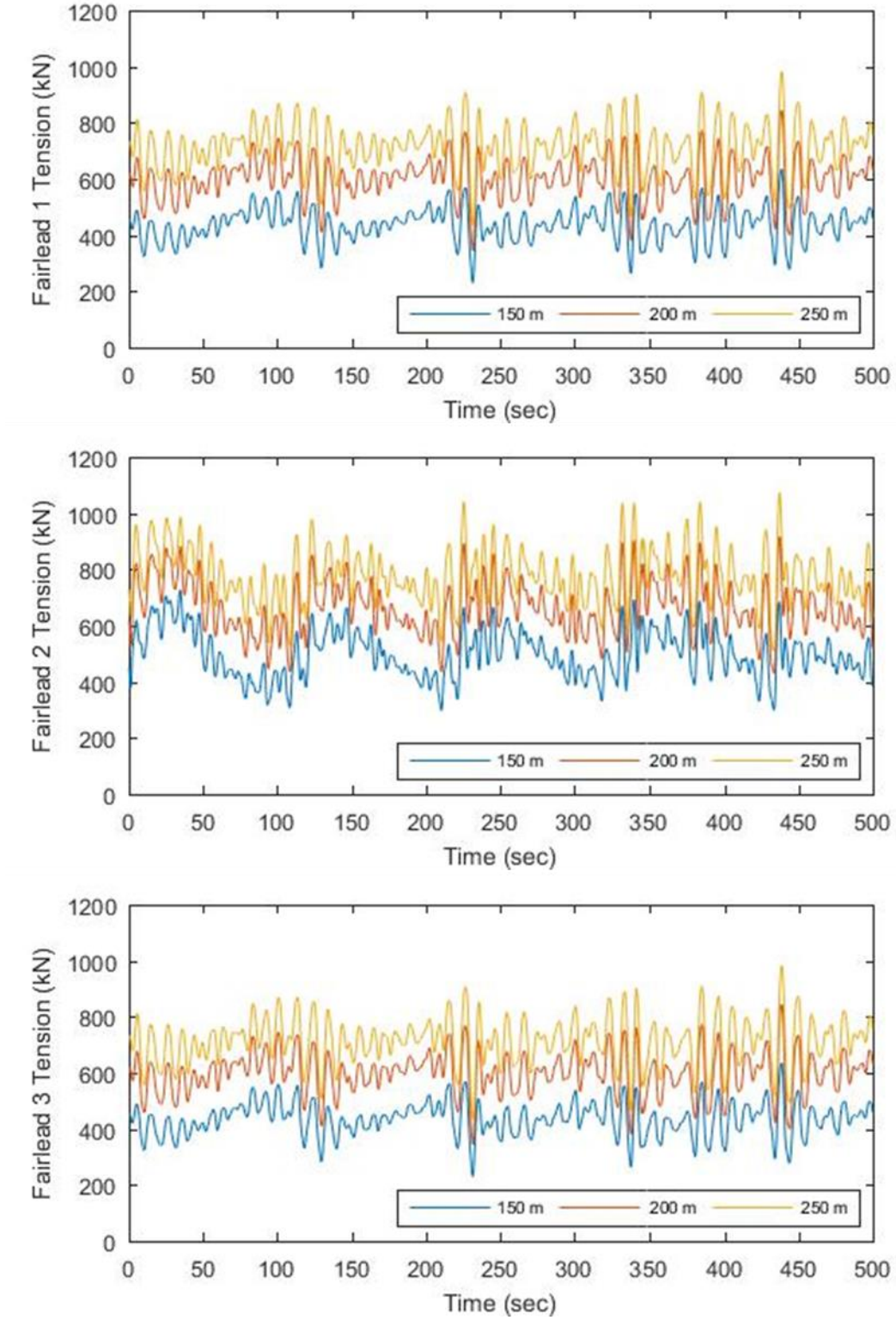

Figure 65: Fairlead tensions of catenary system for examined water depths (case 2)

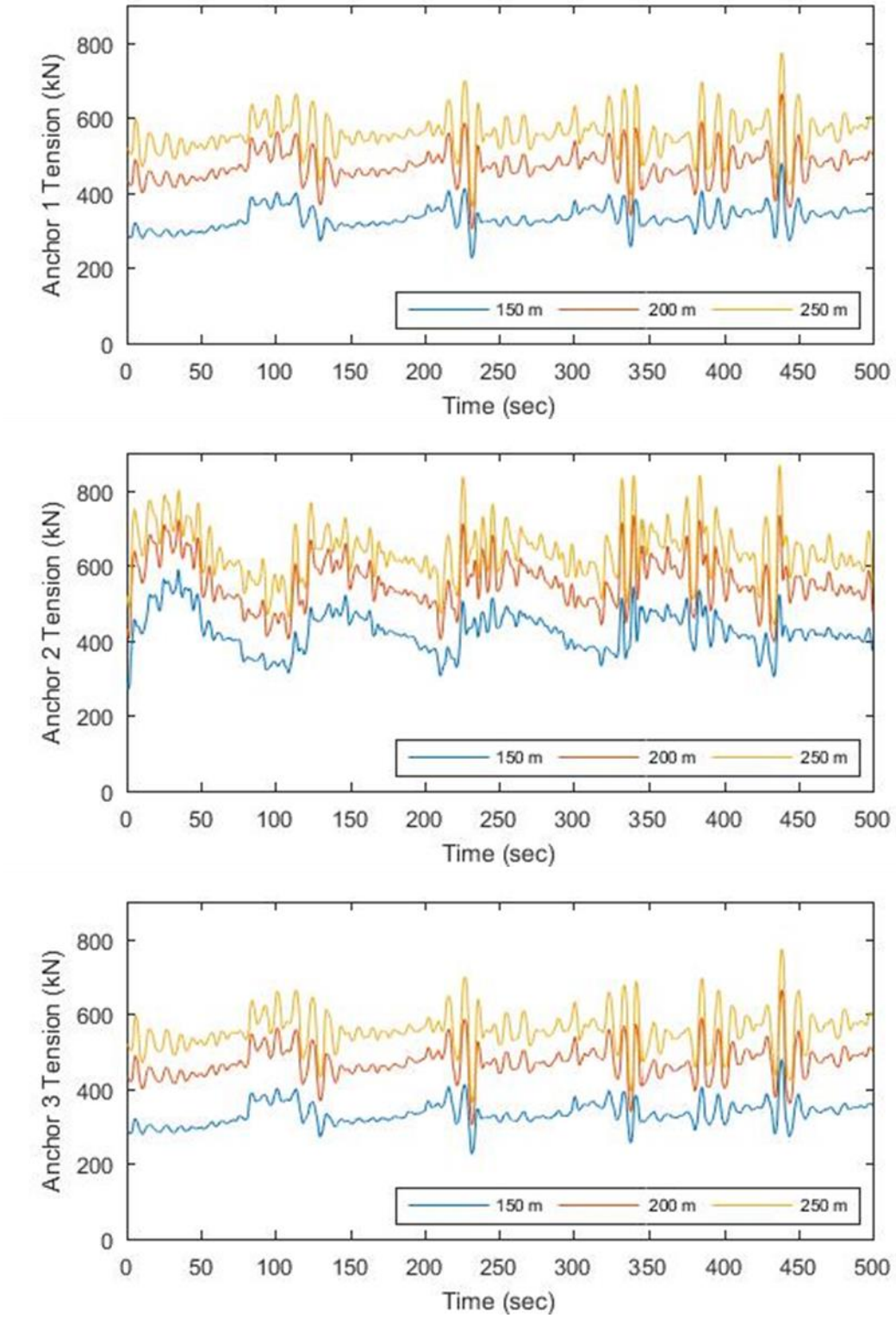

Figure 66: Anchor tensions of catenary system for examined water depths (case 2)

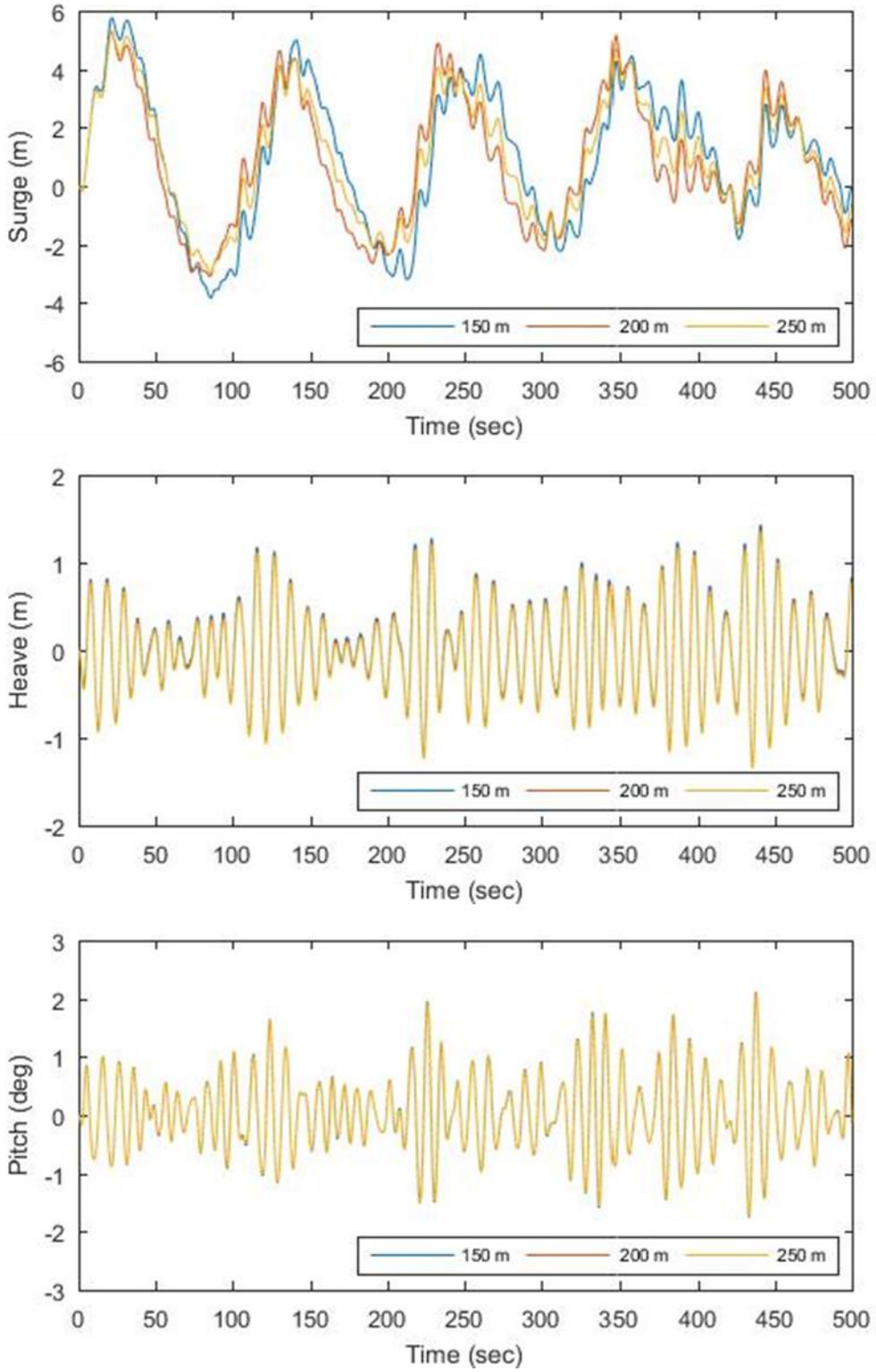

Figure 67: Motions of semi-taut system for examined water depths (load case 2)

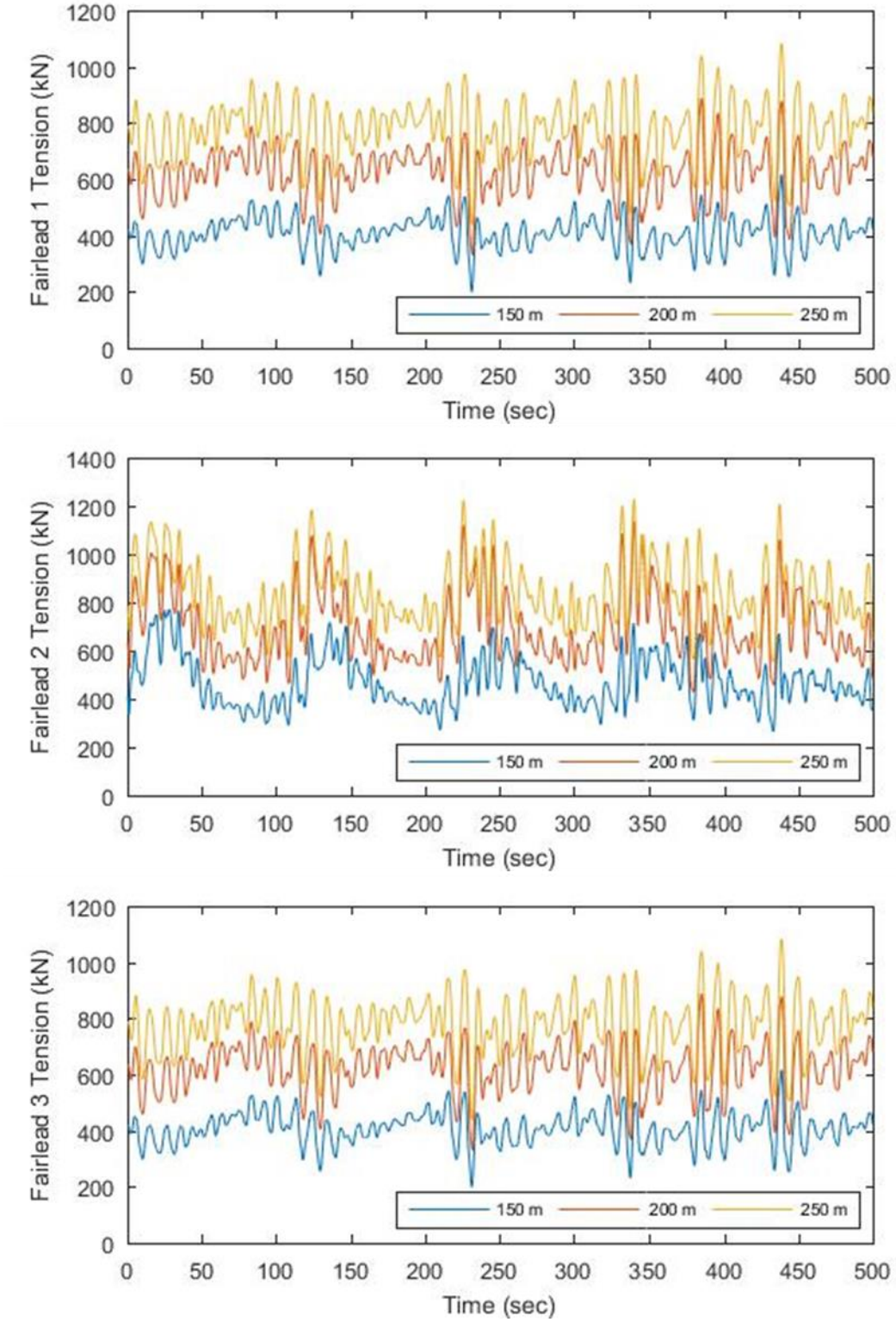

Figure 68: Fairlead tensions of semi-taut system for examined water depths (case 2)

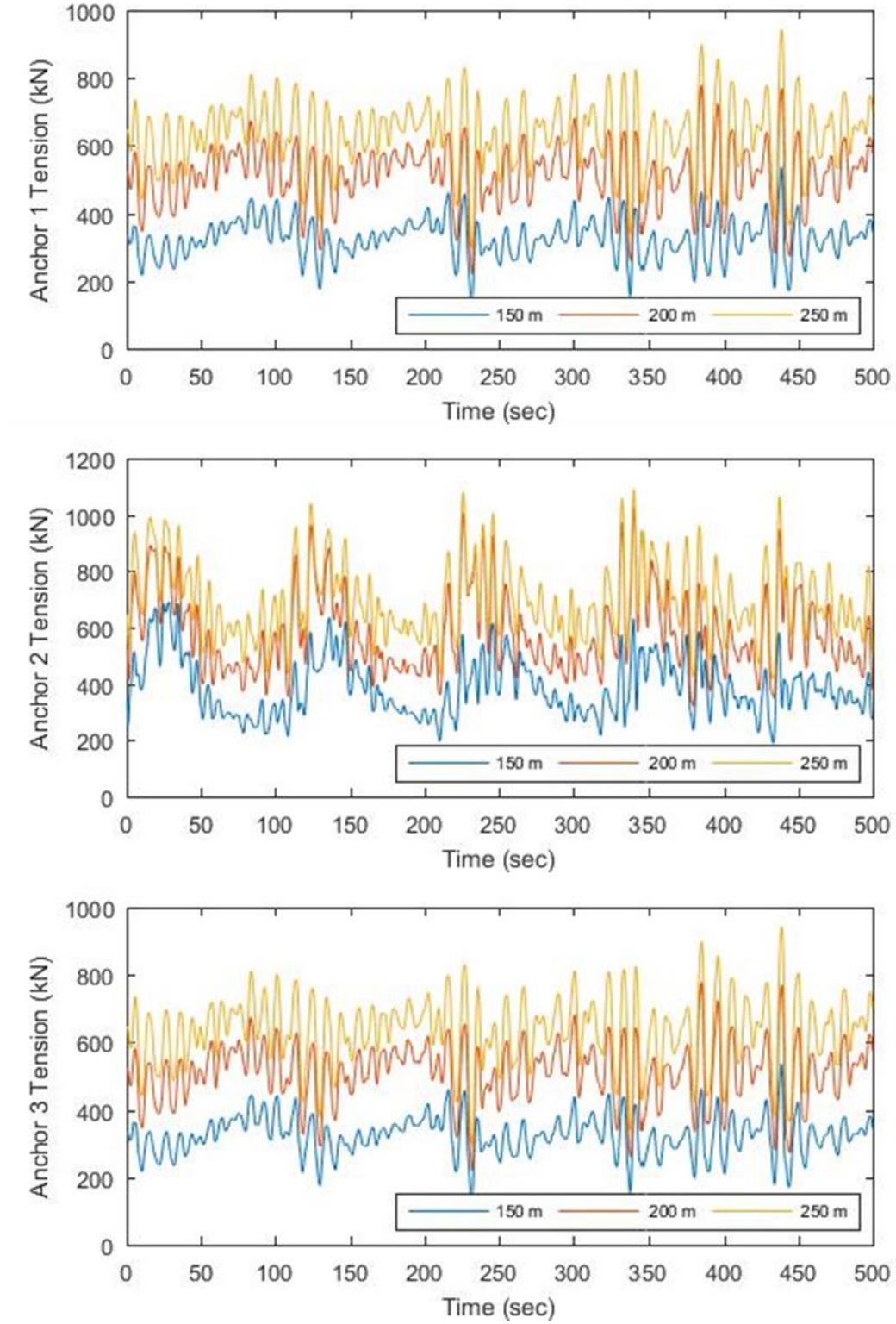

Figure 69: Anchor tensions of semi-taut system for examined water depths (case 2)

Influence of Water Depth Variation – Load Case 3

The sea is defined by a regular wave with steady wind conditions in this section. The results from this simulation are plotted in Figure 70 through Figure 75. Similar to the previous case, the comparison of different depths suggests the average surge motion is not significantly influenced by the different water depth although small variation is observed due to changing mooring configurations. Once again, the heave and pitch comparisons reveal each type of mooring model is very similar regardless of water depth difference. In reference to the tension time series plots in Figure 71, Figure 72, Figure 74 and Figure 75, large differences between the water depths occurred in both slack and semi-taut mooring systems. When wind is included, significant drop-offs are shown in the unloaded mooring lines, although larger extreme values were captured in the most loaded mooring line. In this case, the semi-taut system had significant difference in tension values between different water depths, as opposed to the system using slack mooring lines. A larger variance is seen in the semi-taut mooring tensions in response to the wind excitation which requires horizontal loads to resist. In the semi-taut mooring, the anchor loads are both horizontal and vertical which masks the system sensitive to horizontal environmental loads.

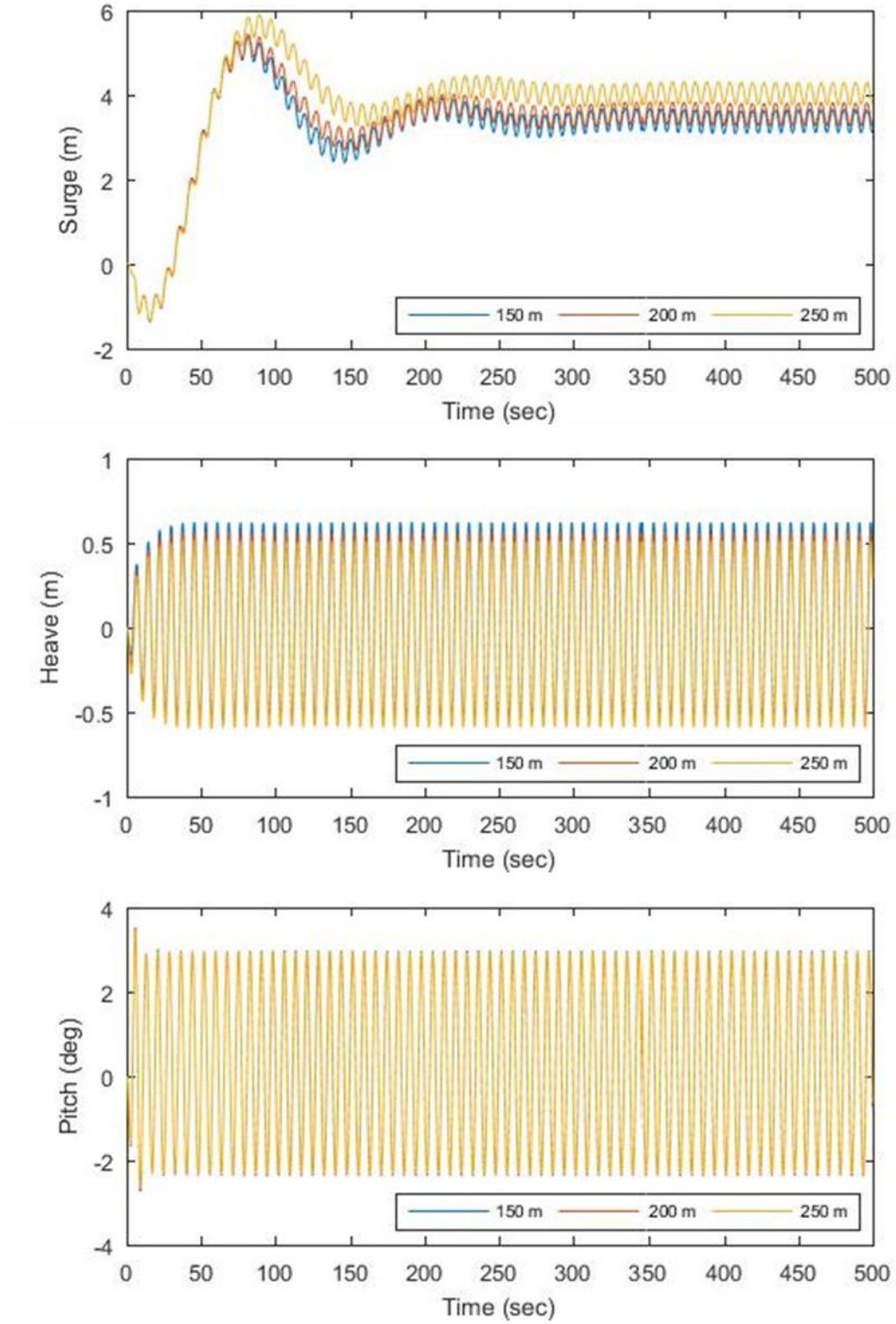

Figure 70: Motions of catenary system for examined water depths (load case 3)

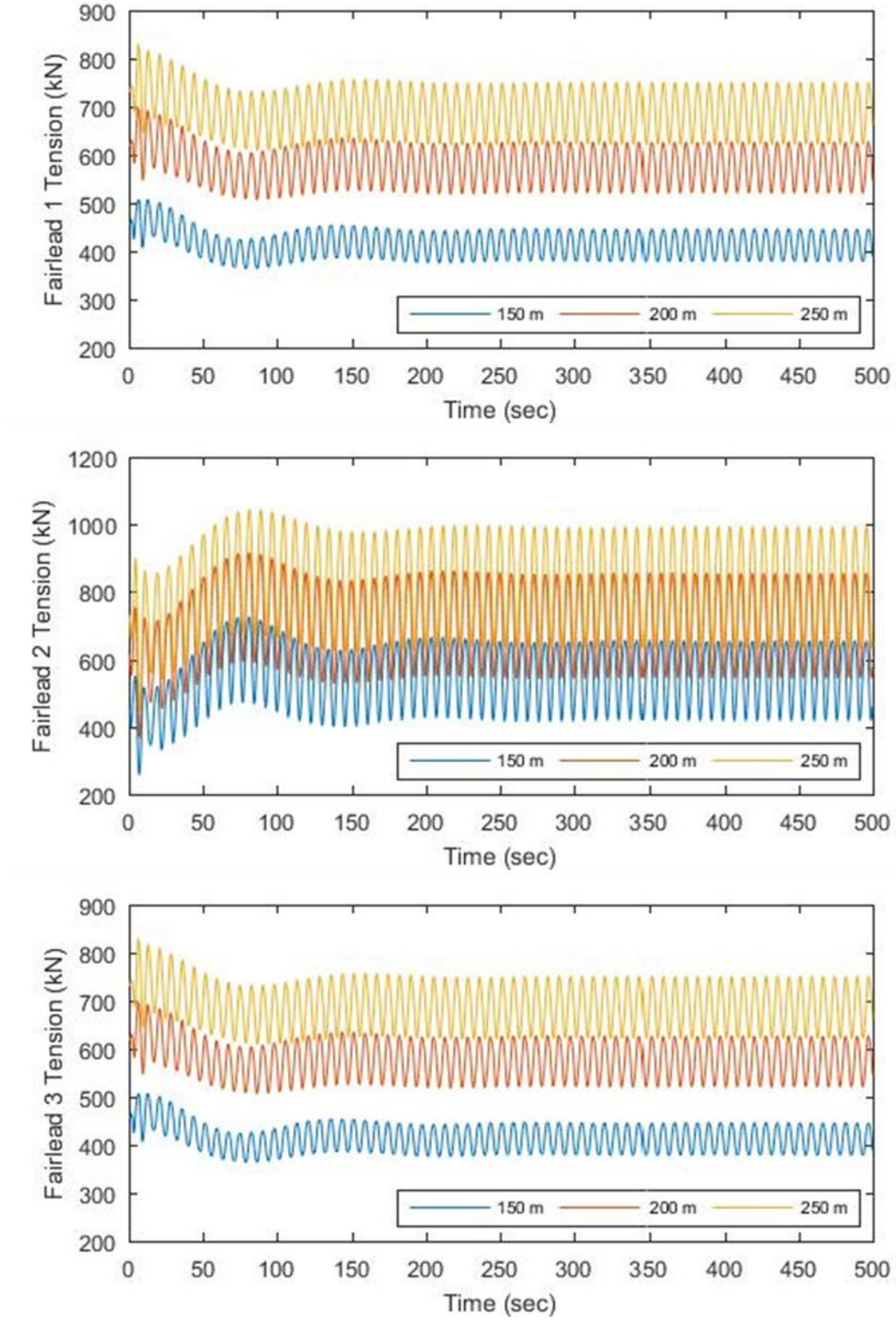

Figure 71: Fairlead tensions of catenary system for examined water depths (case 3)

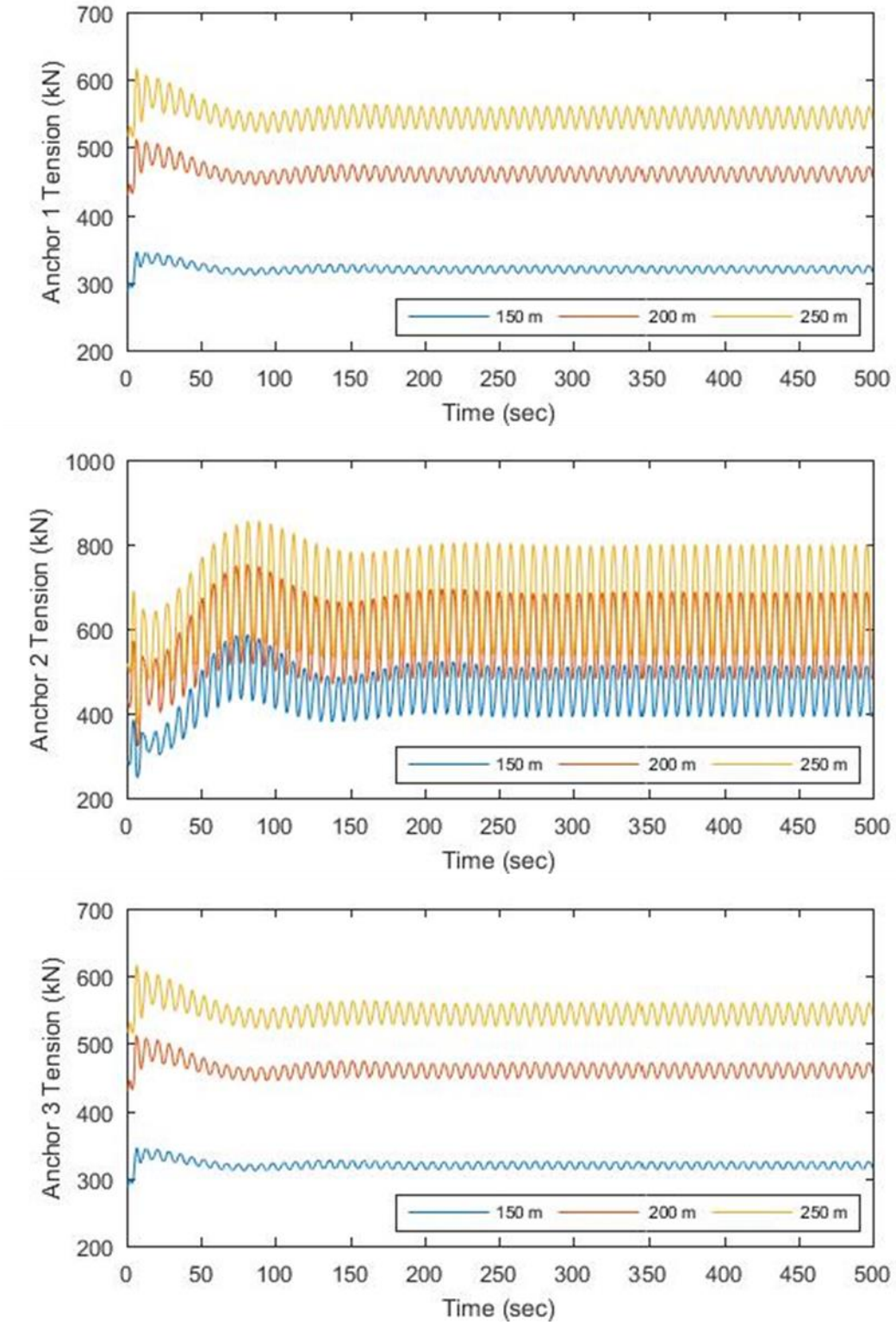

Figure 72: Anchor tensions of catenary system for examined water depths (case 3)

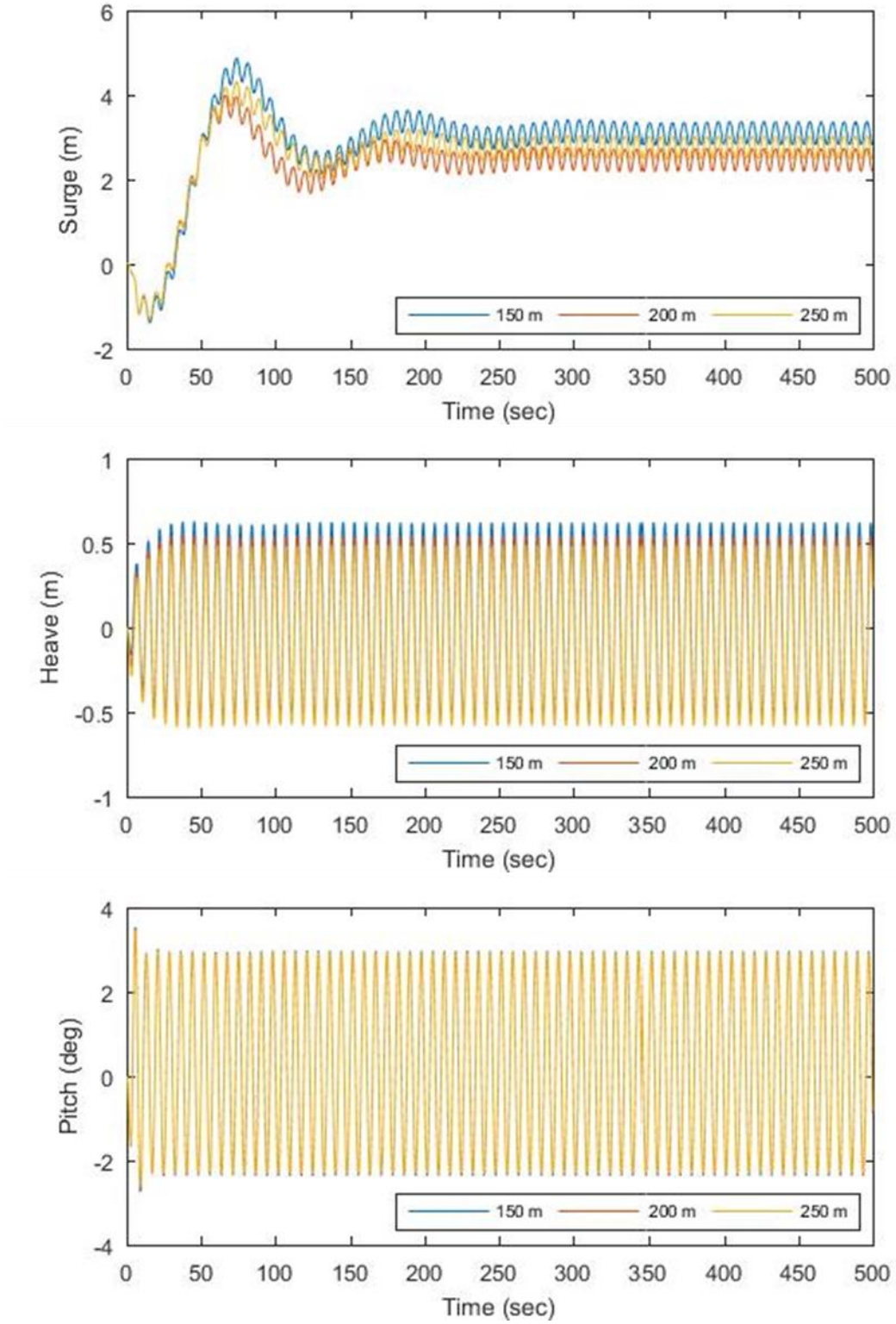

Figure 73: Motions of semi-taut system for examined water depths (load case 3)

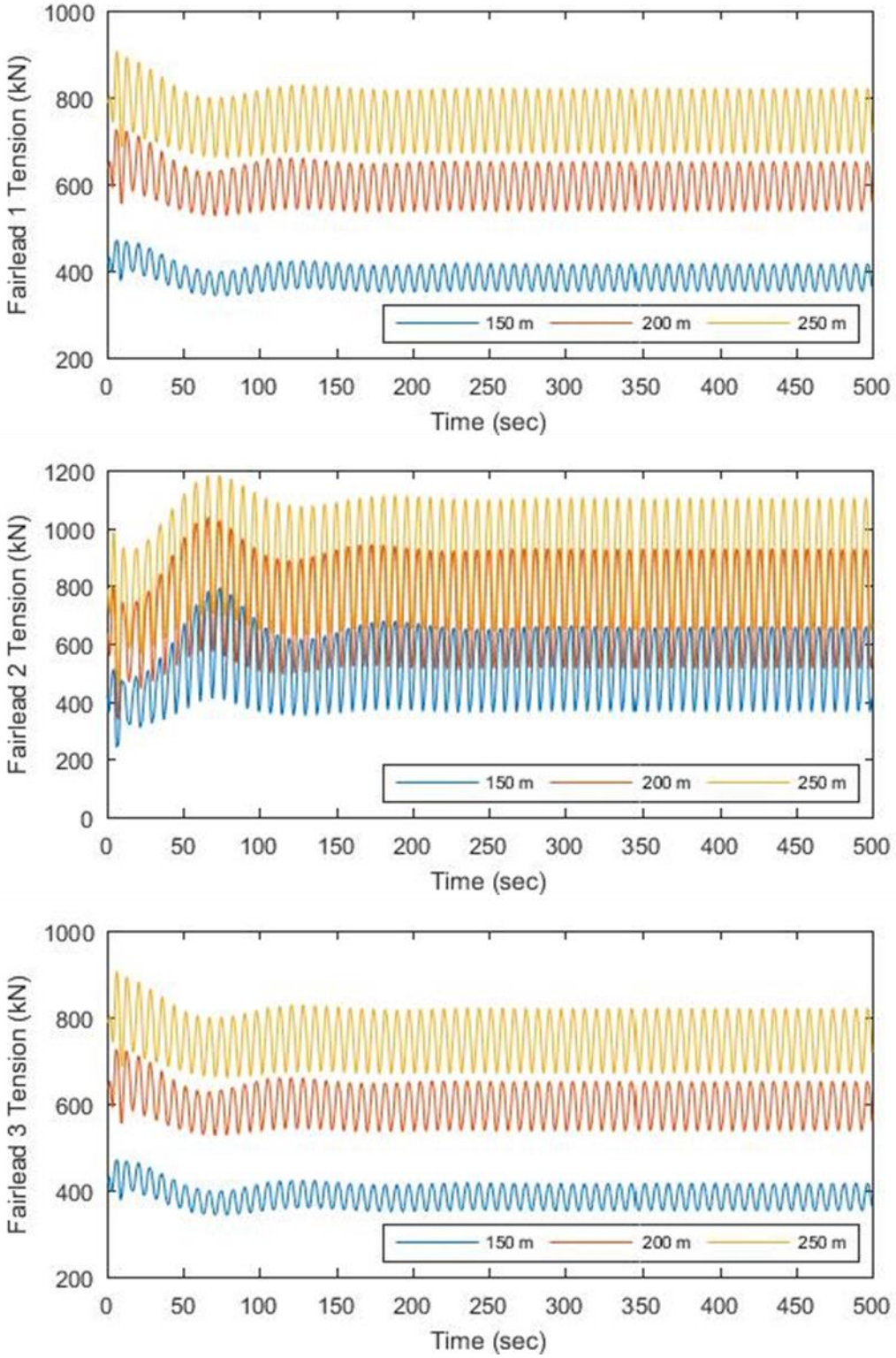

Figure 74: Fairlead tensions of semi-taut system for examined water depths (case 3)

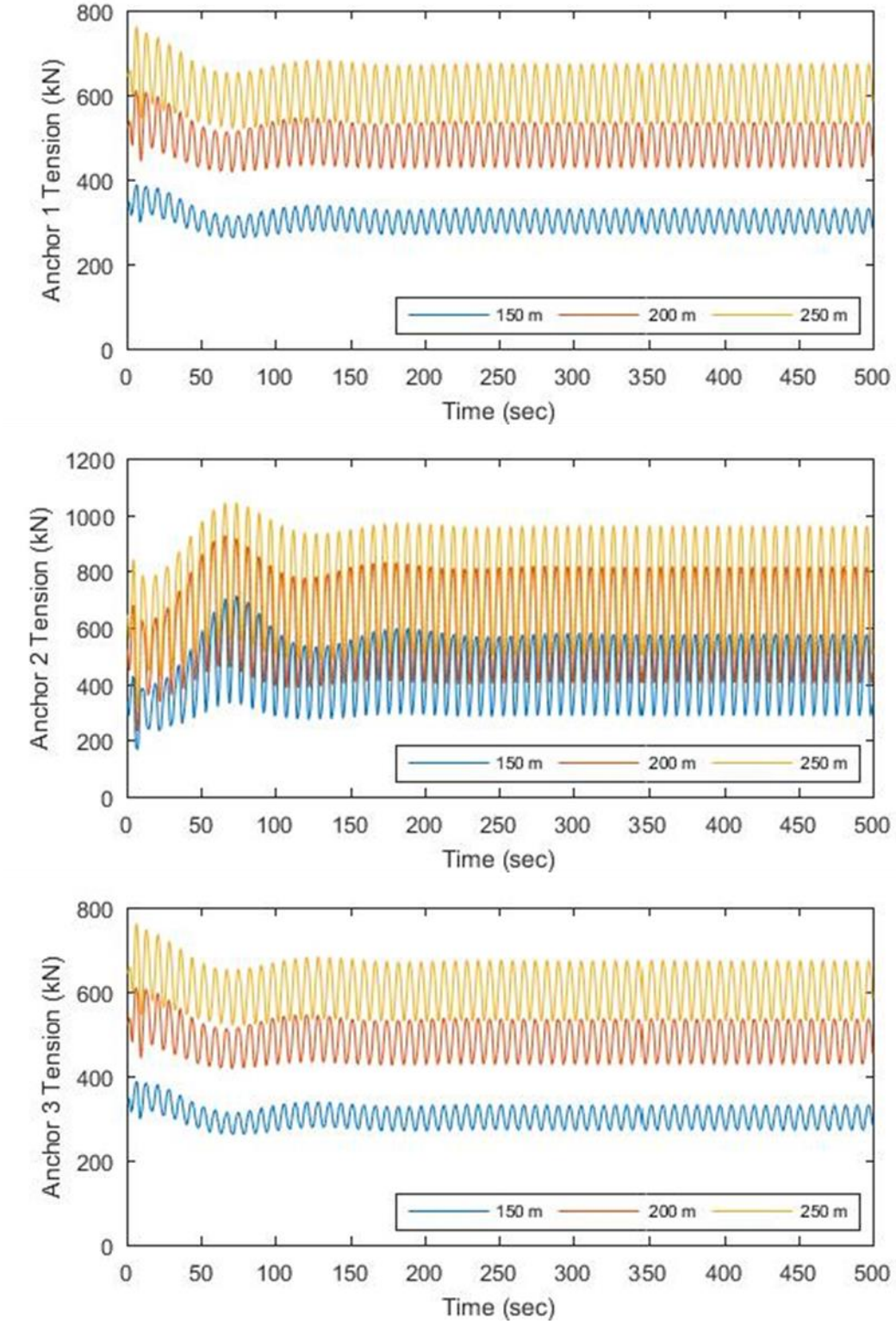

Figure 75: Anchor tensions of semi-taut system for examined water depths (case 3)

Influence of Water Depth Variation – Load Case 4

The next set of comparison involves a condition of irregular waves with sheared wind. Figure 76 and Figure 79 show the comparison of selected responses including surge, heave and pitch time series in different water depths for both catenary and semi-taut system. For the examined time series motions, the differences are seen only in the surge motion, but those are in a very small order. The average mooring line tensions are still 150 m < 200 m < 250 m for the two types of mooring system as found in Figure 77, Figure 78, Figure 80 and Figure 81. Although the catenary system is introducing additional damping by enlarging the total mooring length in deeper water, the amplitudes are smaller than those in semi-taut shape. Hence it can be deduced that the catenary shape could be less sensitive to change in water depth as far as it is deployed in a range of shallow water. For the extreme condition with ultra-deep water, the survivability analysis is required to avoid under-prediction of mooring loads.

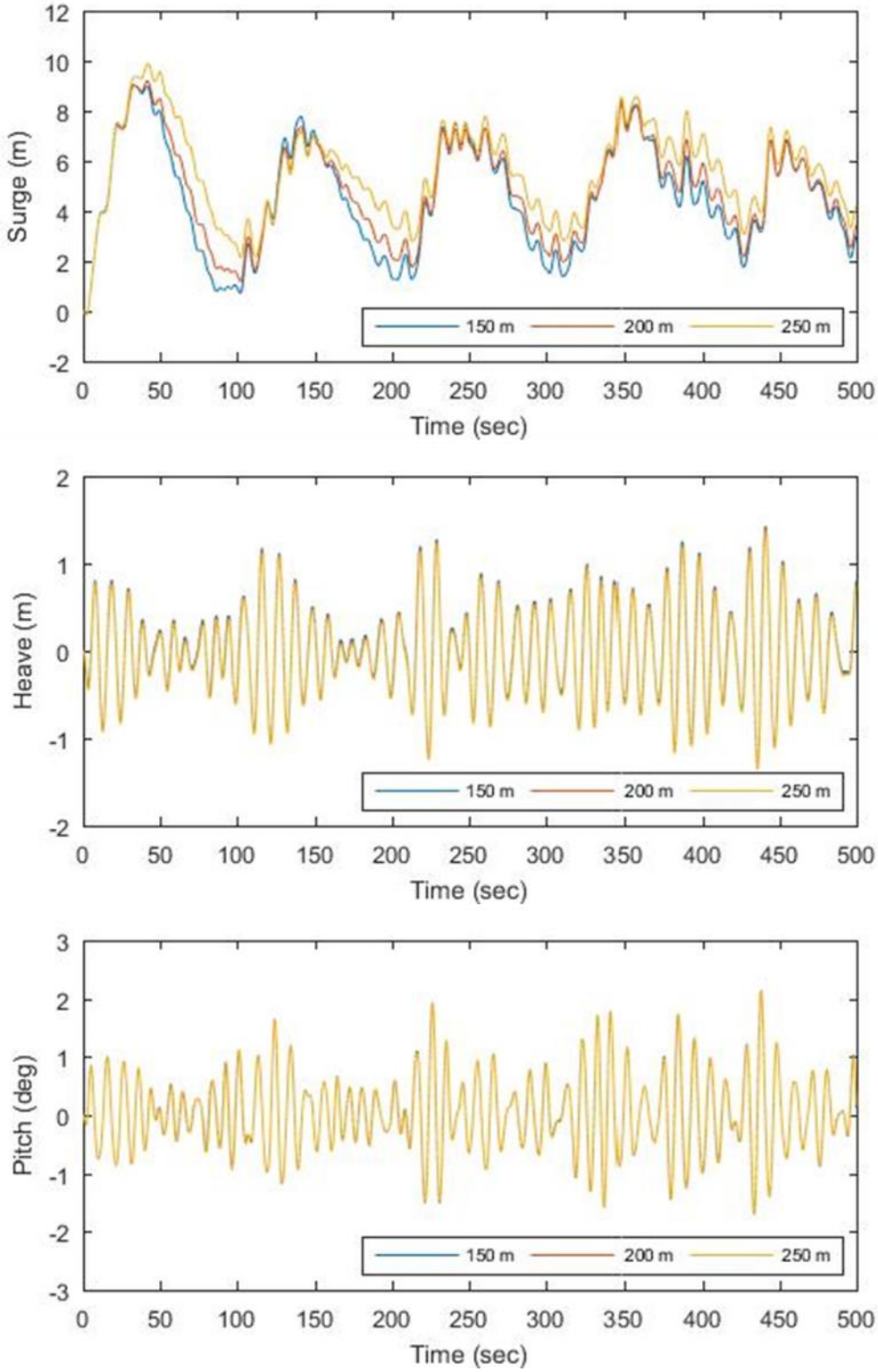

Figure 76: Motions of catenary system for examined water depths (load case 4)

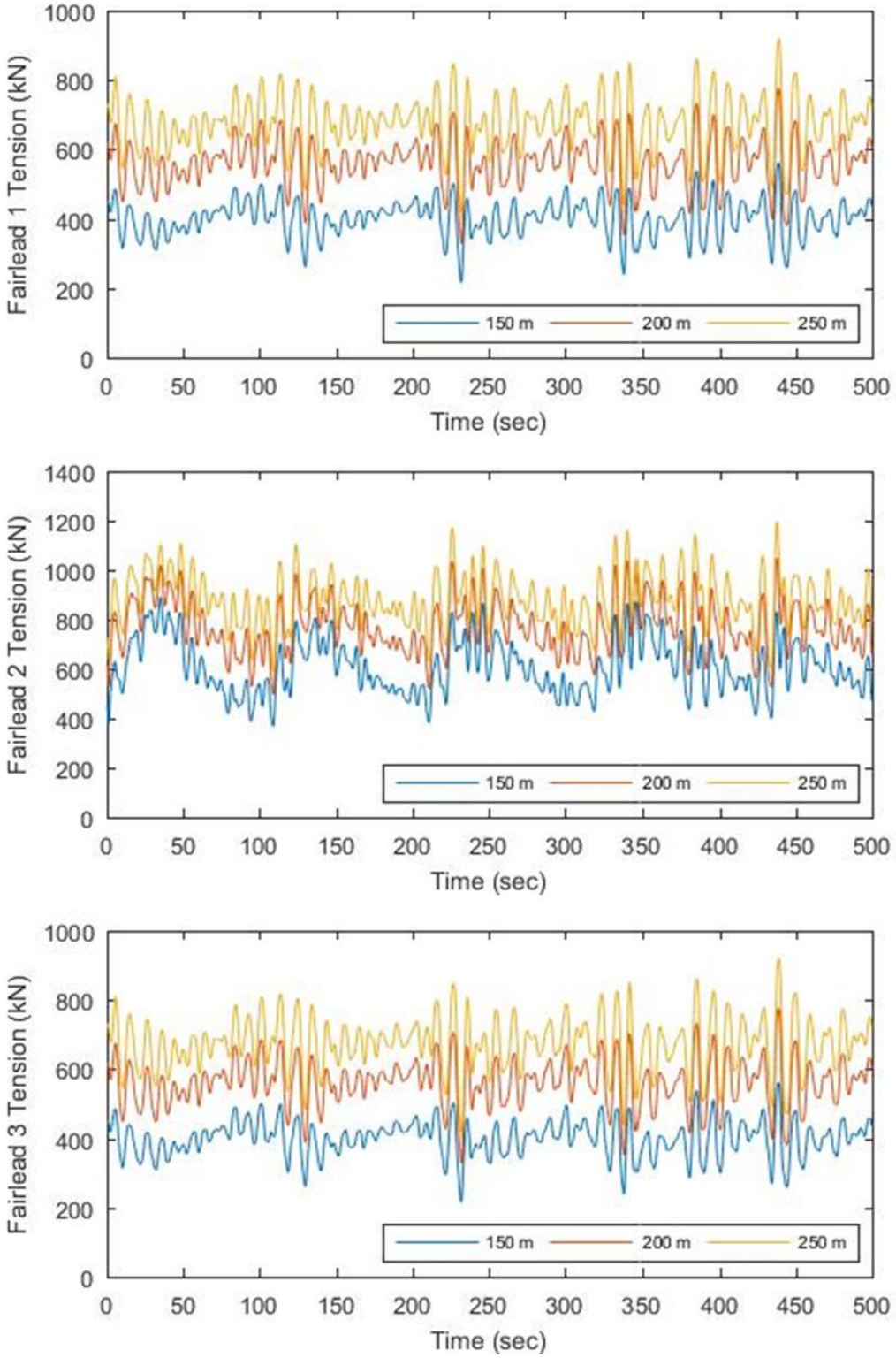

Figure 77: Fairlead tensions of catenary system for examined water depths (case 4)

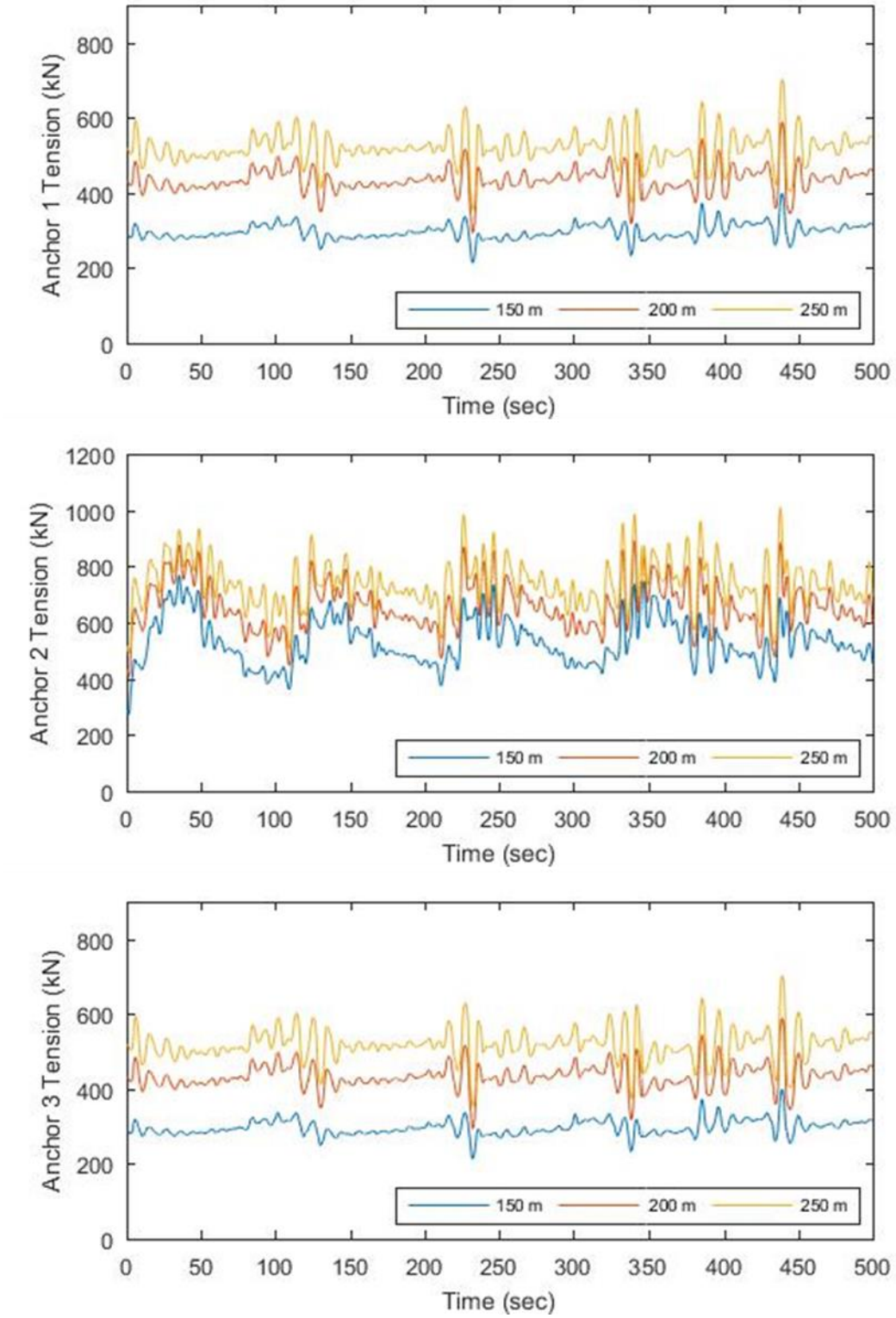

Figure 78: Anchor tensions of catenary system for examined water depths (case 4)

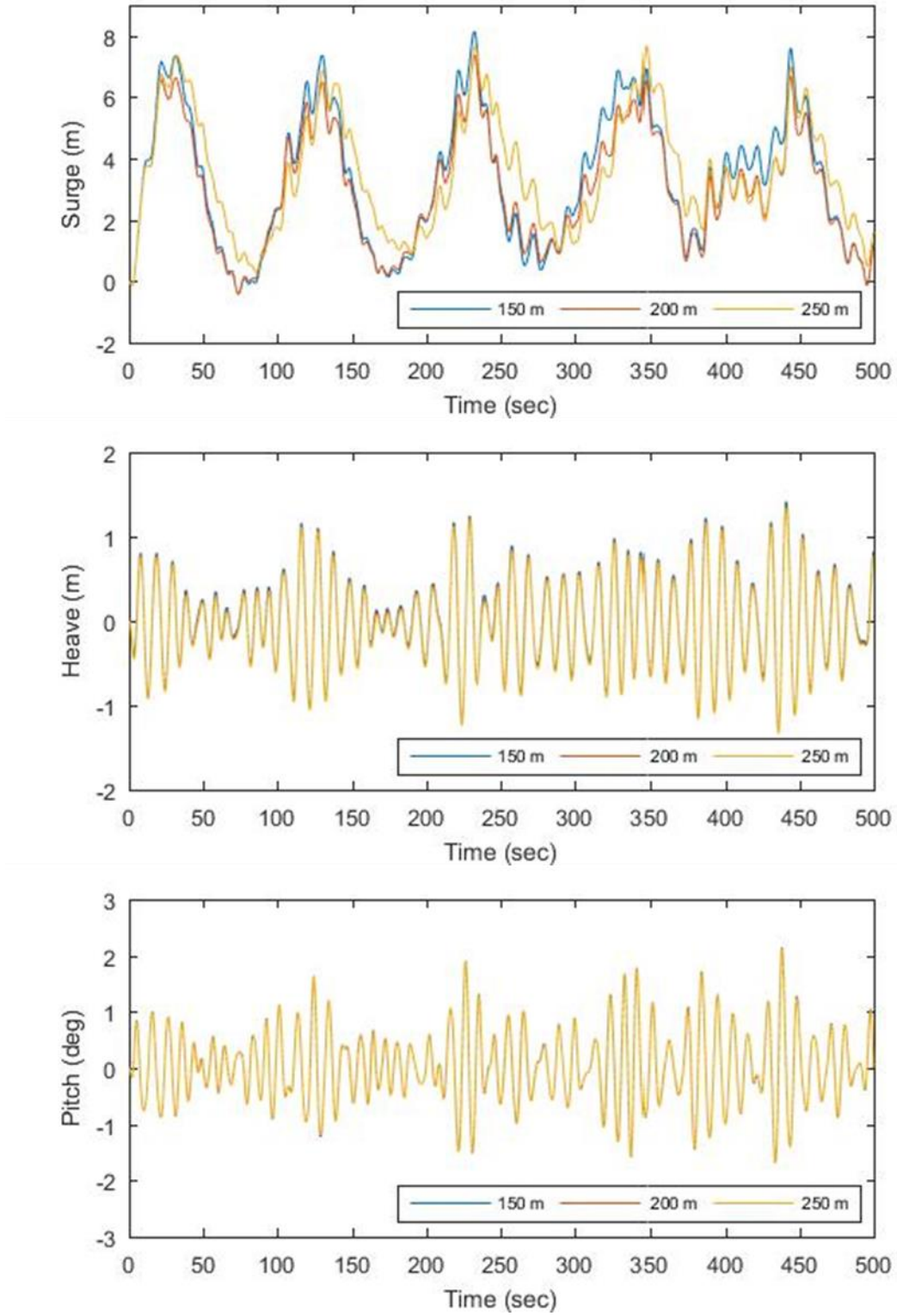

Figure 79: Motions of semi-taut system for examined water depths (load case 4)

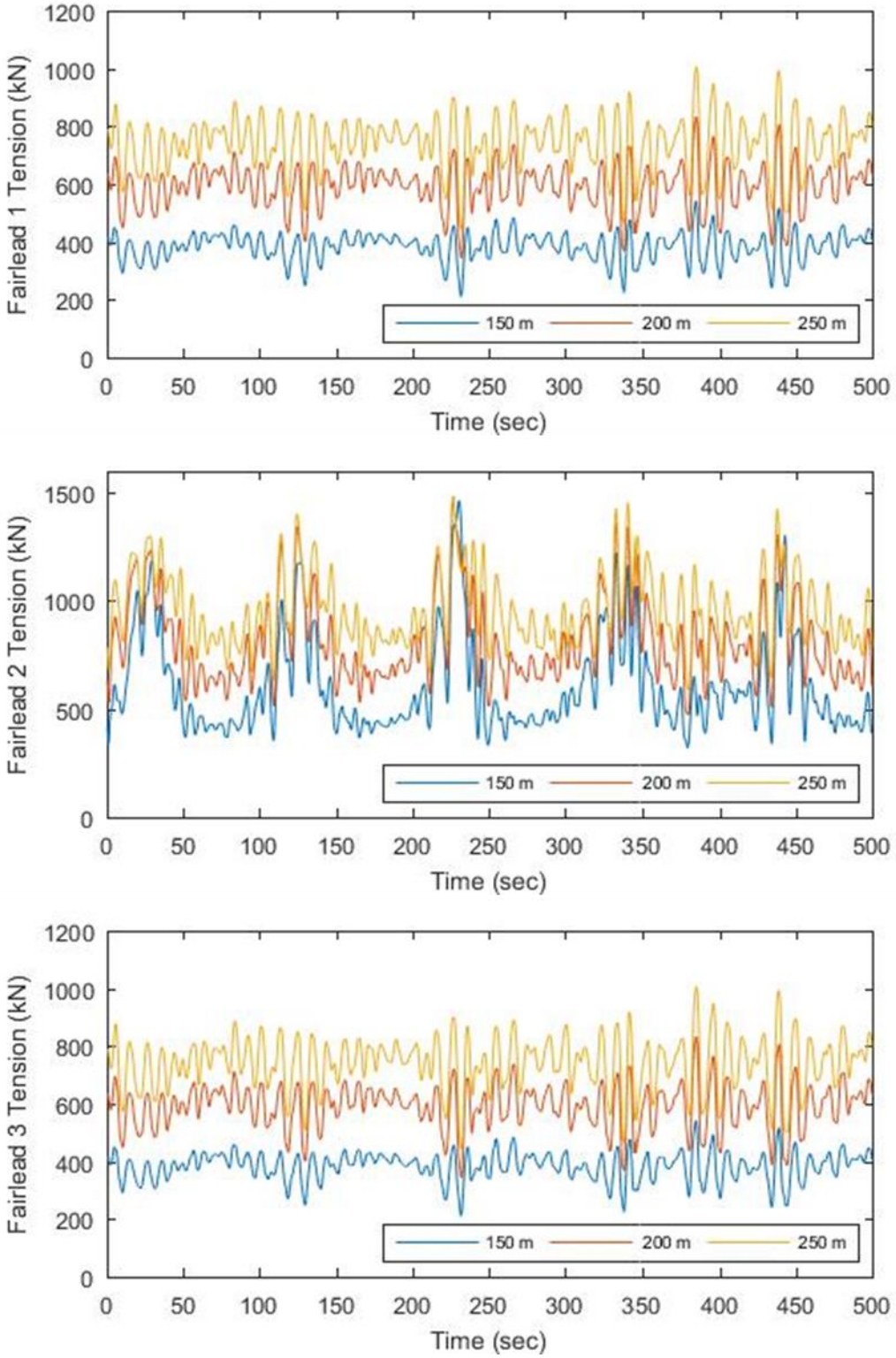

Figure 80: Fairlead tensions of semi-taut system for examined water depths (case 4)

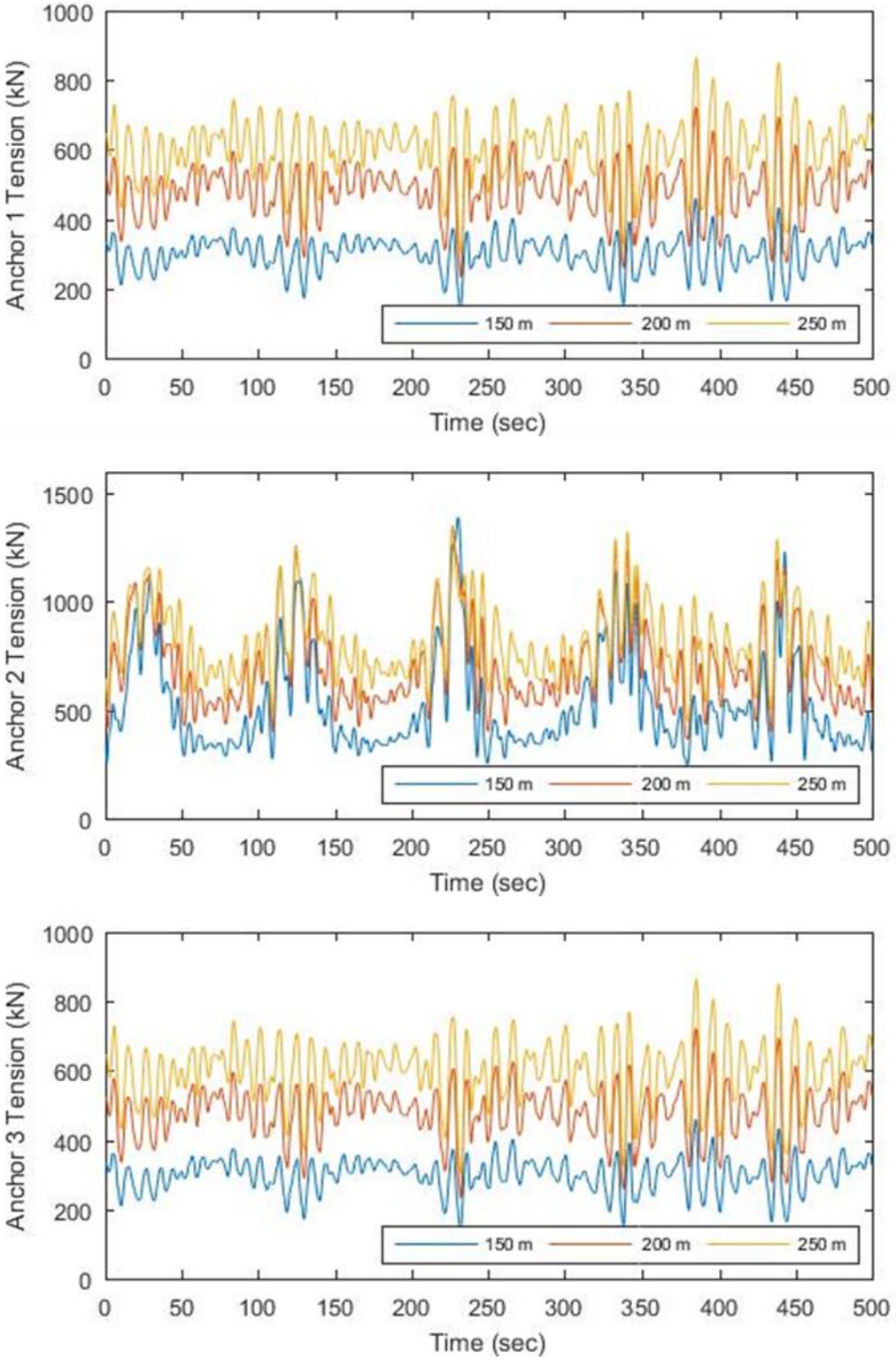

Figure 81: Anchor tensions of semi-taut system for examined water depths (case 4)

Influence of Water Depth Variation – Load Case 5

In Figure 82 and Figure 85, the characteristics of the motions for catenary and semi-taut mooring are compared with three different water depths respectively. The examined environmental condition includes regular waves, sheared wind and power law current profile. It should be noted that time series of each response for both catenary and semi-taut system is not found to be affected by the influence of water depth variation. As far as the surge motions of two mooring systems, little deviation in average values is observed due to the mooring length change. The total mooring line length increases with deeper water depth, and thus the efficient mooring length is decreased with additional damping contribution. The increase in surge with the water depth increase is because the lowered stiffness provides additional translation motions. However, the offset is considered as a negligible amount, which is solely affected by the mooring system.

On the other hand, the modification of the water depth revealed different dynamic behavior of the mooring lines. According to the graphs presented in Figure 83, Figure 84, Figure 86 and Figure 87, the tensions responses for both catenary and semi-taut system are undergoing increased stress with deeper water depth. Consequently, the functionality of the wind turbine is verified to be affected by the different water depth, which means an optimization will be required for other installations.

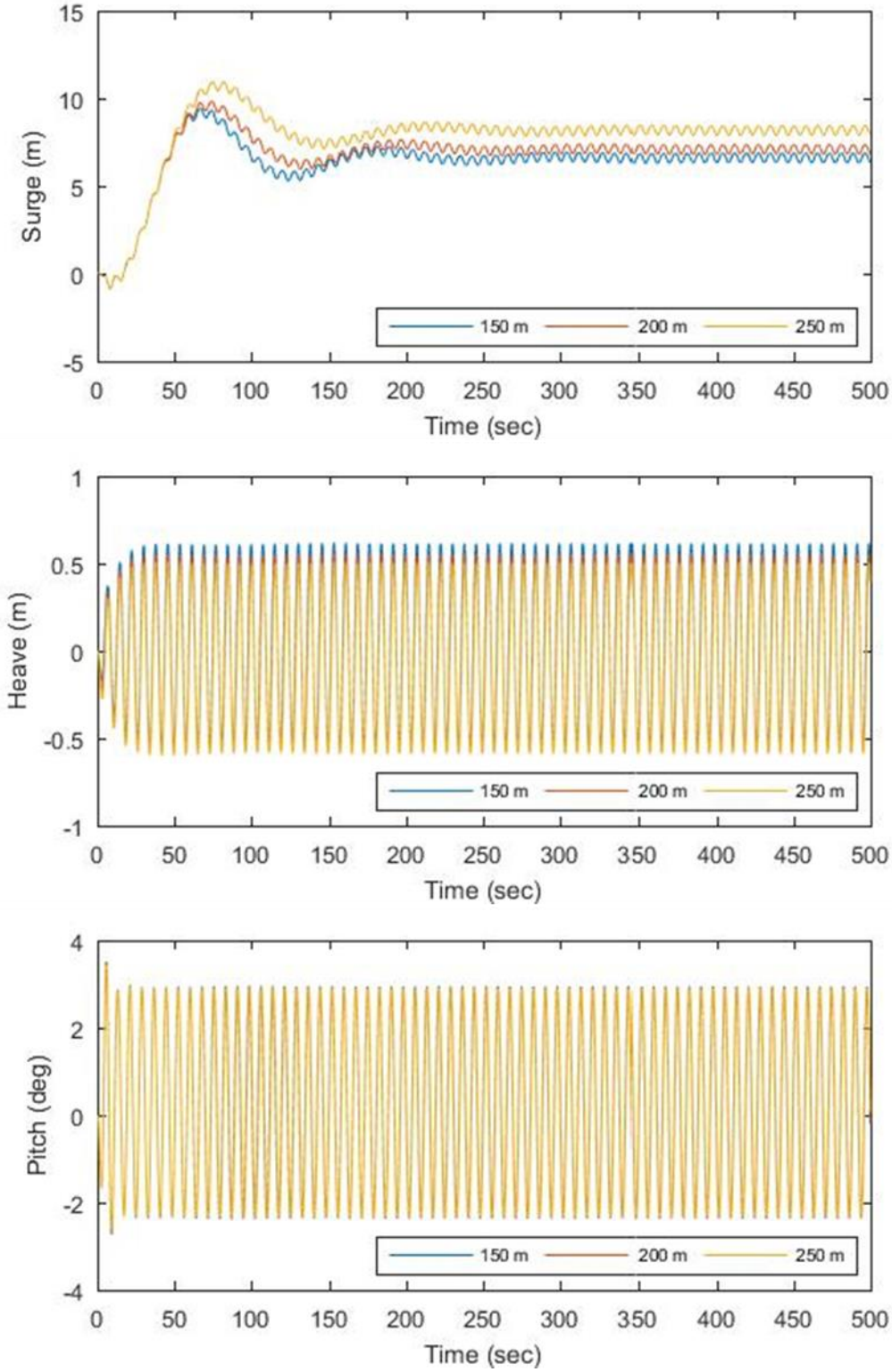

Figure 82: Motions of catenary system for examined water depths (load case 5)

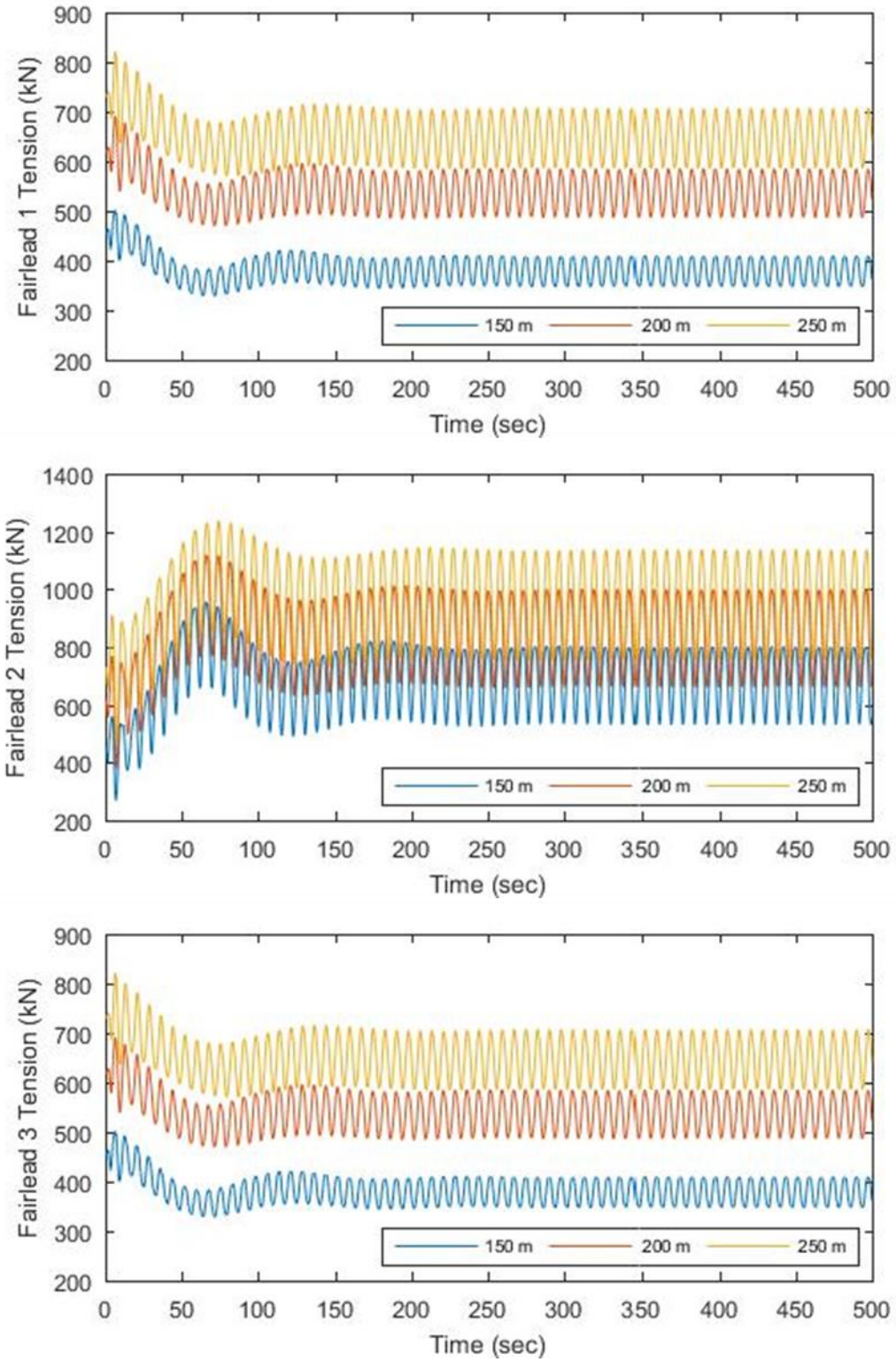

Figure 83: Fairlead tensions of catenary system for examined water depths (case 5)

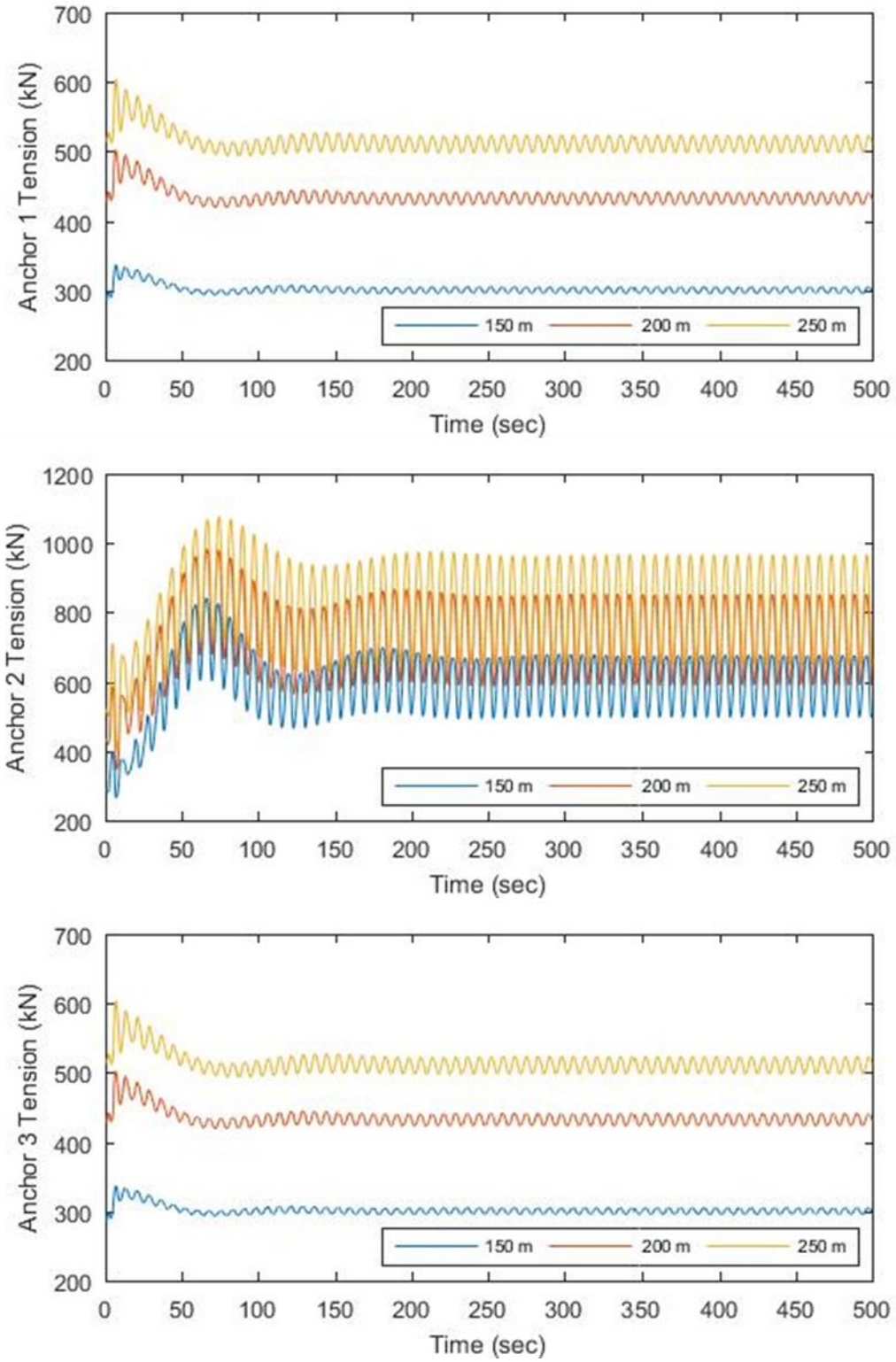

Figure 84: Anchor tensions of catenary system for examined water depths (case 5)

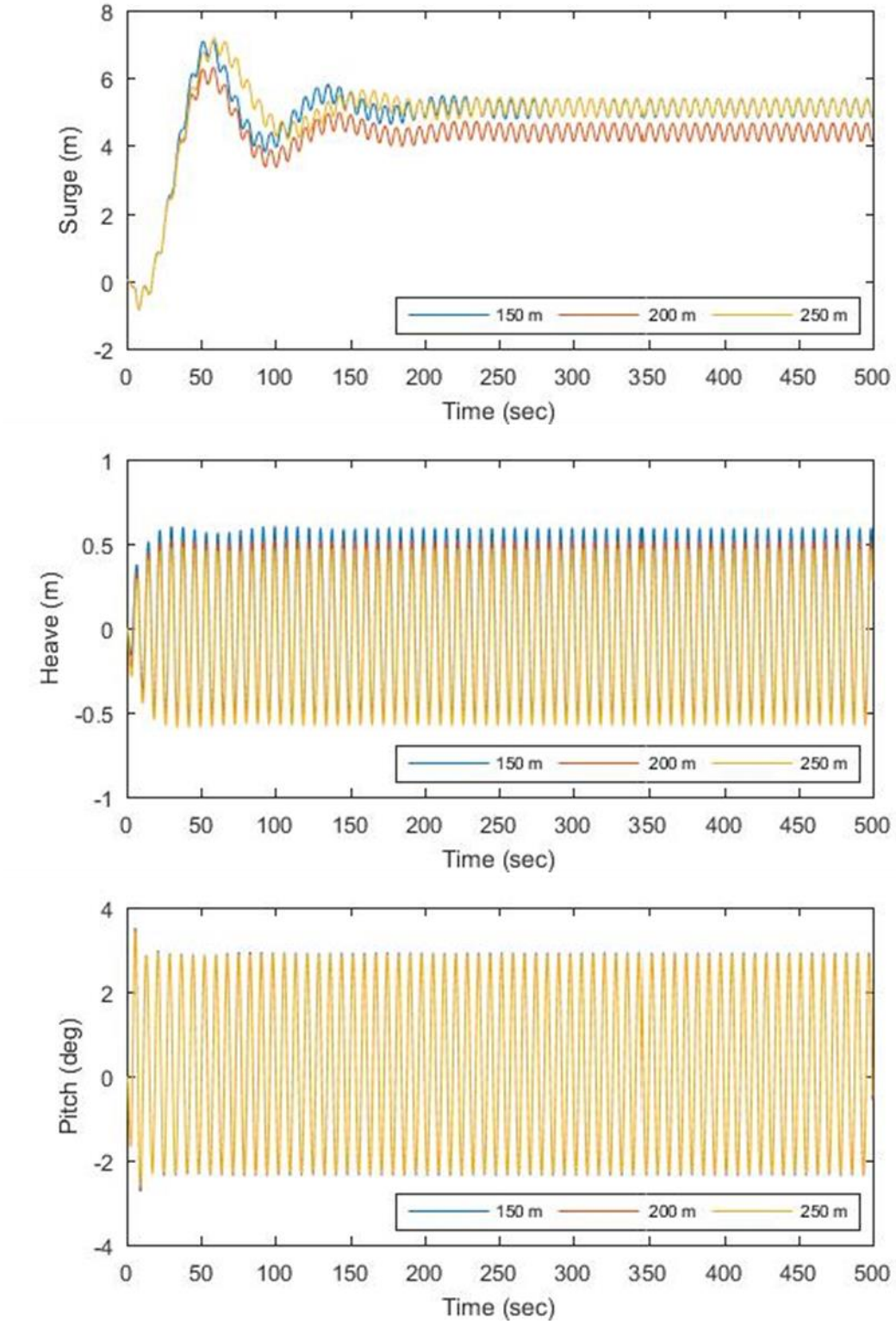

Figure 85: Motions of semi-taut system for examined water depths (load case 5)

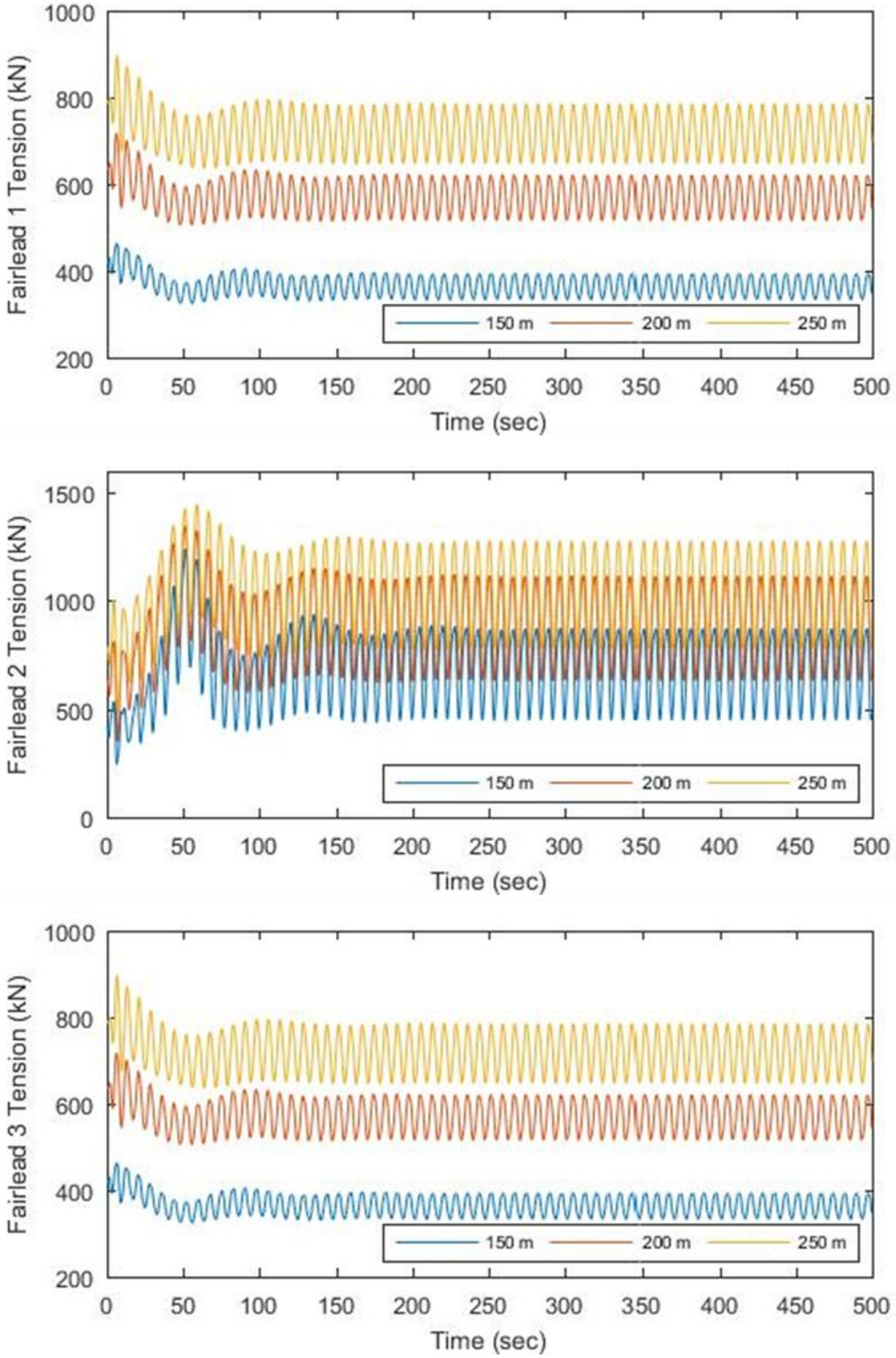

Figure 86: Fairlead tensions of semi-taut system for examined water depths (case 5)

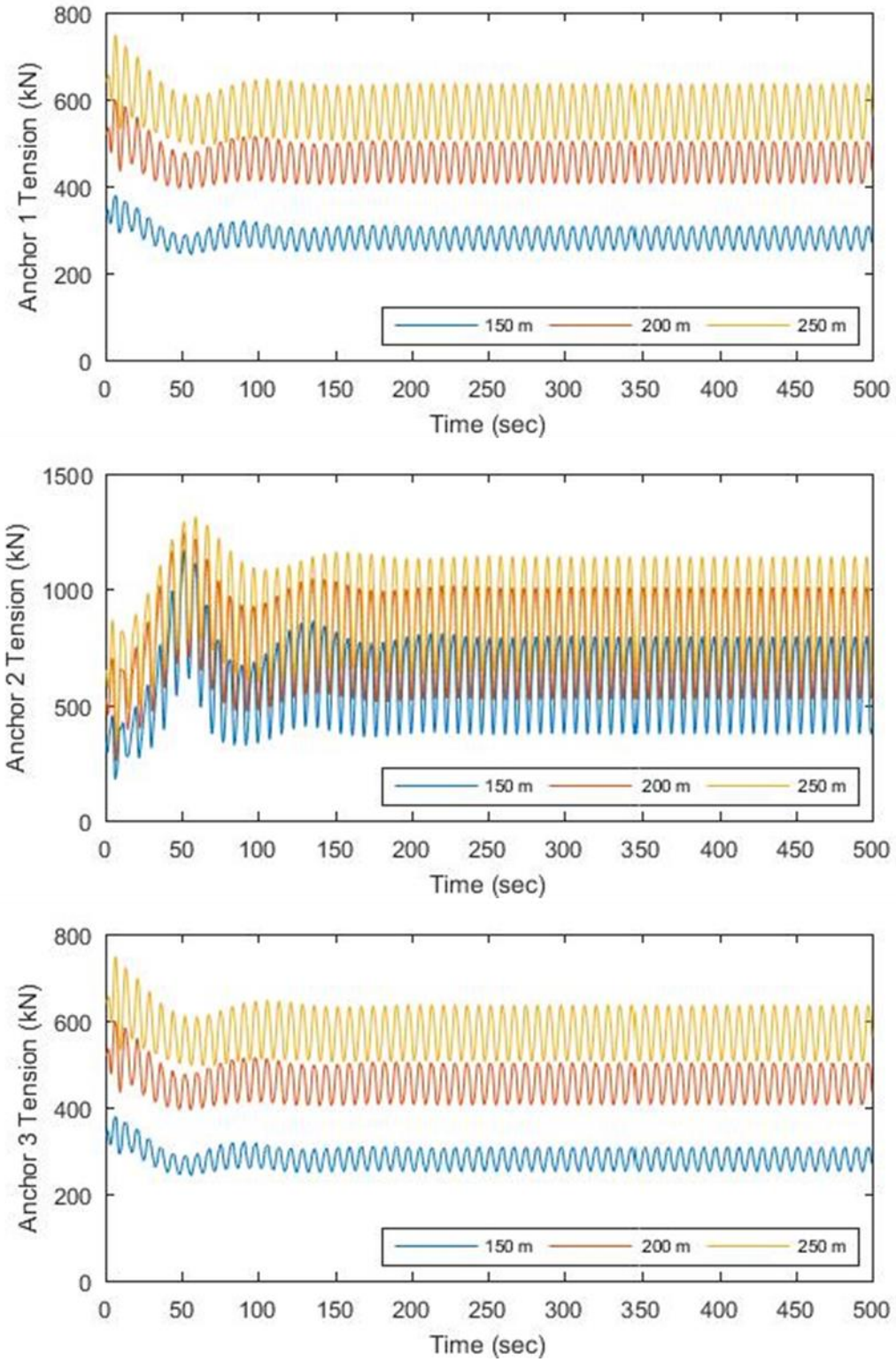

Figure 87: Anchor tensions of semi-taut system for examined water depths (case 5)

Influence of Water Depth Variation – Load Case 6

This section shows the semisubmersible response behavior in which the system is excited by irregular waves, sheared wind, and current with a power law profile. The plots in Figure 88 and Figure 91 illustrate the platform response motions for two systems under examined water depths. The study found all the motion responses to agree in each type of mooring system regardless of the water depth. Differences between the surge responses are negligible since those are attributable to the modification of mooring lengths that corresponds selected water depth. As far as the values that are related with tension responses, the catenary model at shallower water experienced more stress, while the semi-taut model at the shallow condition experienced a greater fluctuation of mooring tensions. The comparisons made in Figure 89, Figure 90, Figure 92 and Figure 93 may suggest that the catenary system could be more stable under examined environmental conditions as the performance is less affected by the water depth than that of the semi-taut mooring.

Despite the fact that the variance in the mooring line tension is less dependent on water depth for catenary system, the lower extreme loads are achieved in the semi-taut cables. To this point, the results covered the presence of current velocity under extreme sea conditions and the collective simulation results suggest that the semi-taut mooring system is more suitable for deep-water operation.

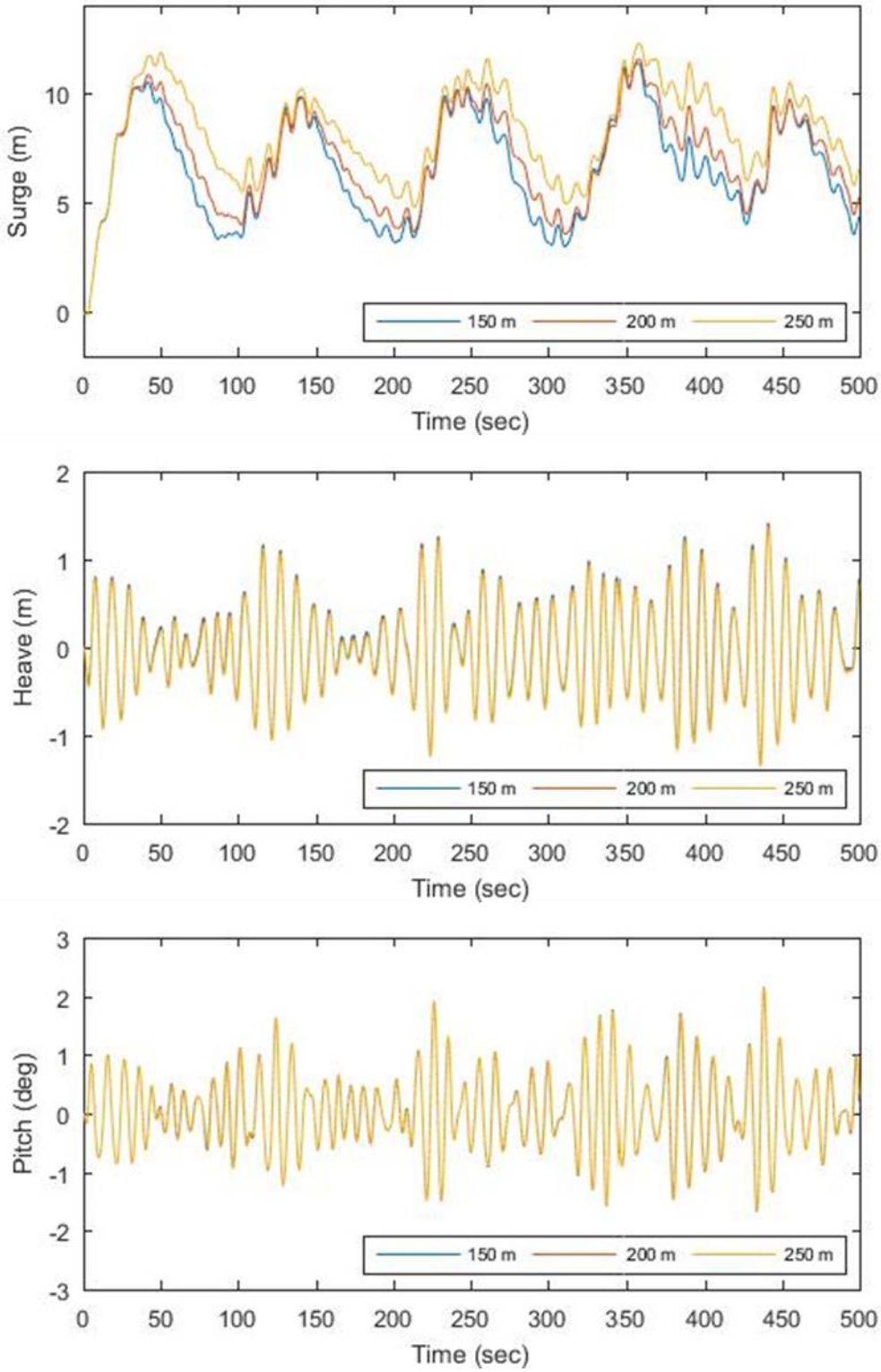

Figure 88: Motions of catenary system for examined water depths (load case 6)

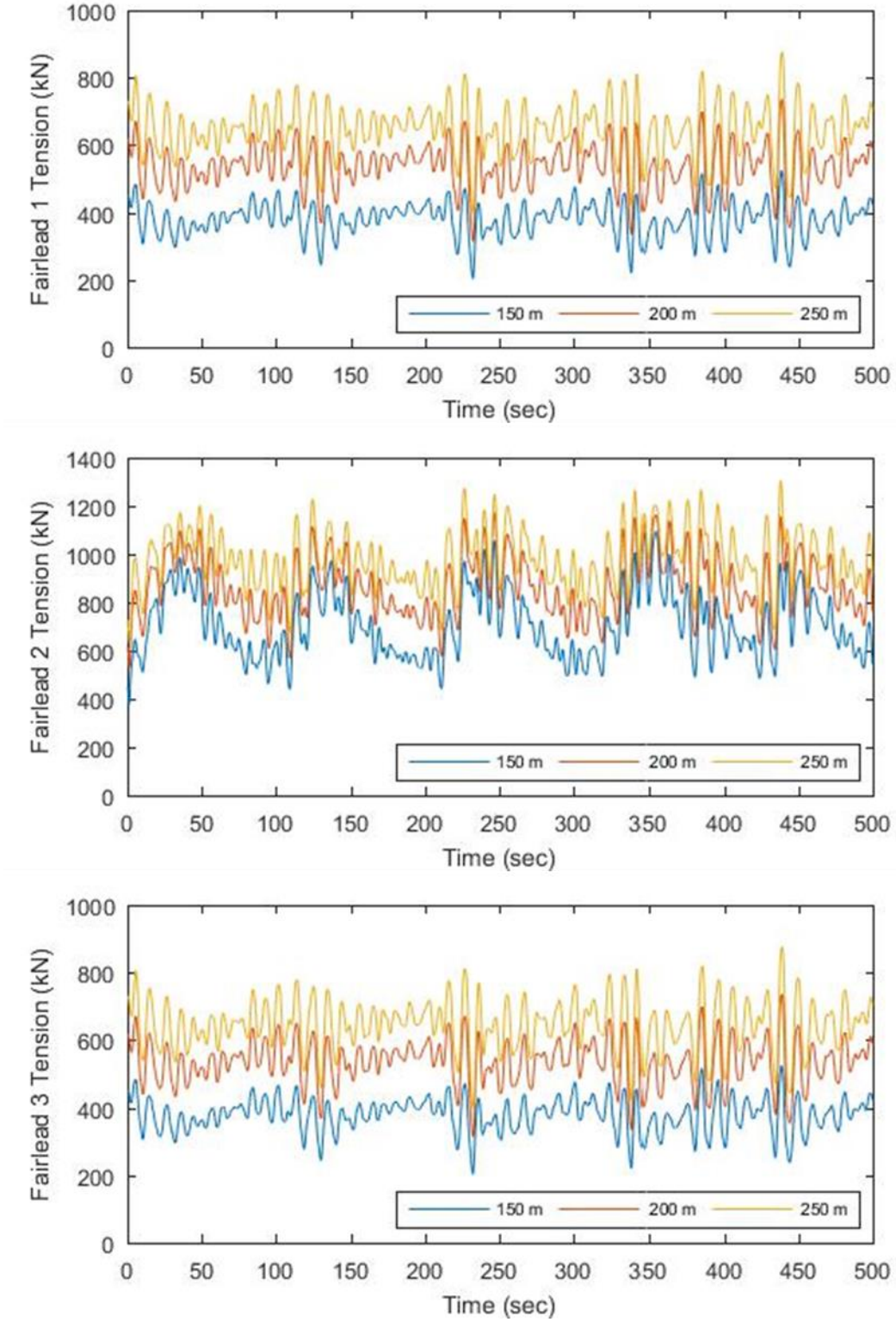

Figure 89: Fairlead tensions of catenary system for examined water depths (case 6)

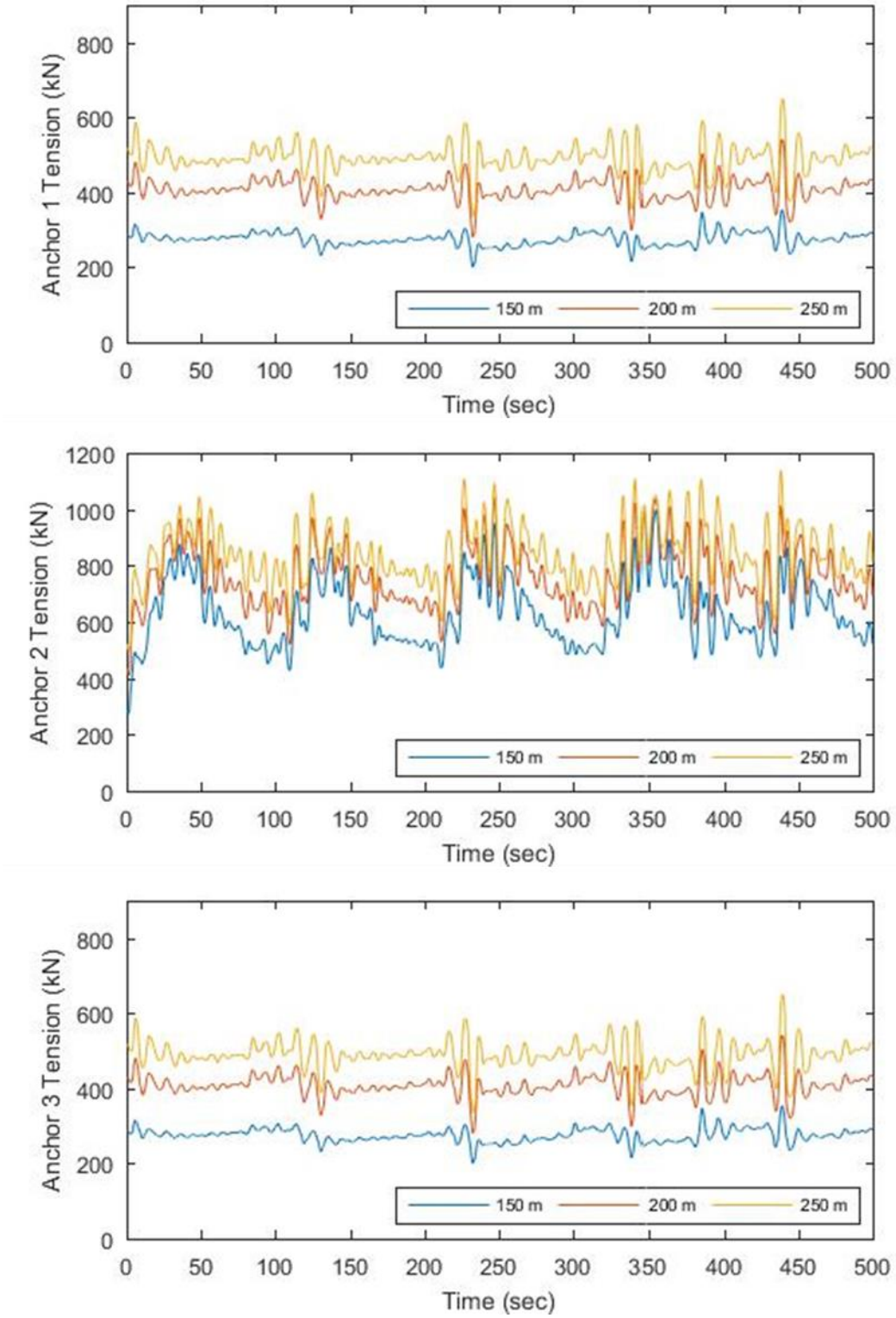

Figure 90: Anchor tensions of catenary system for examined water depths (case 6)

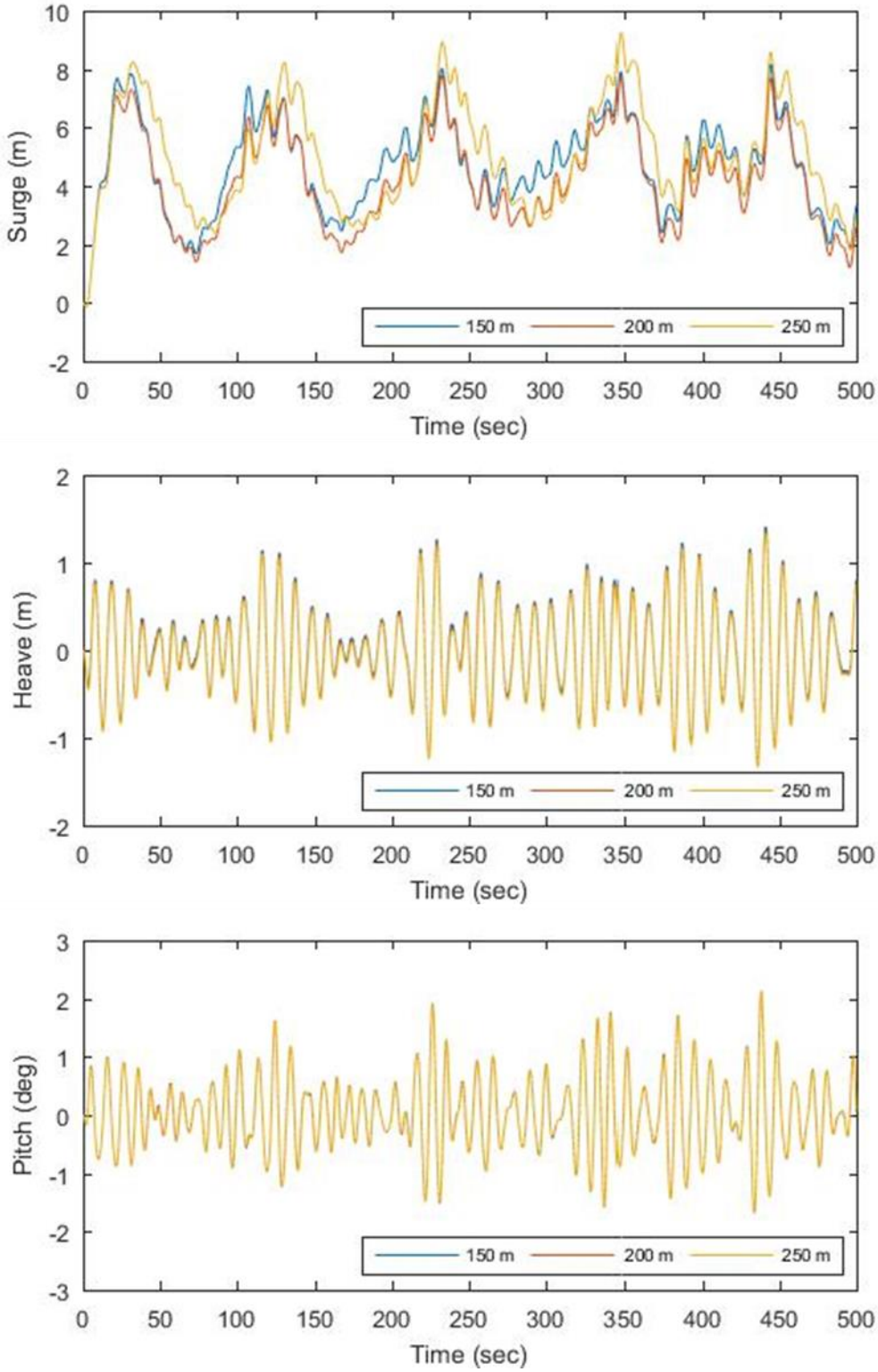

Figure 91: Motions of semi-taut system for examined water depths (load case 6)

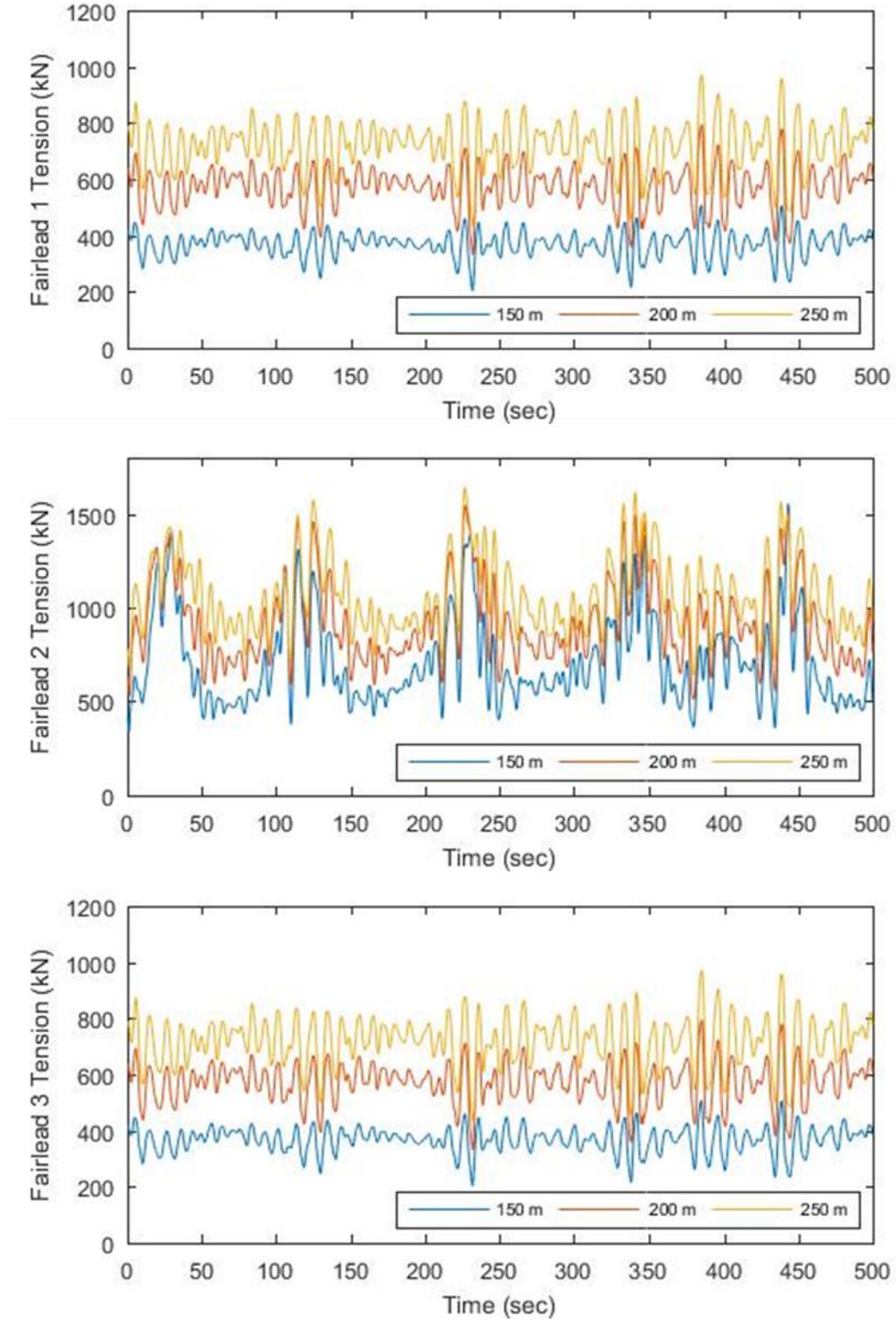

Figure 92: Fairlead tensions of semi-taut system for examined water depths (case 6)

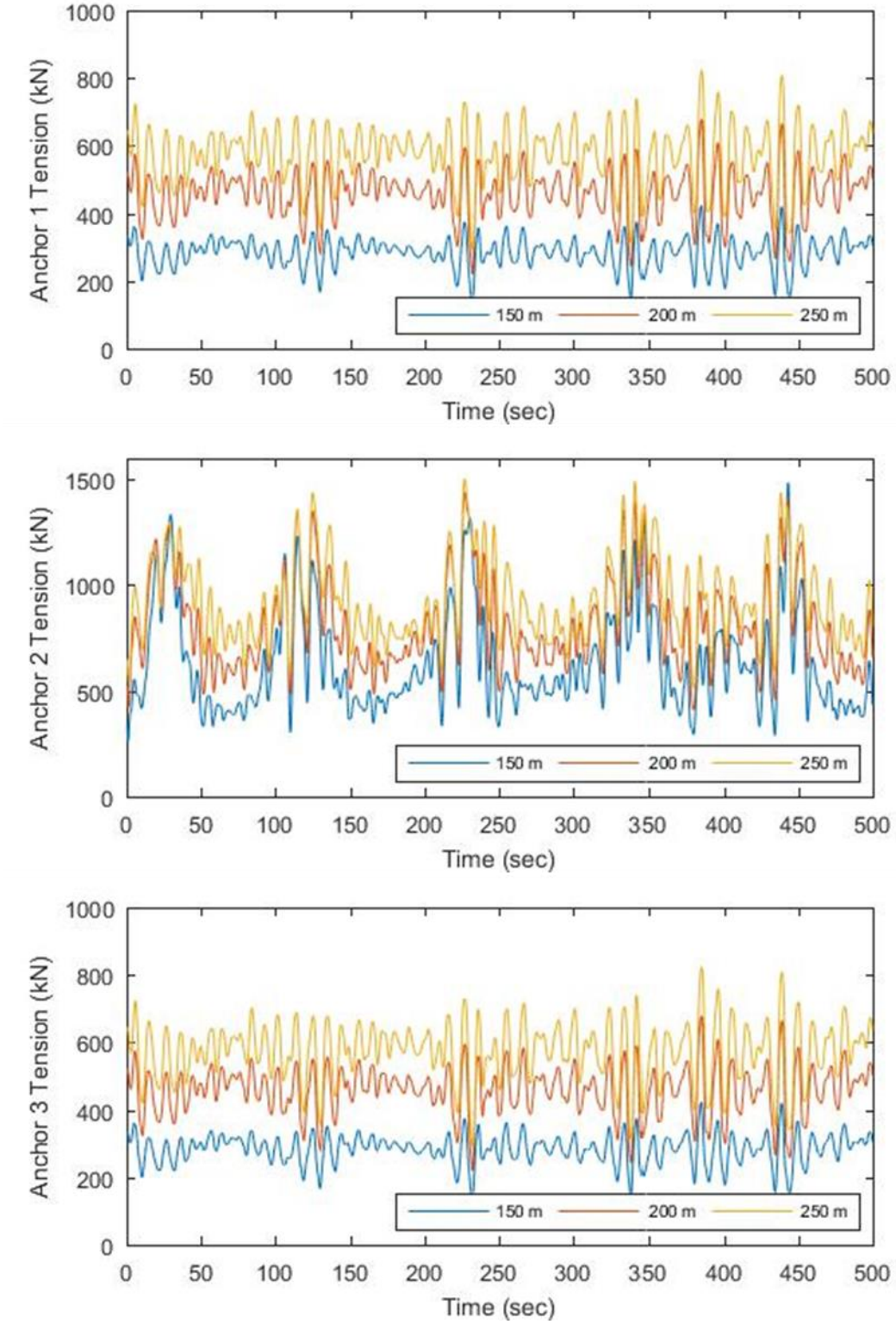

Figure 93: Anchor tensions of semi-taut system for examined water depths (case 6)

Directional Effects of Environmental Load Parameters

In the present chapter, the sensitivity study on the effect of environmental load direction was executed as a final process to validate the applicability of the numerical model. As found in Figure 94, each directional load was examined starting from the original direction of 0 degree with 30 degrees of increments. Wave-wind-current induced environmental load was applied in time domain analysis and the results are shown in Table 7. The simulation results indicate that the load coming in 270 degrees respect to X-axis generated the highest stress at the fairlead of the line that is parallel to the horizontal axis. Then the safety factor was considered to investigate the feasibility of the system under the most extreme directional load (API 2SK, 2005). The rule for calculating safety factor is dividing the maximum yield strength of the line material by the maximum loaded tension. Considering the maximum yield strength of the example material used in this study is 3,870 kN, the system has a value of 2.3 which satisfied the required safety factor of 1.67 set by the API code.

Table 7: Load direction sensitivity analysis result summary

Load Direction (degrees)	0	30	60	90
Max Tension (kN)	1406.4	1564.7	2087.2	2226.3
Safety Factor	2.7	2.5	1.9	1.7
Load Direction (degrees)	120	150	180	210
Max Tension (kN)	1897.9	1698.6	1163.3	1659.2
Safety Factor	2.0	2.3	3.3	2.3
Load Direction (degrees)	240	270	300	330
Max Tension (kN)	1747.3	2237.6	2034.0	1578.3
Safety Factor	2.0	2.3	3.3	2.3

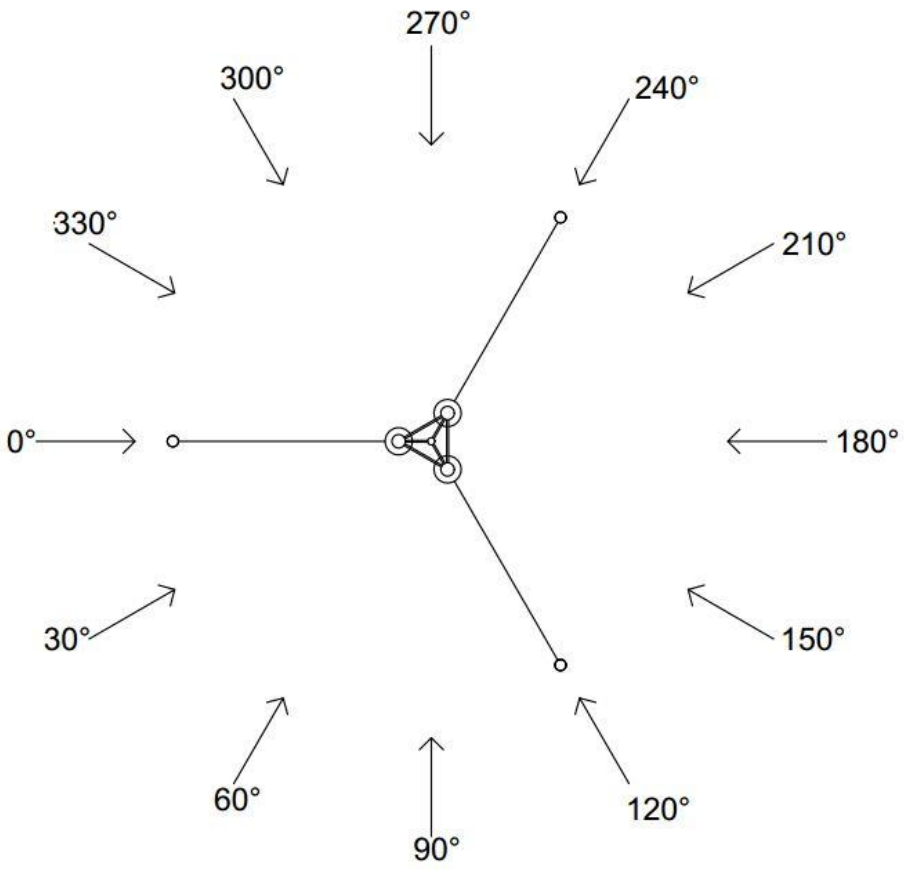

Figure 94: Examined load directions

5. SOIL PROPERTIES

The importance of examining the materials below the bedrock is clear in order to understand the seafloor configuration. Since detailed information of stratigraphy over a large region is neither possible nor necessary, the geological framework of the northern California coastal system is studied to access land slopes and tectonics. As an output of the marine geology research program supported by NOAA and USGS, the literature of the geologic knowledge relative to the study area exists. A general summary of the Northern California coastal system is presented in this chapter, and additional relevant sources are found in the bibliography.

Geologic Framework of Northern California Coastal System

The north California coastal system is a federally protected marine area, and consists of over 18,000 km^2 of ocean with a 511 m shoreline. The region lies between Monterey and San Francisco as a narrow continental shelf and extends offshore by 55 km (Edwards, 2002). The continental shelf segment slopes gradually across the shelf to the shelf break that occurs at a depth of approximately 200 meters. The regional structural framework of the coast of central California is located on the Salinian Block, which is bordered by the San Gregorio Fault and the San Andreas Fault. These two fault systems lie along a margin where the Pacific plate and the North American plate are rifted, causing a tectonic uplift. In response to the uplifted continental shelf, erosion of the deformed rocks exposes the sediments that were once deeply buried underneath. The

general characteristic of the Salinian Block depicts most of the study area as a granitic basement block.

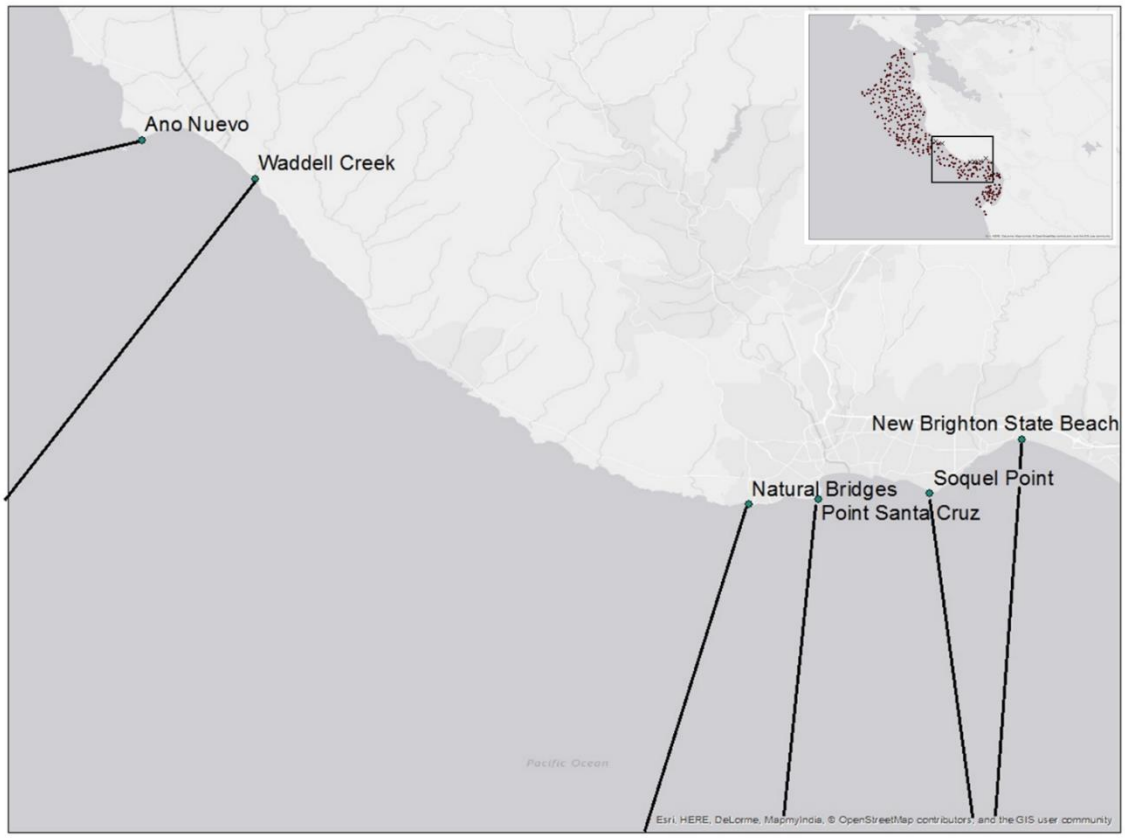

Figure 95: Geologic units within the study area

Four major geologic units are found within the study area as shown in Figure 95. The occurrences of these units are scattered throughout the continental shelf. The Vaqueros Formation is identified as the oldest sedimentary unit among the four units (Anima et al., 2002). This unit predominantly consists of medium-grained sandstone and its locality is near the cliff at Año Nuevo. In the vicinity of the Vaqueros Formation, the

Monterey Formation is spread out along the shore. The unit is mostly composed of siliceous strata including organic-rich mudstone, quartz, and dolomite beds. The Santa Cruz Mudstone is a younger unit, which is composed of siliceous mudstone. The unit overlies along the coastal cliffs from the east side of Moore Creek canyon to the coast at Natural Bridges State Park. At the east side for the cliffs, the Santa Cruz Mudstone is in contact with the Purisima Formation. The consolidated sediments with siltstone, sandstone and mudstone differentiate the Purisima Formation from the other three geologic units (Anima et al., 2002).

For each of these units, the relative geologic knowledge may evaluate the degree of potential for floating wind turbines over the study area. The future potential for wind turbine development, however, requires further study based on randomized sampling of the continental shelf. The information of soil classification often aids in estimating the soil strength based on the type of the seafloor soil.

Information in respect to soil properties are proved valuable for understanding interaction effects on mooring systems. The data can be related to the selection of available mooring technologies through determining the character of seafloor features. In response to the mooring analysis from the previous chapter, this chapter summarizes the geological information from the soil samples to provide a more comprehensive investigation of the station-keeping system. The study area lies on the central California coast. Three hundred and eighty four samples were collected from a multiyear cruise that was initiated by the United States Geological Survey (USGS). Figure 96 shows the map of the coastal region of Northern California and the sample locations.

The soil sampling underneath the water was accomplished by the use of two main devices: box corer and grab sampler. The box corer can recover a removable box containing the sediment of 0.036 m3 (20 cm × 30 cm × 60 cm) from the bottom surface below the ship's deck. When the samples are taken from hard bottoms, grab sampler was used. From these gained samples, Arcmap, a geospatial processing program, will be used to prepare a better understanding of the soil structure interaction. The data samples contain the soil information of surficial depth, sediment distribution, and grain size variation.

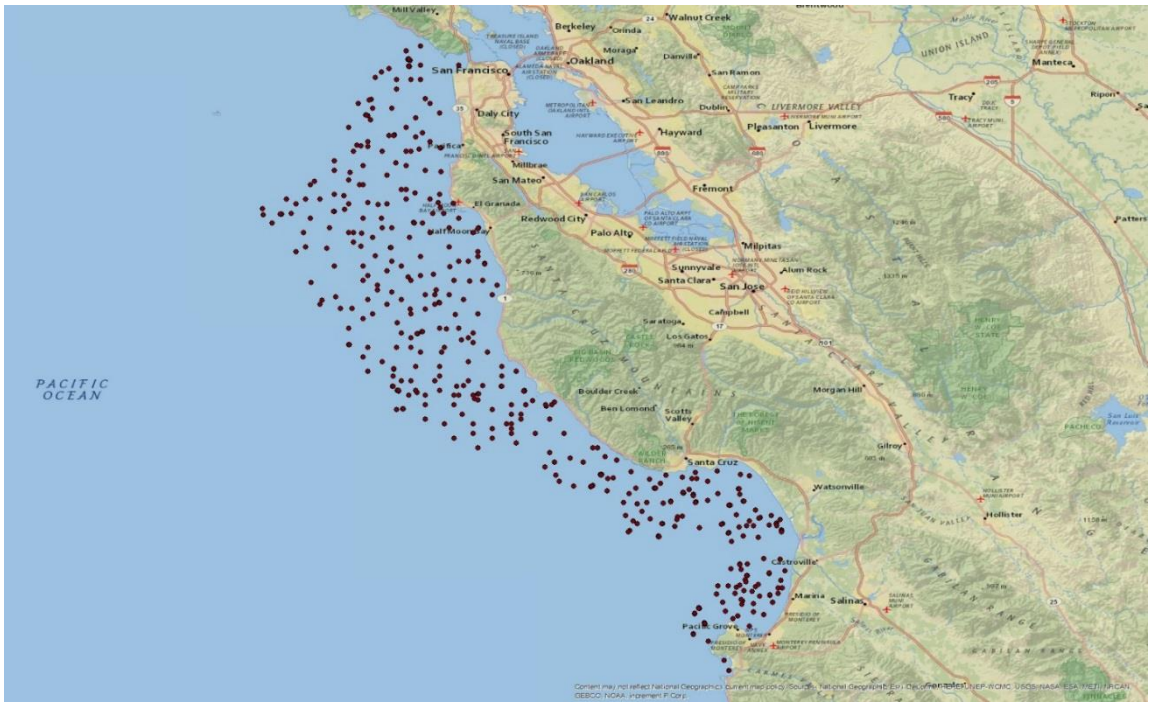

Figure 96: Sample locations

A 12-kHz acoustic profiler was used in the USGS's sampling program to determine the water depth of each sample. The water depth of each sample is mapped as

in Figure 97. The variability of the color transition suggests that the continental shelf gradually slopes seaward from 8 to 150 meters of water depth. In water depths of 51 – 90 m, a narrow band of area extends to the southeast. The darkest blue area contributes to the lower area with the elevation extending to 150 meters below the water surface. Samples show that the seafloor may continue to steepen into the deep ocean, but the study area appears to be located on a shallow basin, ranging in water depth. In general, the study of sea level can glean information on physical characteristics of the soils because the sediment distribution often relates to the transportation distance from shelf to slope.

Figure 97: Water depth of each sample

Mean Grain Size Distribution

Figure 98 shows the distribution of mean grain size of the study area. Based on the mean grain size, the shelf can be subdivided into three zones: inshore shelf, mid-shelf, and outer shelf. The mid-shelf is bordered by the neighboring inshore and outer shelves and extends from the offshore of San Francisco to the southeast. The central shelf region has mean grain sizes ranging from 0.0625 – 0.016 mm throughout the area and separates the near-shore shelf and the outer shelf. The fine grain sizes with sand concentrations occur in both near-shore corridor and outer-shelf band. The variations in soil properties across the study region are further analyzed in regards to the type and state of the soil. For a regional overview, the sea floor in Northern California consists of many different types of sediments, including gravel, sand, silt, clay and mud. The regional distributions of each sediment type are shown in the following figures. The nearshore continental shelf has finer surficial sediments than that on the outer continental shelf. Moreover, a mid-portion of the shelf is composed of soft substratum such as mud and silt.

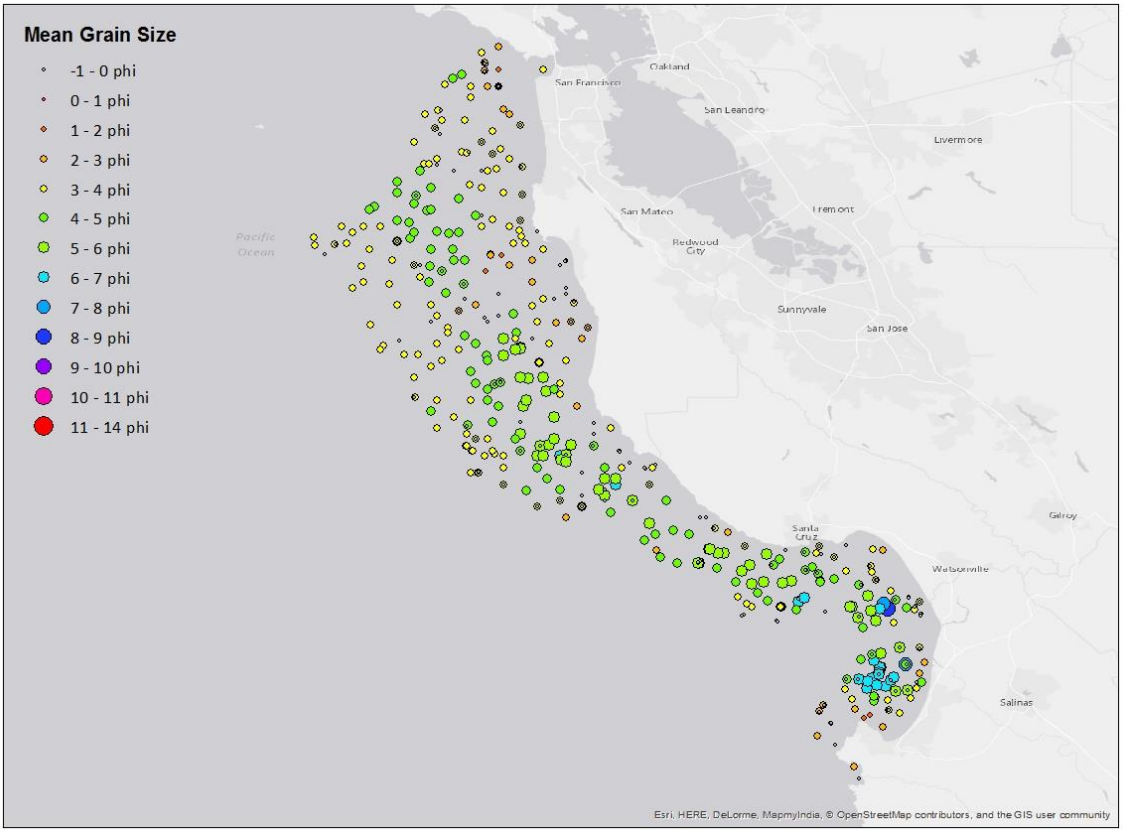

Figure 98: Distribution of mean grain size

Variations in Sediment Texture

To provide information about the sedimentary deposits on the study area, the data points were located on the map if the percentage of sand in each sample was more than 36 percent. Figure 99 illustrates how the shelf is dominated by sandy bottom as a common continental shelf. Information about such textural patterns can be used to refer the sediments by origin as land-derived deposits. For planning a geotechnical design when the marine soil is composed of terrigenous sand, the sediment is assumed to be cohesionless. If sufficient evidence exists to determine whether the sediment is

overconsolidated or nonconsolidated, additional soil engineering parameters can be estimated such as soil shear strength and buoyant unit weight.

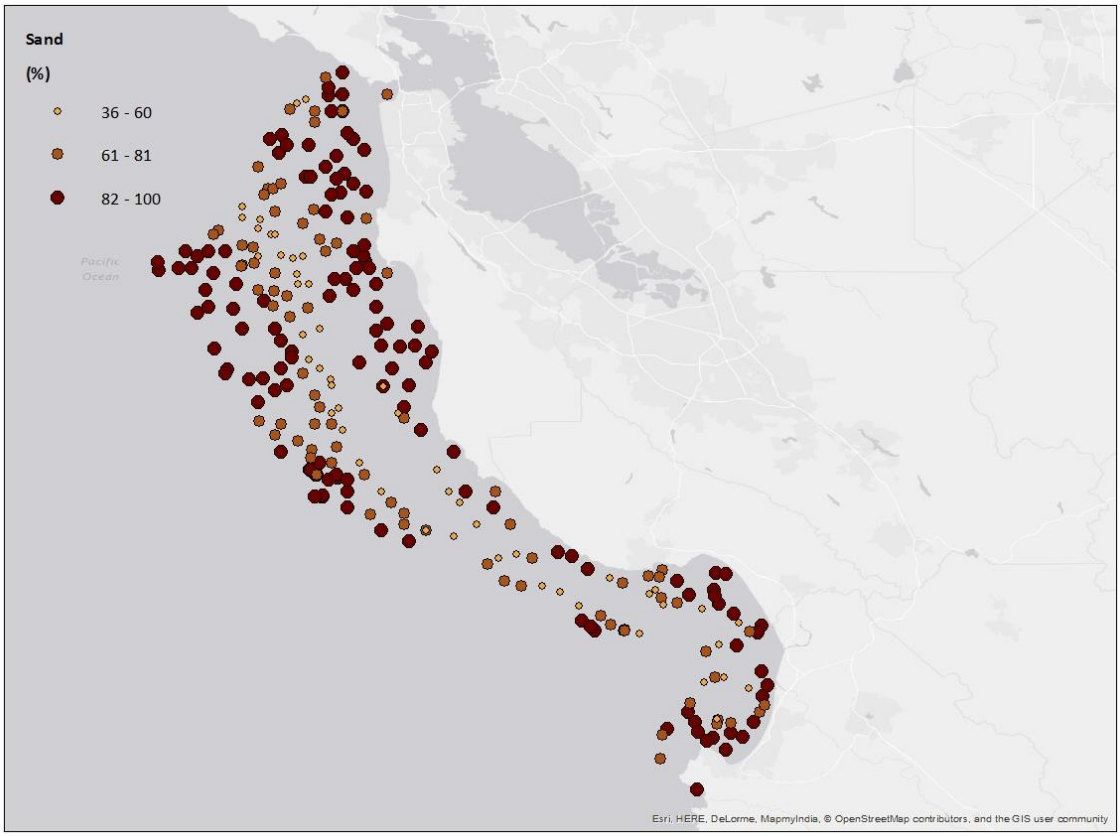

Figure 99: Sand sediment distribution

As the continental shelf descends with steeper floor, a narrow portion of the sanctuary can be found with soft-bottom soil. Figure 100 depicts the increased percentage of silt as the sample data beyond the nearshore area were extrapolated. The considerably silty floor remains narrow throughout the sanctuary, and a band of silt is almost identical to the trace of the mid-water depth from Figure 97. The abundance in

granular soil with silt content in this strip area indicates that the associated sediment has little cohesive strength. No consistent rule can define the degree of consolidation of the floor, and therefore soil properties need to be extended to consider the other combined soil types.

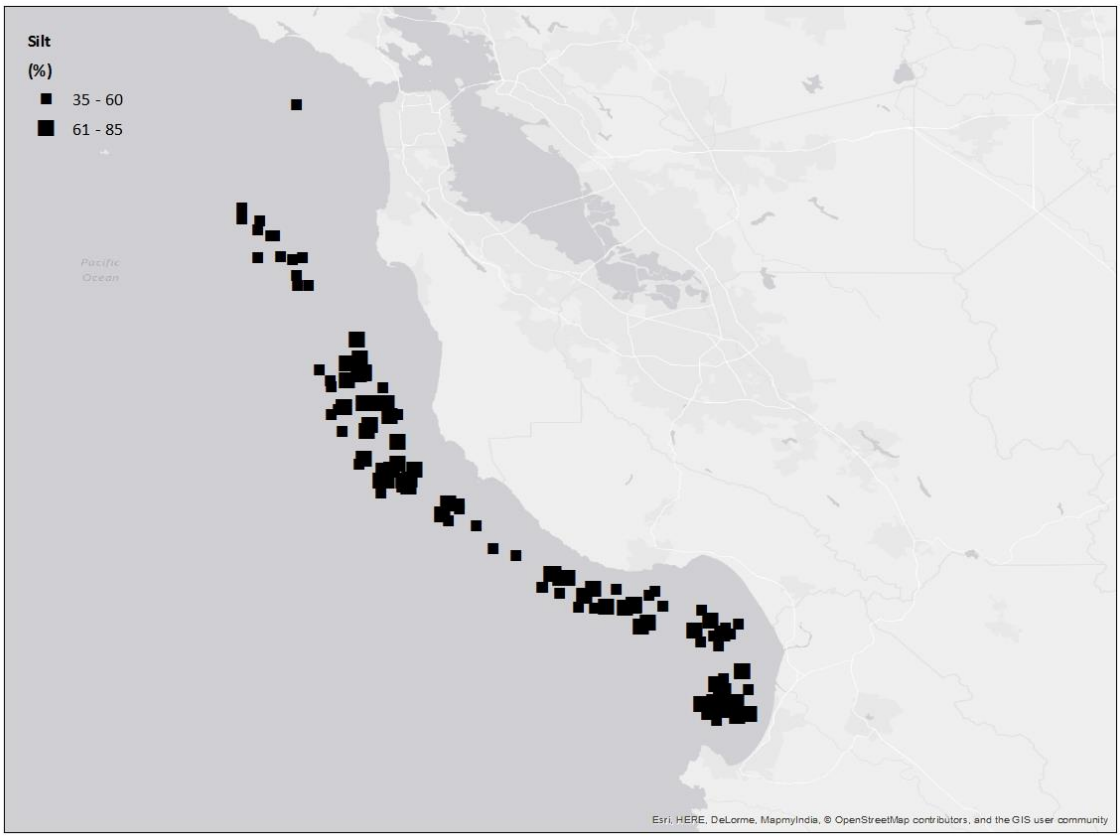

Figure 100: Silt sediment distribution

The distribution of clay type sediment was also documented by locating the cores that represented clay as the major content. The samples shown in Figure 101 consist of more than 24 percent of clay in each sample. The observation of the surficial map clearly

suggests that clay materials are not abundant in the study area. It is not known whether such textural pattern changes throughout the vertical stratigraphy. These facts need to be considered for a site investigation because the presence of clay particles can vary the soil compressibility.

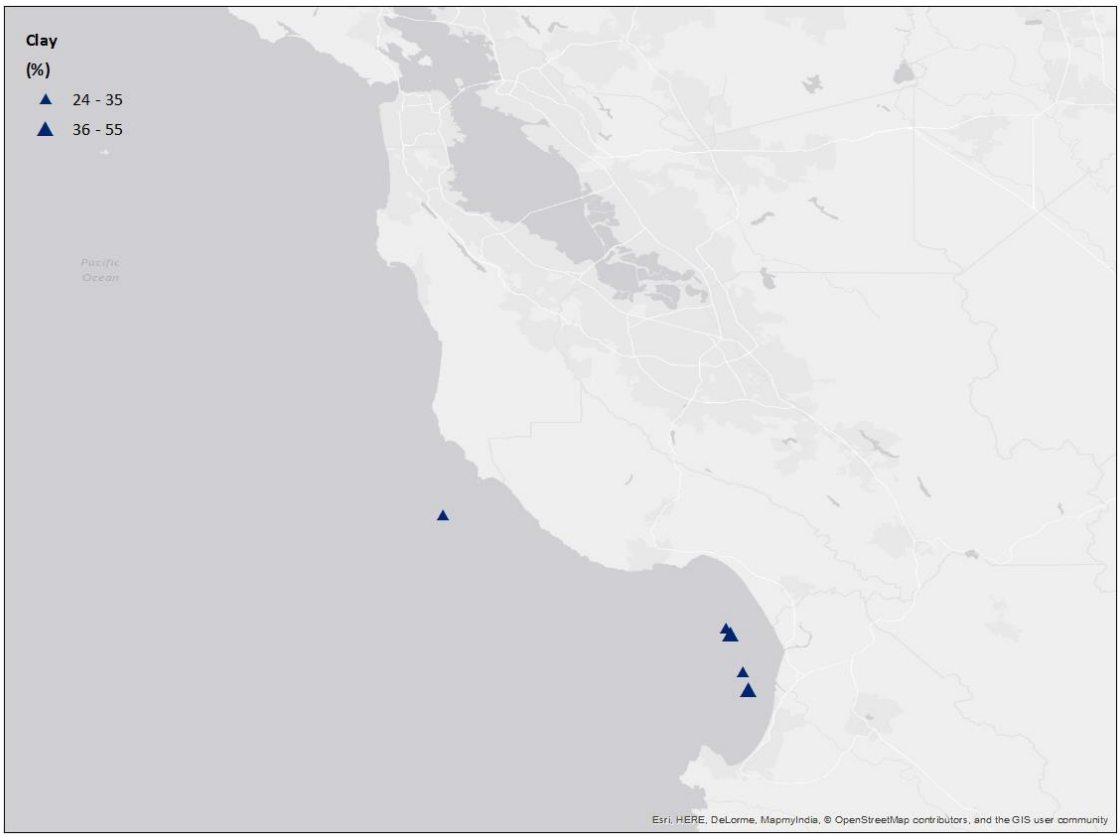

Figure 101: Clay sediment distribution

Additional description of sediment data is found as Figure 102 shows the exposed locations of the gravel sediments. As identified from Figure 102, the gravel sediments are found on the surface at a very low rate. Again, the knowledge of

stratigraphy is uncertain, and thus an effort to minimize the potential complication caused by underlying coarse-grained soil is needed. The geotechnical application can suffer significant disturbances under extreme soil conditions such as hard underlying strata or surficial gravels. Due to the brittle nature of the material, such environment can cause irregular breaking of the rock and limit the penetration depth. However, the problem is not acute as it can be avoided by relocating the device or alternating the system.

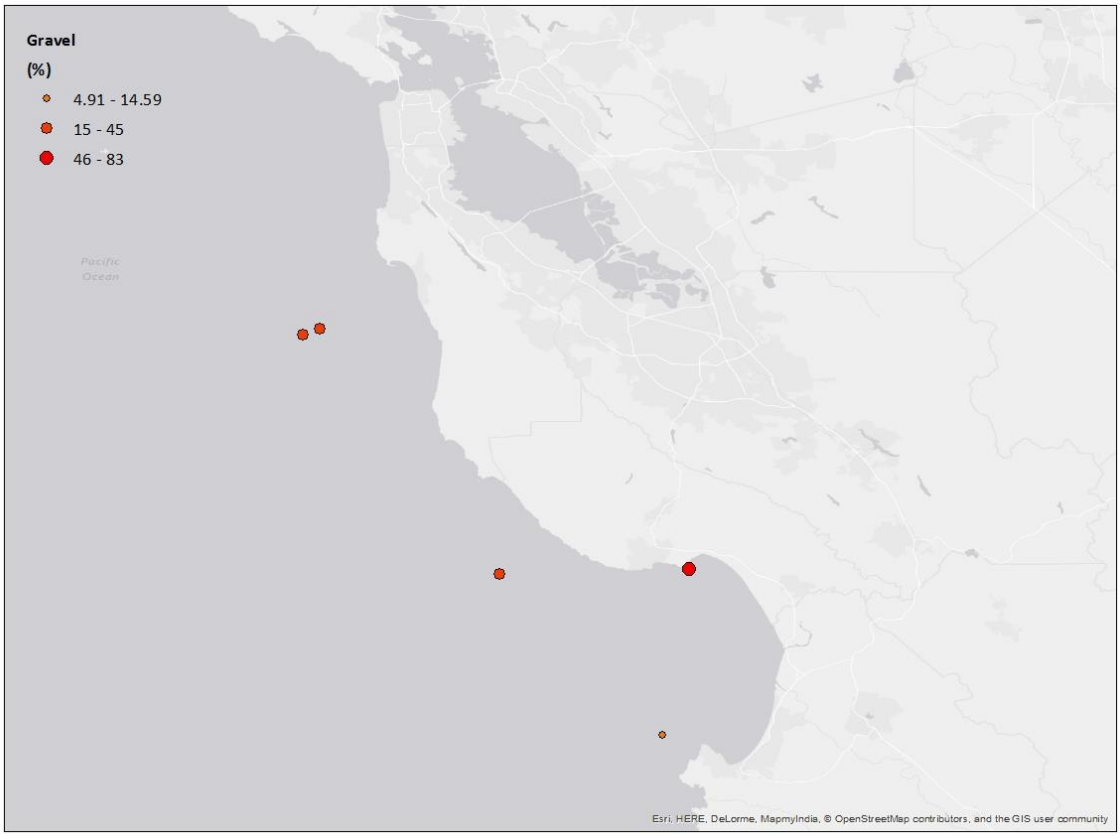

Figure 102: Gravel sediment distribution

The data on mud sediment distribution is found in Figure 103. As the continental shelf extends from the nearshore, the percentage of mud is increased with the water depth. Based on Figure 100, the narrow portion of the shelf is composed of a silt and mud mixture. The occupied mud belt contains silt throughout the central shelf regions according to both figures. The textural analyses of the major sediments reveal that the mid-shelf mud belt is seen between the region of outer-shelf sands and the nearshore sand corridor. When the muds have silt components, the mid-shelf area can be recognized as underconsolidated state due to the permeable characteristic of the soil.

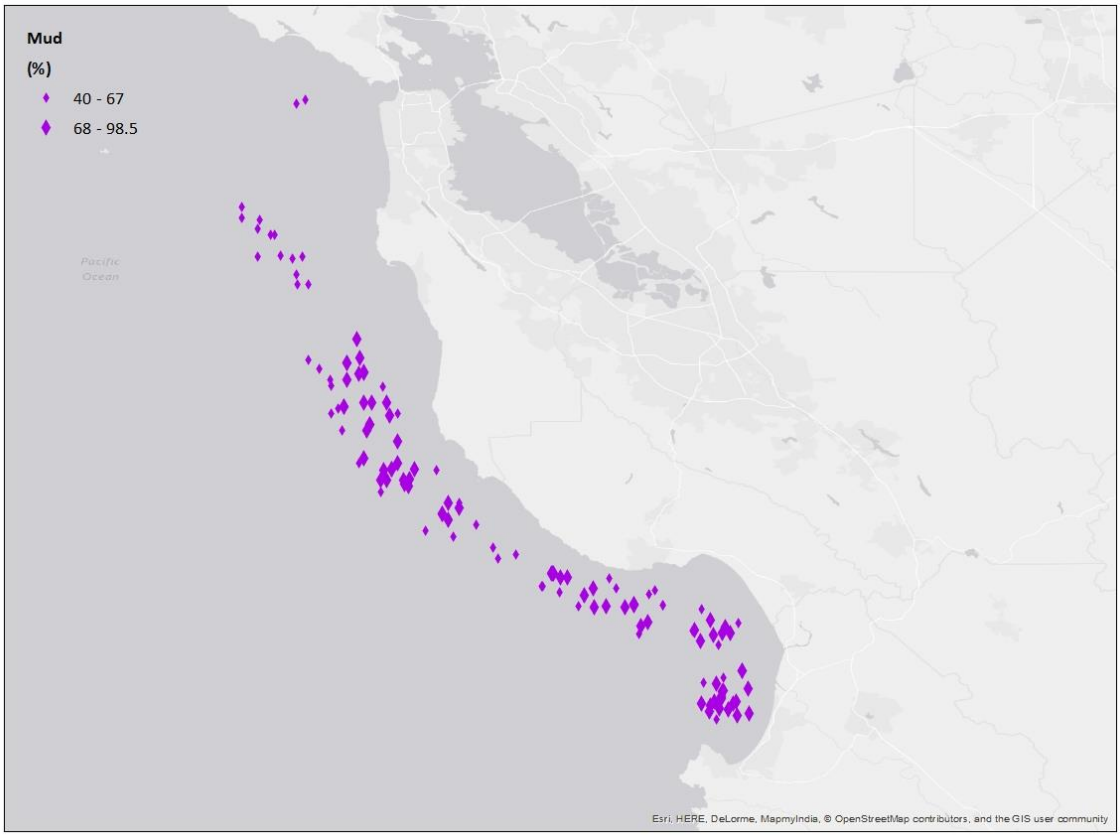

Figure 103: Mud sediment distribution

6. ANCHOR ALTERNATIVES

Information obtained from the study area suggests that the water depth is in the intermediate range where floating offshore wind towers are required to be secured to the seabed by mooring. For floating wind turbines, several types can be considered for anchor application. The type of anchor system is considered in regards to the seabed characteristics in which it may be deployed and the mooring line geometry for which it may be favorable. The purpose of this chapter is to provide assessment on three anchor types and process the available information to examine the potential suitability for a specific site. Then, the context of the anchor usage will progress from a single mooring line attachment to a multiline system. In order for the wind turbines to become commercially viable, a concept for device arrays is assessed by introducing multiline anchor system. The potential anchor types adapting the multiline design include: piles, direct embedment anchors and drag embedment anchors.

Driven Piles

Pile anchors are deep foundation elements that drive hollow steel pipes into the seabed by either driving or drilling. Piles are positioned deep in the soil to achieve the desired holding capacity. The installation is a complex process and requires specialized equipment for underwater operation. For large-scale wind farm applications, the technology may incur unacceptable costs due to the considerable equipment, expertise and time.

A major strength of pile anchors is their high lateral capacities, the magnitude of which are dependent on soil resistance (Karimirad et al., 2014). In addition, the soil friction along the embedded pipe resists the uplift force, allowing piles to transmit loads in any orientation. The high capacities of anchor in both lateral and vertical directions permit any mooring systems to be suitable including catenary, taut and semi-taut.

Driven piles are versatile in seabed types including highly heterogeneous soil deposits compared with other high-capacity anchors when installation vessels and driving equipment are available. They can be installed in soil profiles ranging from soft sediments to hard seafloors. Also, piles have been used on substantial slopes, permitting flexible mooring line scopes. This feature is of particular importance to offshore environment where many potential sites have steep slopes.

Since pile anchors are capable of resisting both horizontal and vertical loads, adapting omni-directional load components is a viable application. Yet, more extensive and better site data will be required unless the design is proceeded extensively conservative with the current level of soil properties.

Pile Driven Plate Anchors (PDPAs)

A pile-driven plate anchor (PDPA) is a steel plate that is driven into the seafloor sediments by conventional methods of pile installation. The PDPA is inserted vertically into a pre-determined depth and then re-oriented to lock its position in the bottom. As noted earlier for driven piles, the PDPA also requires pile-driving equipment, but handling is expected to be simpler due to lower material. It is virtually suited to a wide

variety of soil conditions: soft clay, stiff clay or sand. For installation in soft clays or mud, keying is required to retrieve embedment loss during the action.

The PDPA's reliability on sloping soils parallels that of driven piles and they can demonstrate higher geotechnical efficiency in non-horizontal settings than most other anchor types. Because of its deep embedment, the PDPA can also accommodate layered seafloors. Again, this is similar to driven piles, which can also be installed in seafloors with variable resistance.

Another advantage of the PDPA is its resistance to horizontal loading, which allows amenability to short mooring line scopes such as taut mooring or semi-taut mooring. As a relatively light plate anchor, providing vertical uplift resistance is a significant feature in terms of efficiency. It is noted that the high capacities in uplift as well as lateral directions are suitable for multiline attachments although plate anchors will require a load ring. A load ring is a device that enables plate anchor to transmit mooring line loads to each anchor from multiline attachment. As shown in figure, PDPA appears to be feasible with a multiline mooring configuration as the load ring resolves the issue of out-of-plane loading.

Drag Embedment Anchors (DEAs)

The Drag Embedment Anchor (DEA) is an anchor that has been designed to develop horizontal resistance by dragging the digging part along the sediment surface. Due to its high geotechnical efficiency with low cost, DEA is an attractive anchoring point available today.

The mooring line is attached to the shank of the anchor and the leading edge of the fluke penetrates into the seabed and remains stable with drag. Drag distance during installation should be expected until the mobilizing fluke embeds the anchor into the soil to an equilibrium state. While large resistance to horizontal load is contributing to the holding capacity of the system, low resistance to uplift loads is susceptible to dislodgement of the anchor under vertical loading. Therefore, DEA becomes an inadequate anchor choice for taut mooring systems because vertical restoring force may lead the system to lose station-keeping ability.

The requirement for large mooring footprint restricts the anchorage for only catenary systems. This can be especially significant in sand and stiff clays where drag anchors will embed to a shallow depth, minimizing vertical uplift loadings. In soft clays, deeper embedment occurs in the soil to a depth of three to six fluke lengths, and the increased vertical holding capacity is expected.

On the advantage side, the drag anchor is an efficient performer on soft seafloors. In heterogeneous soils, the behavior of DEA is often erratic. For example, in situations where sediment stratigraphy contains a thick hard layer under a thin layer of soft soil, the anchor will not be able to penetrate into the hard bottom. Consequently, DEAs are rated less reliable in layered seafloors than driven piles or PDPAs.

Topography is another important issue in determining whether DEA is a practical anchor type for a given site. Irregular topography with steep slopes limit the performance of the anchor since pulling on slopes will cause decrease in holding capacity. Having a directional preference also raises an issue for resisting out-of-plane

loading, which is generated by multiline attachments. Although deployable with load ring application, DEAs are not the best candidate for sustaining omni-directional loads.

Geometric Design of Offshore Wind Farms

The applicability of multiline solution for anchor system enables commercialization of offshore wind farm deployment. In contrast to oil/gas industry practices, shared mooring system infrastructure is required to reduce the project cost by lowering the number of anchors needed. The multiline concept proposed in this study considers three mooring lines per anchor. In assessing the efficiency of a design, the benefits are clearly scalable in terms of two quantities: n_{AT}, the number of anchor points per turbine and n_{MA}, the number of mooring lines per anchor (Fontana et al., 2016). When the estimated number of shared anchor points is compared to the number of traditional single line anchors, the reduction in the number will show the degree to which efficiency is achieved. The number of anchors in the wind farm is

$$n_A = n_T \frac{n_{AT}}{n_{MA}} \tag{32}$$

where n_T is the total number of floating wind turbines needed. For a deployment with n_{TA}=3, a multiline windfarm showed 67% reduction in the number of anchors needed when compared to a farm design sharing no anchor points. The geometric layout of the wind farm is shown in figure 1. Note that the array without using the concept of multiline considered the same network.

Based on the analysis, it seems that the proposed concept of floating wind turbines attached to a common structure presents possible cost savings. However, it is

also important to note a more comprehensive research is needed, since the foundations will be subjected to multi-directional and time-variant loads. In this section, a preliminary evaluation of the multiline anchor applied to time-varying loading is presented. The approximation will provide initial insights into the resultant forces at the anchor and the directions. Further study of areas including the considerations of water depth as well as the mooring line configuration are ongoing research topics.

Multiline Anchor Forces

In the case of multiline anchors, multi-directional and time-variant loads are experienced during the windfarm operation. These dynamic responses are important matters during the mooring or anchor selection process. The estimation of the resultant forces at a shared anchoring system will be made to understand some key characteristics of the multiline concept on power production. The example platform used is an OC4 semi-submersible design, which has been used throughout this study. The mooring lines are considered in both catenary and semi-taut configurations. It is assumed that the platform is subject to co-directional wind, wave and current. This is a representative state of windfarm conditions where a turbulent wind field, irregular waves, and power law profile current are fluctuating. The independent oceanographic conditions, however, are assumed simplified model compared to the those modelled with wake effects with spatial correlation. The resultant forces parallel to wind-wave-current direction and perpendicular to wind-wave-current direction are

$$F_{r,0} = T_{a2} - \{T_{a1}\cos(60) + T_{a3}\cos(60)\} \quad (33)$$

and

$$F_{r,90} = T_{a3}\sin(60) - T_{a1}\sin(60) \quad (34)$$

The total resultant force is

$$F_r = \sqrt{F_{r,0}^2 + F_{r,90}^2} \quad (35)$$

Time history of the resultant force at the anchor in the 0° is shown in Figure 104.

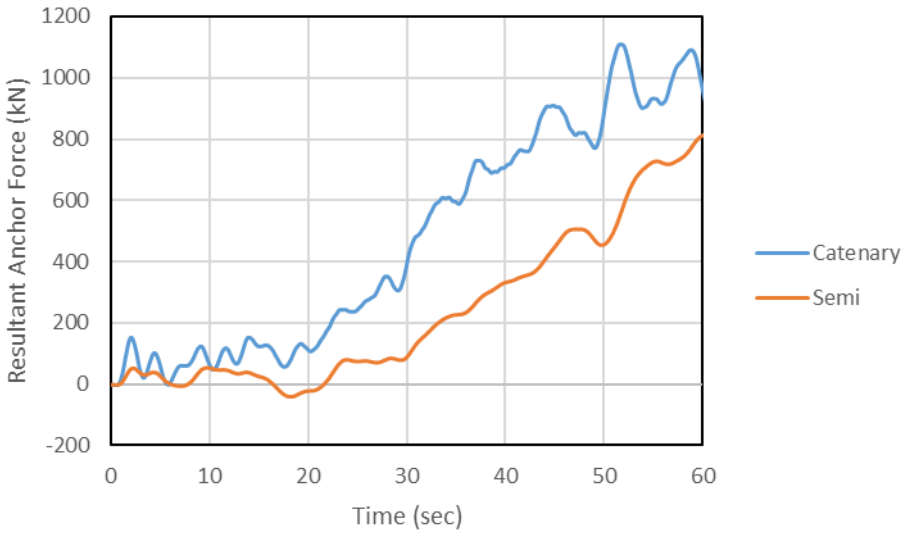

Figure 104: Resultant forces at anchor

Note that the magnitude of the resultant force in the 90° direction is nearly equal to zero due to the counter-pulling effect from lines oriented at evenly spaced directions. As shown in Figure #, the coefficient of variation of the catenary system is 0.73, which is lower than that of semi-taut mooring lines (1.02). The time history analysis for

resultant forces in two different shared mooring systems illustrates that a multiline anchor is likely to see time variant loads especially in the semi-taut structure.

The multi-directional loading is another key characteristic that is worthwhile to consider for shared anchor points. Selection for anchor types can be largely dependent on range of loading directions, as certain types may be restricted to variable directions of the total resultant anchor force. The resultant anchor load comes from the direction

$$\theta = tan^{-1}\left(\frac{F_{r,90}}{F_{r,0}}\right) \tag{36}$$

In the current example, the magnitudes of the resultant anchor components indicate that the load may be coming from a single direction with zero net force of the wind-wave-current field in the perpendicular direction. Although this preliminary study has assumed independence of wave-wind-current fields, environmental loading approaching the windfarm from various directions is typical in reality. Thus, in conventional offshore energy systems, a co-directional wind-wave-current field with the turbine perfectly facing upwind is an ideal condition. It must be noted that variability in oceanographic conditions can significantly affect the holding capacity of certain anchor types, and thus further research is needed to address the issues with multiline anchor subject to unpredictable loading directions.

7. CONCLUSIONS

The model validation was performed using an OC4 semi-submersible floating platform. The OrcaFlex simulation was performed to assess the capability of the module by comparing the results from FAST simulations. In FAST, quasi-static model was used to estimate cable responses, while a discretized cable model was considered in the OrcaFlex model. Several simulations with varying conditions were performed by altering the sea conditions.

A total of six simulations were carried out to ensure consistency between the OrcaFlex coupling module and the FAST program. The coupled DOF responses showed nearly identical results, and it is concluded that both programs are in exceptional agreement under prescribed free-decay conditions. When waves and wind fields were added to the test case, the tension responses at fairleads and anchors showed discrepancies in maximum values.

The results showed the two mooring analysis models, the OrcaFlex and FAST, are fundamentally different with their own basic underlying theories. The analysis suggests that the OrcaFlex model is accounting for effects of excitation loads that are not captured by the quasi-static based model. Thus, OrcaFlex was used as a means to predict mooring characteristics throughout the study to fully reflect the dynamics of the offshore surroundings.

The OC4 semi-submersible models using catenary and semi-taut system were compared to conduct performance study for selecting the preliminary mooring design.

The two types of mooring positioning system had the same mooring line number and angle arrangement and various environmental load conditions were considered in the analysis. The effects of the mooring parameters were investigated by altering the initial design and the optimal semi-taut system was developed.

For the most loaded line, the catenary system is a viable design because of its stable mooring loads (Qiao et al., 2012). The platform offsets in catenary and semi-taut system were similar except for the surge motion. The surge for the catenary mooring system is larger than that for semi-taut mooring system although the average of dynamic mooring line tension for catenary is greater than that for semi-taut.

The difference is because damping contribution for semi-submersible platform changes with mooring line length. The results suggest that the mooring length is decreased with additional damping in semi-taut system. According to the mooring line tensions, the transfers of mooring line tension are related to the length and shape of mooring line, and thus semi-taut system was more vulnerable to severe fatigue problem with higher tension values.

The dynamic behavior of the semisubmersible in three different water depths, 150 m, 200 m, and 250 m was examined. Wave-induced as well as wave-wind induced analyses for different load cases were completed. Finally a comparison of two different mooring types was made with respect to different water depths. Each analysis was performed in time domain.

As far as the motions of the semisubmersible platform, surge obtained similar mean values with the water depth increase for both systems. Generally, the tension of

mooring lines had larger magnitude for both mooring types in larger water depths. The behavior of the floating wind turbine may be dependent on water depths, and certain type of mooring system has more benefits to specific environmental conditions. Meanwhile, water depth variation has little effect on mean heave motion.

For a catenary chain, the motion responses are more significant as the water depth increases while for a semi-taut mooring, the coupled responses are less significant in deeper water. Consequently, the semisubmersible floating wind turbine can easily be secured with catenary system when the water depth is shallow.

The geology of the seafloor was investigated by identifying surficial sediment texture in macro-scale. The study area is located at the Northern California continental shelf, and sample data were extracted to describe surficial sediment type distribution through the use of mapping software. Based on the textural patterns, geotechnical parameters were estimated in order to process a more insightful selection of anchoring system.

Throughout the region, the erosion of sediments is susceptible near the shore due to faulting. Since the deposition of sediment rose to the surface, heterogeneous soil profiles can be expected when determining geotechnical properties. Sand is a dominant surficial sediment type across the continental shelf in the Northern California coastal, a condition that is common for offshore construction. Fine silt and mud were formed a belt on the mid-shelf area, where anchor installations are difficult.

The erosional bedrock typically indicates that the compressibility of sediments is expected to be strong, while fine-grained soils deposited suggest under-consolidated

state of soils. Thus, the survey of the study area suggests that there is an abundance of sand with consolidated state of a soil. In the mid-shelf, the cohesive mud strip is given, and this mud-belt is suspected to be under-consolidated due to the sediments fine-grain size. Overall, the near shore area is a layered seafloor and a granitic basement rock is lying underneath.

Three types of anchors were examined for the potential suitability as anchors for Floating Offshore Wind Turbines. The potential for adapting driven piles, direct embedment anchors, and drag embedment anchors was assessed within the context of securing multiple platforms. The feasibility of this multiline concept was investigated by approximating the resultant forces and loading directions at the anchor.

Considerations for anchor type reveled that driven piles and direct embedment anchors are suitable for the multiline application, except the PDPA needed an external device, known as load ring, which can transfer mooring loads to each anchor due to its directional preference. Because the study area is located at a sand/mud dominant filed with layered stratigraphy, drag embedment anchor was considered relatively inefficient. The result on the resultant force in time series showed more variation for the semi-taut system, and adapting a multiline became less favorable than to catenary system. Although both piles and PDPAs can resist significant amount of restoring forces from the mooring system, PDPA was selected as more commercially viable anchor choice due to its low weight to holding capacity ratio.

Chapters 2, 3, 4, 5, and 6 describe a different consideration for mooring/anchoring combinations. For an array-type floating wind farm deployed in the coastal area near northern California, the major conclusions suggest:

1. The dynamic mooring simulation module was selected as a tool to investigate the platform responses due to its sophisticated capability of modelling offshore systems.
2. The semi-taut system can be an economical solution by reducing both the line tension and footprint of the mooring under various oceanographic settings.
3. The catenary type is more suitable for the study area because the continental shelf is considered a shallow basin where catenary system tends to be more efficient.
4. The soil property data suggest that the example model is likely to be deployed over a near-shore area, mid-shelf, or outer-shelf. The mid-shelf is a site where muddy surface is dominant with under-consolidated state of the soil, while the rest of the sites contain sandy surface with well-consolidated compressibility of the soil.
5. Regardless of which region is used for the site for the floating wind farm, both piles and direct embedment anchors are viable options for the anchoring system. However, the potential for reducing overall project cost allows the PDPA type to be amenable to a multiline mooring configuration.

REFERENCES

Andersen, M. T., Wendt, F. F., Robertson, A. N., Jonkman, J. M., & Hall, M. (2016). Verification and Validation of Multisegmented Mooring Capabilities in FAST v8. International Society of Offshore and Polar Engineers.

Anima, R. J., Eittreim, S. L., Edwards, B. D., & Stevenson, A. J. (2002). Nearshore morphology and late Quaternary geologic framework of the northern Monterey Bay Marine Sanctuary, California. Marine Geology, Volume, 181(1), page. 35-54.

API, R. (2005). 2SK. Design and Analysis of Stationkeeping Systems for Floating Structures. 3rd Edition. American Petroleum Institute.

Beaudry-Losique, J., Boling, T., Brown-Saracino, J., Gilman, P., Hahn, M., Hart, C., Johnson, J., Mccluer, M., Morton, L., Naughton, B.,Norton,G., Ram, B.,Redding, T., Wallace, W. (2011). A National Offshore Wind Strategy. Creating an Offshore Wind Energy Industry in the United States. The U.S. Department of Energy.

Bhattacharya, S. (2014). Challenges in Design of Foundations for Offshore Wind Turbines. Engineering & Technology Reference, Page.9.

Burns, M., Maynard, M. L., & Davids, W. G. (2009). 3D Finite Element Analysis of Ultimate Capacity of Suction Caissons under Multi-Line Loading. Master's Thesis, University of Maine. Orono, ME. USA.

Chung, J., & Maynard, M. L. (2012). Physical Modeling of Suction Caissons Loaded in Two Orthogonal Directions for Efficient Mooring of Offshore Wind Platforms. Master's Thesis, University of Maine. Orono, ME. USA.

Dalyander, P. S. (2014). GMEX_median: The Median of Bottom Shear Stress for the Gulf of Mexico, May 2010 to May 2011 (Geographic, WGS 84). United States Geological Survey.

Diaz, B. D., Rasulo, M., Aubeny, C. P., Fontana, C. M., Arwade, S. R., DeGroot, D. J., & Landon, M. (2016). Multiline anchors for floating offshore wind towers. In OCEANS 2016 MTS/IEEE Monterey, page. 1-9.

Edwards, B. D. (2002). Variations in sediment texture on the northern Monterey Bay National Marine Sanctuary continental shelf. Marine Geology, Volume. 181(1), page. 83-100.

Fontana, C. M., Arwade, S. R., Degroot, D. J., Myers, A. T., Landon, M., & Aubeny, C. (2016). Efficient Multiline Anchor Systems for Floating Offshore Wind Turbines. Volume 6: Ocean Space Utilization; Ocean Renewable Energy, Volume.6.

Hall, M. (2015). MoorDyn User's Guide. Orono, ME: Depart ment of Mechanical Engineering, University of Maine. Retrieved from http://www.matt-hall.ca/wp-content/uploads/2014/11/MoorDyn-Users-Guide-2015-12-15.pdf

Hall, M., & Goupee, A. (2015). Validation of a Lumped-Mass Mooring Line Model with DeepCwind Semisubmersible Model Test Data. Ocean Engineering, Volume.104, Page.590-603.

Jonkman, J. M. (2007). Dynamics Modeling and Loads Analysis of an Offshore Floating Wind Turbine. Doctoral Dissertation, University of Colorado at Boulder. Boulder, CO. USA.

Karimirad, M., Koushan, K., Weller, S., Hardwick, J., & Johanning, L. (2014). Applicability of offshore mooring and foundation technologies for marine renewable energy (MRE) device arrays. In Renew2014, International Conference on Renewable Energies Offshore.

Kim, H., Choung, J., & Jeon, G. (2014). Design of Mooring Lines of Floating Offshore Wind Turbine in Jeju Offshore Area. Ocean Renewable Energy, Volume.9A.

Lin, Z., & Sayer, P. (2015). Influence of Water Depth Variation on the Hydrodynamics of Deep-Water Mooring Characteristics. Ocean Engineering, Volume.109, Page.553-566.

Lindenberg, S., Smith, B., & O'Dell, K. (2008). 20% wind energy by 2030. National renewable energy laboratory (NREL), US department of energy, renewable energy consulting services, energetics incorporated. Retrieved from http://www.nrel.gov/docs/fy08osti/41869.pdf

Masciola, M. (2011). Investigation of a FAST-OrcaFlex Coupling Module for Integrating Turbine and Mooring Dynamics of Offshore Floating Wind Turbines: Preprint. National Renewable Energy Laboratory, U.S. Dept. of Energy, Office of Energy Efficiency and Renewable Energy. Golden, CO. USA.

OrcaFlex Manual. (2006). Orcina Ltd. Daltongate, UK. Retrieved from http://www. orcina. com/SoftwareProducts/OrcaFlex/Documentation.OrcaFlex.pdf.

Qiao, D., Ou, J., & Wu, F. (2012, January). Design selection analysis for mooring positioning system of deepwater semi-submersible platform. In The Twenty-second International Offshore and Polar Engineering Conference. International Society of Offshore and Polar Engineers.

Rabe, P. (2015). On Dynamic Fatigue Loads on Composite Downlines in Offshore Service. Doctoral dissertation, TU Delft, Delft University of Technology. CD Delft, Netherlands.

Randall, R. E. (2016). Underwater and Moored System Design, Texas A&M University, College Station, TX. USA. Print.

Roberts, R. W. (1974). Marine Sedimentological Data of the Washington Continental Shelf. The University of Washington, the Department of Oceanography. Seattle, WA. USA. Retrieved from https://digital.lib.washington.edu/researchworks/handle/1773/16110

Robertson, A., Jonkman, J., Vorpahl, F., Popko, W., Qvist, J., Frøyd, L., Chen, X., Azcona, J., Uzunoglu, E., Soares, C., and Luan, C. (2014). Offshore Code Comparison Collaboration Continuation within IEA Wind Task 30: Phase II Results Regarding a Floating Semisubmersible Wind system. Ocean Renewable Energy, Volume.9B.

Schwartz, M., Heimiller, D., Haymes, S., & Musial, W. (2010). Assessment of offshore wind energy resources for the United States. National Renewable Energy Lab. Golden, CO. USA. Technical Report No. NREL/TP-500-45889.

Thompson, D., Beasley, D. J., True, D. G., Lin, S. T., Briaud, J. L., Seelig, W. N., & Jung, B. (2012). Handbook for marine geotechnical engineering. Naval Facilities Engineering Command. Port Hueneme, CA. USA. Engineering Service Center No. NFESC-SP-2209-OCN.

Tomasicchio, G. R., Armenio, E., D'alessandro, F., Fonseca, N., Mavrakos, S. A., Penchev, V., Schuttrum, H., Voutsinas., Kirkegaard, G., Jensen, P. M. (2012). Design of a 3D Physical and Numerical Experiment on Floating Off-Shore Wind Turbines. Coastal Engineering Proceedings, Volume.1, Issue.33.

University of North Carolina (UNC). (2009). Coastal wind: Energy for North Carolina's future. University of North Carolina at Chapel Hill. Chapel Hill, NC. USA. Retrieved from http://climate.unc.edu/files/2015/12/Coastal-Wind-Energy-for-NC2019s-Future.pdf

Wang, T. Y., Yang, L. J., Xu, Z. G., & Liu, J. K. (2013). Design and comparison of catenary and taut mooring systems for new concept FPSO IQFP in shallow waters. In Applied Mechanics and Materials.Trans Tech Publications, Volume. 353, page. 2670-2675.